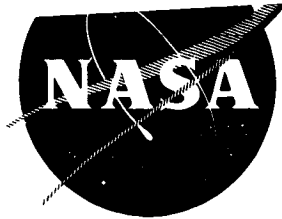


FACILITY FORM 602

N67-31200	(THRU)
(ACCESSION NUMBER)	1
241	(CODE)
(PAGES)	28
CR-72125	(CATEGORY)
(NASA CR OR TMX OR AD NUMBER)	

NASA CR 72125



260-IN.-DIA MOTOR FEASIBILITY  
DEMONSTRATION PROGRAM

Volume VI: 260-SL Motor Nozzle and  
Exit Cone Assemblies

Book 1: Text

Prepared for  
NATIONAL AERONAUTICS AND SPACE ADMINISTRATION

CONTRACT NO. NAS3-6284



AEROJET-GENERAL CORPORATION

SACRAMENTO, CALIFORNIA

GPO PRICE \$ \_\_\_\_\_

CFSTI PRICE(S) \$ \_\_\_\_\_

Hard copy (HC) 3.00

Microfiche (MF) 165

ff 653 July 85

FINAL PHASE REPORT

260-IN.-DIA MOTOR FEASIBILITY  
DEMONSTRATION PROGRAM

Volume VI

260-SL MOTOR NOZZLE AND  
EXIT CONE ASSEMBLIES

Book 1: Text

Prepared for  
NATIONAL AERONAUTICS AND SPACE ADMINISTRATION

8 April 1966

Contract No. NAS3-6284

Technical Management  
NASA Lewis Research Center  
Cleveland, Ohio  
James J. Kramer

**AEROJET-GENERAL CORPORATION**  
A SUBSIDIARY OF THE GENERAL TIRE & RUBBER COMPANY

ABSTRACT

The 260-SL motor nozzle development program was conducted to demonstrate the ability to design, fabricate, and verify the performance of nozzles for the 260-in.-dia motors. A design evaluation program was conducted prior to the final design of the nozzles. A material and process evaluation program was conducted for selecting and defining materials and processes to be used in the fabrication of the nozzles. Three 44-in.-dia and one 120-in.-dia motor nozzles were tested in motor firings and their performance was evaluated to substantiate the design criteria, materials, fabrication procedures, and qualification criteria used, and to verify performance predictions of the 260-SL nozzles. Motors 260-SL-1 and -2 were test fired on 25 September 1965, and 23 February 1966, respectively. Nozzle performance of the two motors were quite similar. The nozzle and exit cone maintained structural integrity for the full firing duration. Erosion performance of the entrance V-44 insulator and all ablative plastic liner components was excellent. The successful fabrication and testing of the 260-SL nozzles demonstrated and confirmed the feasibility and reliability of large ablative nozzles.

TABLE OF CONTENTS

BOOK 1

	<u>Page</u>
I. Summary	1
II. Introduction	5
III. Design Description	8
IV. Original Design Selection	12
V. Design Changes from Original Design	67
VI. Material and Process Evaluation	73
VII. Specifications	134
VIII. Fabrication	138
IX. In-Process Testing and Inspection	169
X. Investigation of Fabrication Processes and Quality Achieved	172
XI. Handling and Handling Equipment	187
XII. Packaging and Shipping	190
XIII. Nozzle Performance	193
XIV. Conclusions	231

List of References

List of Nomenclature

BOOK 2

Appendixes

Ablative Material Property Procedures

A

Test Procedure and Equipment Used for Determination  
of Densification and Heat Transfer Characteristics  
of Thick Ablative Laminates

B



I. SUMMARY

The 260-SL motor nozzle development program was conducted to demonstrate the ability to design, fabricate, and verify the performance of nozzles for the 260-SL motors. This program was successfully completed.

The 260-SL motor nozzle assembly is composed of ablative-plastic liner inserts contained in an 18%-nickel maraging steel structural shell and an exit cone assembly composed of an ablative liner supported by a structural sandwich of aluminum-honeycomb core with inner and outer stainless steel facings and steel end flanges.

A design evaluation program was conducted prior to the final design of the nozzles. This consisted of screening and selection of materials, heat-transfer and structural analyses of the materials and components, and preliminary establishment of material and process specifications. This evaluation program culminated in the design and fabrication of three subscale nozzles for 44-in.-dia motors and one nozzle for a 120-in.-dia subscale motor. The successful performance of these nozzles during motor firing confirmed the adequacy of the materials and fabrication processes for the 260-SL nozzles.

A material and process evaluation program was conducted for selecting and defining materials and processes to be used in the fabrication of the nozzles. The evaluation program included an extensive literature survey in which performance data of materials used in applicable motor nozzles tested by Aerojet and throughout the industry were compiled and analyzed. Completion of four subtasks resulted in final selection of the materials and processes used.

A. Subtask I was conducted to determine the properties of the ablative materials selected, determine their characteristics as related to tape wrapping, and establish tape-wrapping procedures. The materials evaluated were MX-4926

I, Summary (cont.)

a carbon-cloth reinforced phenolic; MX-2646, a silica-cloth reinforced polyamide-modified phenolic; and FM-5131, a silica-cloth fabric reinforced with a modified phenolic.

B. Subtask II involved the development of adhesive bonding technology for assembly of the ablative components into the nozzle and exit cone and assembly of the stainless steel facings, steel attachment flanges, and honeycomb core that comprise the structural part of the exit cone. This included evaluation of adhesives, joint designs, and fabrication methods.

C. Subtask III involved the development of hydroclave cure cycles for the ablative plastic components.

D. Subtask IV demonstrated the fabrication procedures established in Subtasks I and III by fabrication of a half-length throat insert sized for the 120-in.-dia motor (120-SS-1). Material characteristics, tape-wrapping processes, and cure cycles were thus verified.

The 44-SS and 120-SS-1 motor nozzles were tested in motor firings and their performance was evaluated to substantiate the design criteria, materials, fabrication procedures, and qualification criteria used, and to verify performance predictions of the 260-SL nozzles.

The 44-SS subscale motor program enabled the evaluation of the ablative nozzle components, adhesives, and sealants in short-duration motor firings (approximately 20 sec) and assessment of the effects of aft end ignition. Motors 44-SS-1, -2, and -3 were test fired 22 June 1964, 14 July 1964, and 24 February 1965, respectively. The 44-SS motors demonstrated the performance reproducibility of ablative plastic components and verified bond materials and processes. The throat surface recession of the three 44-SS motors ranged from 0.075 to 0.080 in., as compared to a predicted value of 0.094 in.

I, Summary (cont.)

The throat inserts of the motor 44-SS-1 and -2 nozzles were made by a die-cut mold process. These throat inserts were gouged circumferentially during the test firing. The area of the throat insert gouging was replaced for the 44-SS-3 motor with a tape-wrapped component, which did not exhibit any gouging or anomaly after test firing. It was concluded that the die-cut molded process was responsible for the throat gouging. Therefore, the 44-SS nozzles adequately demonstrated the performance of ablative nozzles subjected to aft-end ignition.

The 120-SS-1 motor was fired on 19 September 1964. The nozzle and exit cone assemblies performed satisfactorily throughout the motor firing. The objectives of this test of a large subscale nozzle, which was made as identical as possible to the 260-SL motor nozzles, were accomplished. The nozzle performance was within design limits. The average surface recession at the throat was 0.43 in., compared with a predicted 0.365 in., or a deviation of only 18%.

Two design changes to the 260-SL motor nozzle were made as a result of the 120-SS-1 motor nozzle performance. These were an increase in the thickness of the V-44 rubber entrance insulation and the addition of a layer of cork on the aft external surface of the exit cone. The V-44 rubber entrance insulation of the 120-SS-1 motor nozzle was eroded up to 55% more than predicted. This increased erosion was considered to be principally due to the high erosion of the Germax-modified V-44 material in the aft-head chamber insulation joints, which caused grooves downstream in the insulation. As a precaution, the V-44 insulation of the 260-SL-1 motor nozzle entrance was thickened. The aft external portion of the 120-SS-1 motor exit cone was overheated after the firing due to late quench actuation, which caused some bond failure of the external facing and doublers. This area was protected on the 260-SL motors by the addition of cork insulation over the aft 2 ft of the exit cone.

I, Summary (cont.)

Fabrication of the 260-SL-1 and -2 motor nozzles was accomplished with only minor, acceptable deviations. Major changes in processing procedures resulting from subscale nozzle tests were the performing and curing of the ablative nozzle components in an autoclave instead of a hydroclave and elimination of the perform cycle in fabricating the exit cone liner. Design requirements were met.

Motors 260-SL-1 and -2 were test fired on 25 September 1965, and 23 February 1966, respectively. Nozzle performance of the two motors were quite similar. The nozzle and exit cone maintained structural integrity for the full firing duration. Erosion performance of the entrance V-44 insulator and all ablative plastic liner components was excellent. The average postfiring throat diameter of motor 260-SL-1 nozzle was 1.46 in. greater than the prefiring diameter, yielding an average material loss rate of 5.7 mil/sec during the motor action time of 128.2 sec. The average postfiring throat diameter of 260-SL-2 nozzle was 1.25 in. greater than the prefiring diameter, yielding an average throat erosion rate of 4.8 mils/sec during an action time of 129.8 sec.

The successful fabrication and testing of the 260-SL nozzles demonstrated and confirmed the feasibility and reliability of large ablative nozzles. In particular, the tests demonstrated the adequacy of: (1) the plastic nozzle inserts, fabricated MX-2646 silica cloth and phenolic, tape wrapped, roller debulked, and final cured in 300 psi autoclave cycles; (2) the monolithic plastic nozzle exit cone liner, fabricated of MX-4926 carbon cloth and phenolic and FM-5131 silica cloth and phenolic, tape wrapped, roller debulked, and oven cured at 70 to 75 psi, achieved with nylon tension wrap and vacuum bagging; and (3) the nozzle exit cone liner structural support, consisting of an aluminum honeycomb-stainless steel facing sandwich built up on the liner and bonded with epoxy resin.

## II. INTRODUCTION

### A. PURPOSE OF REPORT

This is the sixth in a series of final reports that will be issued as major phases of the 260-in.-dia motor feasibility demonstration program are completed. This series of reports, when completed, will constitute the major portion of the Final Report on this program.

This report presents the design, material and process evaluation studies, fabrication and performance evaluation of nozzles used in the 44-SS, 120-SS-1 and 260-SL motors, with the exception of the structural and rubber insulation components. The structural components of the 260-SL and 120-SS-1 motor nozzles are discussed in detail in the chamber phase report, Reference (1), and the rubber components are covered in the insulation phase report, Reference (2). Additional posttest analyses of the 260 motor nozzles are discussed in the 260-SL-1 and -2 motor firing reports, References (3) and (4).

### B. SCOPE OF REPORT

This document summarizes in detail the 260-SL motor nozzle development program. The following phases of the program are included in this report:

1. A design evaluation program leading to the design selection of the 44-SS, 12-SS-1 and 260-SL motor nozzles.
2. A material and process evaluation program for selecting and defining materials and processes used in the fabrication of the nozzles.
3. Fabrication of the nozzles.
4. In-process and post-fabrication testing and evaluation of the nozzle components and assembly.

II, B, Scope of Report (cont.)

5. Postfired evaluation of 44-SS, 120-SS-1, and 260-SL nozzle performances.

6. Conclusions.

C. PROGRAM OBJECTIVES

The purpose of the development program was to demonstrate the capability of designing and fabricating large ablative 260-SL nozzles capable of providing the required motor performance. The objectives were to:

(1) evaluate analytically the integrity and performance of each component of the nozzle assembly, (2) select the best available materials and determine the properties and fabricability of the nozzle materials and components, (3) demonstrate the validity of the analytical assumptions, equations and criteria used in designing the 260-SL nozzle, (4) demonstrate the validity of the selection of the materials and fabrication procedures, and finally, (5) fabrication of a sound, reliable 260-SL nozzle.

D. APPROACH

A preliminary design study was conducted which included a literature survey and analysis of existing and previously used nozzle materials and designs. Nozzle designs were selected and analyzed for the 44-SS, 120-SS-1, and 260-SL motor nozzles. A material and process evaluation program was conducted to evaluate selected materials and determine in-process controls and procedures for fabricating and assembling the nozzle components. Materials and in-process specifications were written to incorporate the pertinent data obtained from the material and process evaluation program into the nozzle design, materials and fabrication. Three 44-in.-dia and one 120-in.-dia motor nozzles were fabricated and tested to evaluate nozzle design concepts,

II, D, Approach (cont.)

materials and fabrication procedures to be used in the 260-SL-1 motor nozzle. The results of the subscale nozzle evaluation were used in the final design and fabrication of the 260-SL motor nozzles.

E. PROGRAM SUMMARY

All program objectives were achieved. The selection of materials and the determination of the material properties and fabricability were successfully accomplished in the material and process evaluation program. The capability of all materials and components to be used in the 260-SL nozzles was adequately demonstrated. The performance of the 44-SS and 120-SS-1 nozzles was as predicted and indicated that the analytical predictions and the design concepts were valid. The results of the 44-SS motor tests indicated that the nozzle will have no adverse affect from aft end ignition. The results of the 120-SS-1 nozzle performance indicated areas requiring minor modification of the 260-SL nozzle design to improve the performance and reliability. These modifications were readily incorporated into the 260-SL nozzles. The entire nozzle development program was satisfactorily completed.

### III. DESIGN DESCRIPTION

#### A. 260-SL MOTOR NOZZLE

The 260-SL motor had a single, on-center, fixed nozzle with a 71.0-in.-dia throat as shown in Figure 1. The nozzle geometry consisted of an entrance section with a radius of curvature equal to one throat radius and an exit cone with a 17.5-degree half angle and an expansion ratio of 6.0:1. The nozzle line consisted of ablative plastic inserts. The entrance section contained MX-2646 silica cloth and phenolic at area ratios greater than 2.0:1, with a tape orientation of 80 degrees (nominal) with respect to the nozzle center line. The entrance section had MX-4926 carbon cloth and phenolic, oriented 80 degrees (nominal) and extending between upstream area ratios of 1.1 to 2.0:1. The entrance inserts were over-wrapped parallel to part with MX-2646 silica cloth. The throat insert consisted of MX-4926 carbon cloth oriented 67 degrees (nominal), extending to a downstream area ratio of 1.05:1, and were overwrapped parallel to part with FM-5131 silica cloth and phenolic. The throat extension insert extended to an area ratio of 2.0:1 and had the same materials as the throat insert; however, the carbon cloth was oriented 30 degrees to the nozzle center line. The exit cone (Figure 2) consisted of MX-4926 carbon cloth, oriented parallel to nozzle center line, up to an area ratio of 3.0:1, and FM-5131 silica cloth, oriented parallel to nozzle center line, for the remaining portion of the expansion section. The exit cone inserts were overwrapped parallel to part with FM-5131 silica cloth tape. Silicone rubber sealant was used in the joints between the liner inserts.

The plastic inserts were bonded to the structural components with Epon 913 epoxy adhesive.

The nozzle shell material was 18% nickel maraging steel with a 200,000 psi minimum and 235,000 psi maximum yield strength at 0.2% offset.



III, A, 260-SL Motor Nozzle (cont.)

The shell (Figure 3) contained the entrance, throat, and throat extension inserts and had a design pressure of 870 psia which represented a 1.3 safety factor on the 260-SL motor MEOP.

The exit cone structural shell (Figure 2) was a honeycomb sandwich structure which contained the exit cone inserts. The honeycomb facings were fabricated from 17-7 PH stainless steel with a minimum yield strength of 150,000 psi to 0.2% offset and a minimum ultimate tensile strength of 180,000 psi. Two 0.026-in.-thick sheets were used for the inner facings and one 0.026 in.-thick sheet (with doublers at the splice joints) was used for the outer facings. The sandwich core was a 0.72-in.-thick 6.0-1/4-309 (3000) aluminum honeycomb. The stainless steel facings were bonded to the aluminum core with an Epon 75-25 adhesive film. The honeycomb sandwich contained forward and aft attachment rings made of normalized AISI 4130 steel and AISI 4340 steel, respectively.

An exit cone retainer ring of normalized AISI 4130 steel was used to mechanically retain the plastic inserts and also served as a handling ring during fabrication and assembly.

A minimum number of Buna-N rubber O-rings was provided at the joint interfaces of the ablative inserts.

Gen-Gard V-61 trowelable insulation was used around the exit cone aft ring and cork insulation around the aft 2 ft of the exit cone exterior to provide thermal protection against exhaust-gas heat radiation. Gen-Gard V-44 rubber was used in the nozzle entrance section and was bonded to the nozzle components with Epon 948 epoxy adhesive.

The nozzle and exit cone assemblies weighed approximately 37,000 lb.

### III, Design Description (cont.)

#### B. 120-SS MOTOR NOZZLE

The nozzle for the 120-SS motor (Figures 4 and 5) was essentially a scale reduction of the 260-SL-1 motor nozzle; the same design criteria and materials were used for both. The nozzle had a 30.0 in.-dia throat, and entrance radius of curvature equal to the throat radius, an exit cone divergent half-angle of 17.5 degrees and an expansion ratio of 6.0:1.

The ablative materials and tape orientation were identical to those used in the 260-SL motor nozzle. The location of the ablative materials in the 120-SS and 260-SL nozzles were also similar except the carbon cloth of the 120-SS nozzle extended from an entrance area ratio of 1.6:1 to an exit expansion ratio of 3.5:1

The structural component materials of the 120-SS and 260-SL nozzles were similar. The nozzle shell (Figure 6) design pressure was 965 psia. The honeycomb sandwich had a core thickness of 0.5 in., and 0.018-in.-thick facing sheets. Both exit cone attachment flanges were made of normalized AISI 4130 steel.

The entrance section and the retainer ring insulations were identical to those used in the 260-SL nozzle. No exterior insulation was used on the 120-SS nozzle exit cone. Weight of the nozzle and exit cone assemblies was approximately 4,600 lb.

#### C. 44-SS MOTOR NOZZLE

The nozzles for the three 44-SS motors were identical with the exception of the throat insert. The single, on center, fixed nozzle had a 13.1 in.-dia throat (Figure 7). The exit cone had a 17.5 degree half-angle

III, C, 44-SS Motor Nozzle (cont.)

and an expansion ratio of 2.5:1. The nozzle liner consisted of three inserts. The entrance section insert had MX-2646 silica cloth oriented 72 to 87 degrees (with respect to the nozzle center line) overwrapped with MX-2646 silica cloth parallel to the part. The throat insert extended from a subsonic area ratio of 1.6 to a supersonic area ratio of 1.3 and consisted of MX-4926 carbon cloth oriented 60 to 75 degrees and overwrapped parallel to part with FM-5131 silica cloth. The carbon throat insert was composed of stacked die-cut segments in the 44-SS-1 and -2 nozzles and in the forward portion of 44-SS-3 nozzle throat insert. The aft portion of the 44-SS-3 throat insert was tape wrapped (Figure 8). The exit cone insert had MX-4926 carbon cloth tape wrapped at an orientation of 45 to 60 degrees and overwrapped parallel to part with FM-5131 silica.

The nozzle shell (Figure 9) was made of AISI 4340 steel with a 150,000 psi yield strength at 0.2% offset. The nozzle shell design pressure was 819 psi, which represented a 1.5 safety factor on the 44-SS motor MEOP.

An exit cone retainer ring of AISI 4130 steel was used to mechanically retain the plastic inserts and was attached to the nozzle shell with 42 NAS1022N8 nuts and AN8-13A bolts. Gen-Gard V-44 insulation was used in the nozzle entrance section and Gen-Gard V-61 trowelable insulation was applied around the exit cone retainer ring to provide protection from the exhaust gases.

The nozzle assembly weighed approximately 540 lb.

#### IV. ORIGINAL DESIGN SELECTION

##### A. 260-SL MOTOR NOZZLE

##### 1. Nozzle Geometry

The 71.0-in. initial throat diameter was a motor performance requirement established from interior ballistic design and performance parameters.

The exit cone divergent half-angle of 17.5 degrees was stated in the Work Statement. The optimum sea-level expansion ratio based on average thrust was 6.0:1 for the 260-SL motors.

The nozzle entrance radius curvature, which was equal to the throat radius, was based on an analytical evaluation of several different radius curvatures. A series of nozzle entrance shapes was evaluated in the Minuteman nozzle contour development program for nozzles with throat diameters slightly larger than 2.5 in. An additional series of entrance shapes for nozzles with throat diameters slightly larger than 3.5 in. was evaluated in the Minuteman nozzle immersion program. Pertinent data from these two investigations are shown in Figure 10. Both sets of data indicate that, for radius ratios (entrance wall to throat) between 1.0 and 4.0, differences in motor performance are insignificant. Both programs used aluminized solid propellants. Because losses due to two-phase flow in a nozzle are considered to be greater for small nozzles than for very large nozzles, no performance decrements for the large nozzles would be expected for the foregoing range of wall radius values.

Aerodynamic experiments also were conducted in support of Minuteman motor development. In these investigations, which are based upon ideal gas flow and are independent of nozzle size, nozzle entrances, having radii of 0.5, 1.0, and 2.0 times the throat radius, were evaluated. One

IV, A, 260-SL Motor Nozzle (cont.)

result of the aerodynamic studies was the excellent correlation obtained between cold-flow model data and the observed erosion characteristics in geometrically similar rocket motors. In particular, the correlation studies demonstrated the direct relationship between relative heat-transfer rates obtained by quantitative aerodynamic measurements in the nozzle entrance and the erosion distribution in corresponding regions.

Wall Mach number distributions in nozzle entrances, having curvature-radius to throat-radius ratios of 0.5, 1.0, and 2.8 are presented in Figure 11. For each condition, the shape of the curve tends to minimize convective heat-transfer rate. However, in the region immediately upstream of the throat ( $-0.3 < x < 0$ ), the entrance with a radius ratio of 0.5 reaches a condition of peak heat-transfer rate ( $M = 1.0$ ) at a substantial distance upstream of the critical locations which were established for entrances with radius ratios of 1.0 or greater. Moreover, the critical locations for the larger radius ratios are substantially the same. It is concluded that there is little advantage in designing for radius ratios larger than 1.0, and, for radius ratios of the order of magnitude of 0.5, the undesirable condition exists that excessive local flow acceleration locates the region of peak heat-transfer rate a substantial distance upstream.

Profiles of the flow at the throat station were obtained in the aerodynamic experiments for radius ratios of 0.5, 1.0, 2.0 and 2.8. These profiles appear in the form of Mach numbers in Figure 12. It is evident that the Mach number profile gradients are increasingly severe as the radius ratio is reduced. Subsequent investigation of local momentum flow and pressure across the throat station indicates that a substantial decrease in discharge coefficient and internal thrust existed for the nozzle with the upstream radius ratio of 0.5 relative to the other ratios, although no noticeable difference was noted for radius ratios of 1.0, 2.0, or 2.8. No effect on specific impulse was established for any of the configurations;

## IV, A, 260-SL Motor Nozzle (cont.)

however, this is primarily because of the decrease in mass flow corresponding to the decrease in thrust level. It is concluded that there was no advantage for either thrust level or performance in incorporating a radius ratio larger than 1.0 and that it would be undesirable to incur thrust losses and possible downstream effects of mass-flow profile distortion association with smaller radius ratios. This conclusion has particular validity for very large nozzles for which two-phase flow approximates characteristics of ideal gas flow.

A method of analysis which includes nozzle geometry in terms of axial position and the rate of change of local nozzle wall radius with axial position was used to determine the effect of entrance radius ratio on local heat transfer coefficient. This method utilizes the momentum integral equation, together with some basic experimental data for skin friction in turbulent flow, to calculate the hydrodynamic boundary layer thickness and momentum thickness along the nozzle wall. Reynolds analogy between heat and momentum transfer was then employed to determine the local heat transfer coefficient.

Using the above method, which was programmed for the G.E. 225 computer, the ratio of the local heat transfer coefficients for radius ratios of 2 and 0.5 to the heat transfer coefficient for a radius ratio of 1 were calculated. The results of this analysis are presented (Figure 13) in terms of the ratio of heat transfer coefficients, noted above as a function of the nozzle area ratio. It is indicated by this plot that for the subject motor and propellant, the increase in throat heat-transfer coefficient is approximately 4% for a radius ratio of 0.5 and the reduction in throat heat-transfer coefficient is approximately 3.5% for a radius ratio of 2. It is also indicated that, for the assumed initial conditions, the variation on local film coefficient for the various radius ratios is insignificant for area ratios larger than 2.

From the above study, it can be concluded that the influence of radius ratio on heat transfer and the resulting erosion is negligible. The

IV, A, 260-SL Motor Nozzle (cont.)

trend noted was a general decrease in heat transfer with increased radius ratio. The net decrease of only 7.5% for a four-fold change in radius ratio is not sufficient to warrant the added length and weight of the inlet region attendant with large radius ratios.

2. Material Selection

The use of ablative plastic as the throat insert material was stated in the Work Statement. Ablative plastic was also used on all other ablation surfaces of the nozzle for compatibility with the throat material in fabrication and in-process control methods.

Ablative tape material was selected for fabricating the nozzle inserts because tape-wrapped plastic nozzle parts have been widely used and have demonstrated greater reliability and uniformity in erosion than molded plastic parts. Ablative plastic inserts can be pressure-molded either from chopped fabric or from tape-wrapped laminates. Although the material cost of chopped fabric is cheaper than tape fabric, the requirements of expensive large dies and high pressures for molding chopped fabric greatly offsets the material cost advantage.

Phenolic-resin-impregnated carbon cloth was selected for the throat and high ablation areas of the nozzle. A literature survey was conducted in which experimental data on ablative materials were obtained from motor tests conducted both at Aerojet and throughout the industry. A summary of the pertinent results is presented in Figure 14. Although a direct comparison of all test data was not possible because of varying test conditions and fabrication techniques, selective screening permitted both qualitative and quantitative comparison of portions of the data. For example, tubular nozzle data could not be compared quantitatively with conventional nozzle

IV, A, 260-SL Motor Nozzle (cont.)

data; however, the tubular nozzle data (Figure 14) enabled the qualitative comparison of three carbon cloths and two graphite cloth materials. This qualitative comparison indicated that MX-4926 carbon cloth had the lowest surface recession rate. Also, results obtained with end-burning grain configurations could not be compared quantitatively with those obtained with core grains. Selective comparison of the results shown in Figure 14 indicate that carbon cloth and graphite cloth materials have similar surface recession rates. In addition to the literature analysis, various ablative plastic materials were comparatively evaluated, using the Aerojet material evaluation rocket motor (MERM); the mechanism for comparison was their surface recession rates. The candidate materials and the test results are shown in Figures 15 through 17. The results of the MERM tests indicate that the recession rate of carbon cloth and graphite cloth are similar. The average recession range of 2.89 to 3.66 mil/sec was small for the five best materials, which included three carbon cloths (MS-4926, FM-5072, and FM-5063) and two graphite cloths (MS-4551 and FM-5014G). The lowest maximum recession rate was obtained with MX-4926; carbon cloth also has the advantage of lower cost and superior properties. The material cost of carbon cloth is approximately 25% less than graphite cloth, and carbon cloth has higher strengths and a lower thermal conductivity as shown in Figure 18. The consistency in recession rate and material properties is dependent upon the quality control of the raw material and fabrication procedure. With the completion of process evaluation work prior to initiation of fabrication and with the rigid quality control imposed during fabrication, reliable nozzle parts with carbon cloth are ensured.

Phenolic-resin-impregnated silica cloth was selected for the low ablation areas of the nozzle. The use of silica cloth at high area ratios of the nozzle has been widely demonstrated by numerous successful motor firings. Its relatively low cost and ease of fabrication are particularly attractive for large size nozzles.



IV, A, 260-SL Motor Nozzle (cont.)

The quality of the raw materials, both carbon and silica cloth is controlled by the rigid physical and mechanical requirements of the material specifications. The capability of the candidate materials to meet these requirements must be established before they are accepted for use.

The carbon cloth materials that were evaluated for acceptance were MX-4926 and FM-5072. These materials were previously evaluated in the MERM motors and were found to have similar recession rates. The room temperature properties of these materials (Figure 18) are different but they are expected to be within the requirements of the specification. The MX-4926 material was selected because of its low recession rate, its excellent room temperature properties, and its successful use in smaller nozzles (Figure 14).

The silica cloth materials that were evaluated include MX-2646, MX-2600 and FM-5131. In addition to determining if the requirements of the specification were met, these materials were evaluated for fabrication compatibility with the carbon cloth material. MX-2646 was selected for the entrance-section liner and overwrap because of its superior mechanical properties. FM-5131 was selected for the exit-cone liner and overwrap of the throat, throat extension, and exit-cone sections because of its lower cost.

The location of the changeover from carbon cloth to silica cloth was selected so that a minimum of carbon cloth would be used and yet ensure that the ambient temperature material (thickness below the heat affected depth) would be sufficient to maintain the structural integrity of the insert. The changeover location at the nozzle entrance is at the 1.60 area ratio. At that area ratio, the silica cloth recession depth is 1.15 in. and the 100°F temperature depth is 1.50 in. The remaining material thickness of 1.43 in. is at ambient temperature. At the exit-cone area ratio of 3.78, the silica cloth recession depth is 0.37 in., and 0.78 in. of ambient temperature material

IV, A, 260-SL Motor Nozzle (cont.)

thickness remains. The material thickness at ambient temperature is calculated considering twice the recession rate. If the locations were moved toward the throat section, the thickness of ambient temperature material would be decreased because of higher recession depth and, therefore, the structural integrity of the insert would be adversely affected. If the locations were moved away from the throat section, additional carbon cloth would be required.

The ablative liners were overwrapped parallel to the mating surfaces with silica cloth to provide a thermal barrier should delamination occur in the inserts and to provide more rigidity during handling. The selection of silica cloth rather than cheaper materials (glass and asbestos) was to ensure maximum thermal protection to the steel shell and to afford fabrication compatibility with the ablative liner materials. The ablation temperature of silica cloth is 3500°F as opposed to 2200°F for glass cloth and 1200°F for asbestos cloth.

3. Determination of Material Thickness

The insert thickness requirements were based on the amount of internal stresses in the insert. The stresses are caused by internal pressure of the exhaust gases, thermal gradients through the insert, and radial stresses due to differential restraint of the expanding materials. All of these effects were calculated and superimposed to obtain the final stress distribution through the insert. Minimum margins of safety of the nozzle components are shown in Figure 19.

a. Heat-Transfer Analysis

A heat-transfer analysis was conducted to determine the thermal gradient at various stations of the nozzle and exit cone. The thermal

## IV, A, 260-SL Motor Nozzle (cont.)

gradient through the insert is the surface recession, char depth, heat-affected zone (100 to 500°F) and the remaining ambient-temperature thickness. The analysis was based on actual motor environmental conditions without applying a safety factor. Applying such factor to the chamber pressure, flame temperature, or heat flux can render the results unrealistic. The thermal analysis of a rocket nozzle consists of predicting the transient-temperature distribution in the various nozzle components. However, when the surface material exhibits ablative characteristics, the ablation depth and char depth are also significant factors. The analytical prediction of these quantities requires the evaluation of the surface heat flux. Surface heat flux is used to evaluate the boundary conditions which are subsequently used in solving the transient conduction equation. This heat flux is equal to the product of the convective heat transfer coefficient and the difference between the adiabatic wall temperature and the wall temperature:

$$Q_c = h_c (T_{aw} - T_w) \quad (\text{Eq 1})$$

where:

- $Q_c$  = convective heat flux, Btu/sq ft-sec
- $h_c$  = convective heat transfer coefficient, Btu/sq ft-sec-°R
- $T_{aw}$  = adiabatic wall temperature, °R
- $T_w$  = wall temperature, °R

The convective heat-transfer coefficient of equation (1) was evaluated using the Colburn equation which was developed originally for fully developed flow in circular ducts. Although the flow in nozzles does not correspond to the flow in constant area circular ducts, data obtained from numerous motor firings with nozzles geometrically similar to this nozzle has indicated that accurate results are obtained using the Colburn equation to evaluate the heat transfer coefficient.

## IV, A, 260-SL Motor Nozzle (cont.)

By substituting the equation of mass flux and continuity into the Colburn equation, the following relationship is obtained:

$$h_c = \frac{0.023 C_w P_c C_p}{\left( \frac{P_c C_w D_t}{\mu} \right)^{1/5} (Pr)^{2/3}} \left( \frac{A_t}{A} \right)^{.9} \quad (\text{Eq 2})$$

where:

- $C_w$  = propellant mass flow coefficient,  $\text{sec}^{-1}$
- $P_c$  = chamber pressure, lb/sq ft abs.
- $c_p$  = specific heat at constant pressure Btu/lb-°R
- $A$  = local nozzle area, sq ft
- $Pr$  = Prandtl number
- $A_t$  = throat area, sq ft
- $D_t$  = nozzle throat diameter, ft
- $\mu$  = absolute viscosity, lb/ft sec

Analytical and experimental studies of nozzles similar to this nozzle indicated that the contribution to the surface heat flux due to particle impingement and radiation was negligible compared to the convective contribution. Based on this finding, the total heat flux is approximated by equation (1).

As noted previously, the thermal response characteristics of the nozzle components are obtained by solution of the transient conduction equation, with the appropriate boundary conditions. For the 260-SL motor nozzle, the depth of heat penetration is slight compared to the local radius of curvature at the heated surface and the temperature gradient parallel to the nozzle surface is small compared to the temperature gradient normal to this surface. For these reasons, the following simplified transient conduction equation is used:

## IV, A, 260-SL Motor Nozzle (cont.)

$$\frac{\delta}{\delta r} \left( K \frac{\delta T}{\delta r} \right) = \rho c \frac{\delta T}{\delta \theta} \quad (\text{Eq 3})$$

where:  $K$  = thermal conductivity, Btu/sec ft-°F  
 $r$  = radial coordinate, ft  
 $\rho$  = density, lb/cu ft  
 $c$  = specific heat, Btu/lb-°R  
 $\theta$  = time, sec

The boundary conditions used in solving the transient conduction equation are obtained from an energy balance at the heated surface. At this surface, the heat flux to the surface is equal to the heat flux leaving the surface in the absence of ablation.

When the surface material reaches its "effective ablation temperature", the boundary condition becomes:

$$Q_c = h_c (T_{aw} - T_a) = -K \left( \frac{\delta T}{\delta r} \right)_{r=r_i} + \rho h_{eff} \left( \frac{\delta r}{\delta \theta} \right)_{r=r_i} \quad (\text{Eq 4})$$

where:  $T_a$  = effective ablation temperature, °R  
 $h_{eff}$  = effective lower heat of ablation, Btu/lb

The general thermal analysis program discussed above was written for the IBM 7090 computer and is used to determine surface recession depth, char depth, and temperature gradients. Recession characteristics are expressed as a function of two material properties: ablation temperature and heat of ablation. These properties are determined from both simulation testing and actual motor firing results. The ablation temperature is a measure of the maximum surface temperature that a material can sustain in ablating. The heat of ablation is a measure of the material's capability to absorb energy in

IV, A, 260-SL Motor Nozzle (cont.)

ablating and restricting heat transfer. The motor pressure and thrust vs time data and heat of ablation values are input into the computer until a correlation is obtained with actual measured recession at a selected nozzle station. By assuming the ablation temperature and heat of ablation to be approximately constant, these values are used to determine surface recession at other nozzle stations. Minimum values of heat of ablation and ablation temperature are used in determining recession rates, and thus result in conservatively predicted recession rates.

Results of the 260-SL-1 nozzle heat-transfer analysis at various area ratios are presented in Figures 20 through 32. The thermal properties of the materials are listed in Figure 33. The butadiene rubber in the entrance cap region was not included in the analysis so that a conservative analysis of this critical region would result. The burnout dimensions at various area ratios are summarized in Figure 34. The variation in throat diameter is approximately linear during web time as shown in Figure 35. The calculated burnout recession and char depth at the throat of the 260-SL-1 are 0.47 and 0.85 in., respectively. The depth of heat penetration at the throat, as defined by the 100°F isotherm, is 1.2 in. Figure 35 also indicates that the throat variation increases very little during tailoff. The ablation throughout the nozzle follows these general characteristics.

The ablation depth of the carbon cloth decreases with increasing area ratio. At an area ratio of 1.41 upstream of the throat, ablation, char, and 100°F depths at burnout are 0.37, 0.78, and 1.15 in., respectively. At an area ratio of 3.37 in the exit cone, the ablation, char, and 100°F depths in MX-4926 are 0.095, 0.65, and 1.1 in., respectively.

Because of the lower ablation temperature and heat of ablation of the MX-2646 silica cloth, the ablation depth is greater than the ablation depth of the MX-4926 carbon cloth for similar exposures. The

IV, A, 260-SL Motor Nozzle (cont.)

ablation, char, and 100°F depth predicted for MX-2646 at an entrance cap area ratio of 1.6 are 1.15, 1.31 and 1.49 in., respectively. The exit cone ablation depth at an area ratio of 3.78 is 0.37 in. and decreases to 0.22 in. at an area ratio of 6.

Figures 20 through 32 present the predicted temperatures as a function of depth at 40, 80, 110, and 140 sec after ignition. These data indicate that only negligible heating of the silica cloth back-up material occurs.

Figure 36 shows temperature vs depth for silica cloth when exposed to the thermal environment at the throat of the 260-SL-1 nozzle at 40, 80, 110, and 140 sec duration. The total ablation for this material is 1.62 in., or approximately four times the ablation predicted for the MX-4926 material. The variations in throat diameter with time for MX-2646 and this environment are shown in Figure 37. The depth of heat penetration at burnout is approximately 1.9 in., or approximately 60% greater than the penetration for MX-4926. The advantages of MX-4926 as a throat material are: (1) the required thickness and increase in throat diameter are substantially more with MX-2646 silica cloth than with MX-4926 carbon cloth, and (2) the density of the MX-4926 is approximately 80% that of MX-2646.

Scaling techniques for determining recession rates of large motors from small motor data are based on heat transfer theory. Although the analytical surface recession rates have been correlated with actual motor firings, only in a relatively small number of motors have carbon cloth materials been used. However, the correlation with carbon cloth materials is expected to be valid. Data obtained from related programs conducted by Aeronautical Systems Division and Aerojet provided additional information for verifying the scaling technique.

## IV, A, 260-SL Motor Nozzle (cont.)

To predict the recession rate of a given material in two nozzles that have different ballistic parameters and/or different geometries, the procedures discussed below are used.

First, the following material properties must be known for a given material; density, specific heat, thermal conductivity, heat of ablation, and ablation temperature. Secondly, the heat-transfer rates are determined from the ballistic data, geometry, and propellant type. The effective heat of ablation is then assumed to be independent of heat flux. The recession rate will thus be only a function of heat input, while the char layer depends only on the appropriate specific heat and conductivity. Finally, all values are used as input to the general thermal analysis program (IBM 7090 computer) and the resulting recession rate and temperature profiles are numerically calculated. The char layer is found as a function of time by plotting the temperature gradient and noting the depth below the surface of the 500°F isotherm.

If the char depth or temperature profile is unimportant, the instantaneous recession rate of the same material in two different nozzles can be determined by a simplified equation as follows:

$$\dot{a}_1 = \dot{a}_2 \left( \frac{P_1}{P_2} \right)^{0.8} \left( \frac{D_2}{D_1} \right)^{0.2} \frac{\Delta T_1}{\Delta T_2} \quad (\text{Eq 5})$$

where:  $\dot{a}$  = recession rate, mil/sec  
 $P$  = chamber pressure, psia  
 $D$  = throat diameter, in.  
 $\Delta T$  = difference between adiabatic wall temperature and wall temperature, °R  
 Subscripts 1 and 2 are the two nozzle conditions.



IV, A, 260-SL Motor Nozzle (cont.)

This form is valid for approximating the instantaneous recession ablation rate when one reference firing condition is known. Extreme care is necessary when applying the above equation over a long time interval if either the pressure or the throat diameter change significantly.

The above equation was applied to the MERM test data to determine the recession rates for a 260-in.-dia motor with a 66.4 in.-dia throat. The results obtained from this simplified approximate scaling method are presented in Figure 38. The maximum instantaneous recession rates compare approximately with the recession rates determined previously by the IBM 7090 analytical program. For example, the maximum surface recession rate of 3.8 mil/sec for MX-4926 compares to the 4.0 mil/sec obtained by the detailed method. The average recession rates obtained with the approximate method are considered to be unusually low; the lowness of these average values is believed to be the result of the significant pressure and diameter changes of the MERM firings. Verification of the approximate scaling formula for less severe diameter and pressure changes has been successful.

The recession rates of MX-4926 carbon cloth and FM-5014G graphite cloth were obtained from several motor firings and projected to the 260-SL-1 motor nozzle conditions by use of the approximate scaling technique. The data was taken from MERM, Minuteman, Polaris, XM-86, Tapco and United Technology motor firings (Figure 14). Recession rates obtained at various exit cone area ratios were corrected to throat conditions before scaling to the 260-SL-1 motor. The results (summarized in Figure 39) indicate that the projected recession rates of carbon cloth and graphite cloth are similar. The validity of the MX-4926 data of Minuteman motors 52 TW-6 and 54 TW-7 are questionable because of the presence of liquid injection TVC ports and the questionable accuracy of the analytical technique for correcting data at high area ratios to an area ratio of 1.0.

IV, A, 260-SL Motor Nozzle (cont.)

To verify that the thermal analysis procedures would apply to the throat regions, the ablative nozzle of motor 54 SS-2 of the Large Solid Rocket Program was analyzed as follows:

First, the instantaneous throat area was calculated by applying the same equations used for the MERM data reduction. Pressure and corrected thrust were obtained from the 54 SS-2 motor test data report. The calculated prefiring throat diameter used was 6.4 in., and the final average diameter was calculated as 8.84 in. at 117 sec. This difference in throat diameter represents a 0.25% deviation from the measured 10.5 mil/sec average recession rate given in the test report.

Next, the IBM 7090 Computer Program was used with thermal property values applicable to carbon cloth with a 90-degree orientation. Exact thermal property values were not available for the materials actually used in the 54 SS-2 nozzle. Throat heat-transfer rates were computed for the measured pressure history and geometry. Various values of the effective heat of ablation were then considered and the total ablation calculated as discussed above. These results are indicated in Figure 40. As noted, the effective heat of ablation value for the nozzle material that gave the exact total ablation observed in the 54 SS-2 motor firing was 7920 Btu/lb. The ablation temperature was determined to be 4040°F.

With all material parameters held constant, stations in the entrance section and throat (Figure 41) were similarly analyzed. The heat-transfer rate by convection at a given area ratio then represented the only variable. The general agreement between the computed and measured recession is excellent with exception of the uneven nature of the actual throat erosion, which was probably caused by unsatisfactory fabrication control.

IV, A, 260-SL Motor Nozzle (cont.)

Similar calculations were performed for the exit cone insert and also are presented in Figure 41. Agreement between the calculated and measured recession is excellent at upstream stations; the erosion near the exit plane is higher than predicted. It is believed that exact agreement was not obtained because of the adverse influence that the jet tabs might have had on erosion in the exit plane.

This comparison of predicted and measured recession in the 54 SS-2 nozzle verified the analytical procedures and assumptions discussed above. In addition, the negligible influence of radiation and particle impacts on the total heat transfer in the entrance region was verified. Another factor apparent from this study is the need for accurate ablation data; significant deviations could be introduced in the erosion profile throughout any nozzle if the material properties used were erroneous.

Predictability and uniformity of surface recession are dependent on the knowledge of ablative plastic material properties and quality control of the material and fabrication techniques. Delamination, spalling, and/or chunking that have occurred with both graphite cloth and carbon cloth are attributed to moisture and volatile inclusion as a result of unsatisfactory fabrication techniques.

b. Stress Analysis

The magnitude of the thermal stress in the nozzle and exit cone inserts cannot be explicitly determined. The material strength and modulus of elasticity in the elevated temperature zone of the insert result in compression in the inner layers and tension in the outer layers of the insert. Unfortunately, mechanical and physical properties of the ablative plastics at elevated temperatures are limited and only estimated values can be used in the stress analysis.

IV, A, 260-SL Motor Nozzle (cont.)

The compressive stresses on the inner surface of the insert could exceed the allowable compressive strength of the material depending upon the assumed material strength and modulus of elasticity. The consequence of an excessive compressive stress will be an increase recession rate. A designed safety factor of 2 on recession rate was used to compensate for the uncertainties. The tensile stress on the outer surface also may vary depending on the assumed material properties and results in a change of the insert thickness requirement. The thermal stress analysis indicated that a minimum of 1.6 in. of ablative insert material is conservatively required at the end of firing for the throat section, which has the maximum thermal gradient (Figure 42).

Results of the throat-insert thermal stresses vs material allowables analysis (Figures 43 and 44) indicate that the compressive stresses are below the allowables. Also, the tensile stresses are well below the tensile stress allowable of 3800 psi.

In addition to thermal gradient stress calculations, the nozzle throat insert was analyzed for structural adequacy when subjected to ejection forces. A differential pressure load, for which the calculation was based on the design chamber pressure of 871 psi, was assumed to be acting to eject the throat insert. Although the bond strength between the insert and the nozzle stack was calculated to be sufficient to resist the ejection load, a mechanical stop is provided by the throat overwrap for added reliability. The stop is designed to be adequate in both bearing and interlaminar shear strength to resist the ejection load.

The throat extension insert thickness is the same as the aft end of the throat insert because of nozzle geometry. Since both thermal gradient and internal pressure decrease along the insert, the resultant stresses in the throat extension insert are less than at the aft end of the

IV, A, 260-SL Motor Nozzle (cont.)

throat insert. Sufficient material thickness remains at the 2:1 area ratio joint so that a mechanical retention of the throat extension insert can be provided. The mechanical retention prevents transfer of the ejection load to the exit-cone insert and prevents ejection of the extension insert in case of exit cone malfunction.

The entrance cap insert was analyzed for structural adequacy due to chamber pressure which is the primary stress factor in this region; the thermal stresses were shown to be adequate in the throat insert which is a more critical thermal stress region than the entrance insert. To be conservative, the chamber design pressure of 871 psi and the material thickness below 500°F were used in the analysis. It was also assumed that the V-44 rubber does not contribute any strength. The meridional and hoop stresses at various stations of the entrance cap insert (Figure 45) are shown in Figures 46 and 47. The minimum margin of safety was 0.37.

The exit cone insert thickness was selected to provide a high margin of safety with respect to tensile stresses on the outer surface because of the lack of elevated temperature material properties. Stresses due to hoop pressure and thermal loads are well within the allowables as shown in Figures 48 through 50. To resist delamination, a minimum thickness of 0.25 in. ambient-temperature ablative liner material (silica cloth) was provided. Twice the predicted recession rate was considered in providing the 0.25 in. material, which exists at area ratio 3.7, or the maximum surface recession location.

The silica cloth overwrap thickness is 0.5 in. This thickness provides adequate insulation for the structural shell in the event delamination occurs in the ablation surface liner. The overwrap material also provides strength to the insert during handling and assembly.

IV, A, 260-SL Motor Nozzle (cont.)

4. Orientation of Laminates

A study of the effect of laminate orientation on surface recession was conducted on previous nozzle firings conducted by Aerojet and others in the industry. The study concluded that minimum surface recession occurs when the laminations are oriented 45 to 67 degrees to the gas flow. Within the 45 to 67 degree range, minimum char depth occurs at approximately the 45-degree orientation. The silica cloth and carbon cloth entrance sections are oriented 72 to 87 degrees to the nozzle center line. This orientation approaches 45 degrees to the gas flow to provide minimum surface recession and allows mating with the throat-insert laminate orientation. The carbon-cloth throat insert has laminations 60 to 75 degrees to the nozzle center line, and the throat-extension insert has laminations 45 to 60 degrees to the nozzle center line to provide for the best combination of minimum surface recession, good fabrication, and minimum tape width. The mating joint between the carbon-cloth entrance section and throat insert will necessarily have short-length laminates because of a change in laminate orientation between these parts. However, by the use of these orientations, the area of the short-length laminates are reduced and the tendency for them to delaminate is minimized. The mating surface between the throat and throat extension inserts is oriented parallel to the laminations of throat insert so that the effects of the existence of short pieces of cloth which tend to delaminate and spall at the low area ratios is minimized.

Laminate orientation of the carbon-cloth and silica-cloth inserts of the exit cone was selected to be 3 to 18 degrees to the nozzle center line to facilitate fabrication and to provide locking of each laminate against delamination. It was anticipated that warp (straight) tape could be used to fabricate the inserts with this orientation because of the large diameters and shallow angle. Final selection of the tape (straight or bias cut) should be based on the fabrication capability to meet the orientation angle.

IV, A, 260-SL Motor Nozzle (cont.)

The silica cloths that overwrap the ablation surface liners are oriented parallel to the bonding surfaces to provide maximum protection against gas passage to the steel shell in case of liner delamination. With parallel orientation, the maximum width of tape cloth is used to guard against gas penetration and the tendency to delaminate within the overwrap is minimized. The thermal conductivity is lowest in a direction perpendicular to the laminates, thus providing the best insulating properties.

5. Effect of Aft-End Ignition

An analysis of the effect of instantaneous increase in pressure at the exit cone due to aft end ignition was conducted and found to have no consequential effect on ablation or thermal gradient through the insert. This analysis is presented in the phase report on the ignition system, Reference (5).

6. Structural Components

a. Nozzle Shell

Discussion of the 260-SL nozzle shell is presented in Reference (1). However, a brief discussion is presented herein to provide a general understanding of the design. The nozzle shell material is 18%-nickel maraging steel for compatibility with the chamber. The material has a 200,000 psi minimum yield strength at 0.2% offset. The quality of the material was controlled in accordance with Aerojet specifications AGC-34316 and AGC-34315 for forgings and plates, respectively, which were also applicable to the motor chamber.

IV, A, 260-SL Motor Nozzle (cont.)

A reduction in strength of 5% throughout the nozzle shell was assumed to allow for weld efficiency combined with weld mismatch, resulting in 190,000 psi as the allowable stress. The maximum weld mismatch as specified by the drawings was 10% of the minimum thickness (90% continuous membrane) for all welds.

The nozzle shell design pressure was 871 psia, which had a 1.3 safety factor on the 260-SL motor MEOP. The design pressure was the same as that for the chamber. The results of the structural analysis of the nozzle shell are summarized in Figure 51. The stations analyzed are defined in Figure 52. The complete stress analysis is presented in Reference (6).

The entrance configuration of the nozzle shell had a double conical angle. The steep initial angle was selected for compatibility with the chamber joint, and a shallower cone angle forward of the throat section was selected to minimize the entrance liner insert thickness and to permit inclusion of the mechanical stop for the throat insert.

The shell thickness was selected to minimize deflections of the nozzle inserts. The limiting deflection was selected to reduce the stress levels of the inserts to within allowable limits. As shown in Reference (6), the minimum margin of safety of the insert was 0.37 with the designed minimum shell thickness of 0.75 in.

The 7-degree taper angle was selected for support of the throat insert so that the insert is wedged in place against the ejection loads. The taper angle also served to center the insert and to obtain the proper bond line between the insert and the steel shell during assembly.



IV, A, 260-SL Motor Nozzle (cont.)

The forward attach joint was designed for compatibility with the chamber aft joint and had the structural capacity for a 4-degree jet deflection bending moment.

The aft attach joint was designed for structural adequacy under both hydrostatic test and static firing conditions. For the hydrostatic test condition, the joint enabled attachment of the test plug and mating piston. The hydrostatic proof pressure of 737 psig was used for joint design. For the static firing condition, the joint supported the exit cone assembly. The hydrostatic test requirements of this joint were more severe than the firing loads.

The nozzle shell was hydrostatically tested while assembled to the chamber in the vertical position. The nozzle shell was located at the top and a 102.3-in.-dia piston was located at the aft attach joint. The piston load was transmitted to the forward skirt of the chamber by means of external structures to simulate the skirt load during motor firing. The proof pressure of 737 psig was measured at the piston surface thus subjecting the complete motor case to a minimum pressure of 1.1 MEOP.

b. Exit Cone Shell

A honeycomb structural shell was selected for the exit cone section because of its light weight and good structural characteristics. A honeycomb structure has an inherent rigidity for bending moment, so that its capacity for TVC loads, particularly jet-tab or liquid-injection TVC systems, could be included with little additional weight.

Preliminary designs of nonhoneycomb exit cone structures were evaluated. Two versions of a semi-monocoque design using I-beam or hat section rings with longerons were found to be 15 to 50% heavier than a honeycomb structure.

IV, A, 260-SL Motor Nozzle (cont.)

The 17-7 PH stainless steel was selected for the honeycomb facings because of its mechanical and physical properties. Its thermal expansion coefficient is compatible with the end flange rings and plastic liner. This stainless steel has a high rigidity to weight ratio, can be welded readily, and has the desired strength and modulus of elasticity for a light weight structure. Aluminum was rejected as a facing material because of its high thermal expansion as compared to the plastic insert. The differential in thermal expansion could cause bond separation during the cooling period following cure at elevated temperature. The selected strength level for the 17-7 PH steel is a minimum of 150,000 psi at 0.2% offset yield with an ultimate tensile strength of 180,000 psi minimum.

Aluminum was selected as the honeycomb core material so that the exit cone is flutter proof against dynamic vibration and normal flexing. Aluminum and glass-phenolic honeycomb core were considered before selection. The aluminum honeycomb core was found to be commercially available, is easily fabricated, and exhibits better physical properties than glass-phenolic honeycomb. Aluminum core has a shear modulus 2 to 5 times higher than that of glass-phenolic core, thus providing a substantial saving in weight and cost. The aluminum honeycomb selected was No. 6.0 - 1/4 - 30P (3003) per MIL-C-7438C. A permeated cure type was initially chosen to vent volatiles that might occur during fabrication. Volatile content was found to be insignificant and non-permeated cores were finally selected because of better mechanical properties.

Although a 0.023-in. sheet that is continuous in the hoop direction would have been structurally adequate for each of the inner and outer facings, two sheets were actually used for the inner facing to simplify fabrication and to eliminate the necessity for close tolerance control. The two sheets of the inner facing were overlapped in the complete circumferential direction to eliminate machining of the honeycomb core. The outer facing was

IV, A, 260-SL Motor Nozzle (cont.)

a single sheet thickness with doublers at the splice joints of the sheet. The doubler width was selected to provide sufficient bond strength. Each thickness of sheet was welded to form a continuous sheet in the longitudinal direction.

The 0.023-in. thickness was selected for the facing sheets based on the structural requirements due to internal pressure. The internal pressure was calculated using supersonic flow theory and the chamber design pressure of 871 psia, which includes a 1.3 safety factor over the MEOP. The margins of safety for the inner and outer facings were 0.03 and 0.62 respectively Reference (6).

There was no structural requirement due to firing conditions for the 0.72-in. thickness and the density of the aluminum core selected; they were chosen to provide a good structural bond between the core, facings, and the end rings and to provide structural rigidity during handling and shipping of the exit cone assembly.

The honeycomb sandwich was analyzed for buckling stability, face dimpling, and shear in the aluminum core (Reference 6). Buckling in the honeycomb sandwich is due to the sum of the exit cone weight and the axial component of the internal pressure load. Shear in the aluminum core is due to the transfer of the axial load from the inner facing to the outer facing. The margins of safety for all three conditions were high.

The honeycomb facings were bonded to the forward and aft end attachment rings with sufficient length to provide adequate bond strength. A high margin of safety was used in all bond joints for added reliability because of the difficulty in nondestructive inspection of bonded joints. Self-tapping screws were provided as redundant fasteners for attaching the doubler and outer facing to the end rings to prevent peeling of the doubler bond.

IV, A, 260-SL Motor Nozzle (cont.)

The effects of discontinuities between the honeycomb sandwich and end rings were analyzed at a station adjacent to the forward ring. The assumed condition was conservative in that the ring was infinitely rigid with respect to the sandwich and the sandwich structure was considered a semi-infinite cylinder. The resultant margin of safety was 0.79. The cross sectional areas of the end rings were gradually reduced for transition into the honeycomb sandwich structure to reduce the effect of discontinuity.

The forward attachment ring was designed to transmit the total compressive load acting on the exit cone structural shell to the nozzle shell. The axial component of the compressive load is transferred by bearing between the flange faces and the radial component is transferred by the shear lip in the ring. The magnitude of these loads was small.

An aft attachment ring was provided for withstanding loads during ignition deployment, handling the exit cone assembly during fabrication and assembly, and for supporting the assembly during shipment. Stress analysis indicated that the structure was adequate for ignition loads and for a maximum of 7g acceleration during handling.

Both the forward and aft attachment rings were fabricated of normalized AISI 4130 steel. This low-cost material is readily available and is compatible in thermal expansion with the honeycomb facings and plastic insert. The strength of this material is sufficient to meet the structural requirements.

The exit plane ring was provided to retain and to minimize movement between the liner and structural shell in the event of bond failure. The ring was aluminum to reduce weight and was segmented to simplify fabrication and assembly.

IV, A, 260-SL Motor Nozzle (cont.)

7. Sealants and Adhesives

The gaps at the forward and aft joints of the throat insert were provided to permit thermal growth and to alleviate mating problems of the inserts. A silicone-rubber sealant (Aerojet specification AGC-34076, Class 5) was selected as the gap filler. The selection of this sealant was based on its successful use in the 100-in.-dia motor and GAM-86 motor programs. The sealant extrudes easily when squeezed while maintaining a flame and gas seal. The surface of the rubber compound will char when exposed to flame; however, based on previous test data, the ablation depth was expected to be only 0.125 to 0.5 in. below the adjacent ablation surfaces.

A minimum number of O-rings were provided at ablative insert joint interfaces to prevent direct gas paths from propagating behind the inserts. Buna-N rubber (per MIL-R-6855 at 60 Shore A hardness) was selected as the O-ring material because this material has good abrasion tear, resistance to flexing, excellent compression set, and good resistance to cutting. The properties of Buna-N rubber are superior to those of silicone rubber except for the 200°F higher temperature resistance capability of the latter. However, the lower temperature resistance is not detrimental in this application.

Epon 948 was selected as the bonding agent between the entrance-cap rubber insulation and ablative insert because of its long-duration aging characteristics. As aging time increases, the physical properties of Epon 948 improve, whereas the physical properties deteriorate in other materials such as Epon 913.

An adhesive with the desirable properties of low-cure temperature, high shear strength, and high elongation was selected for bonding the ablative inserts to the steel nozzle shell. The capability of low-temperature

IV, A, 260-SL Motor Nozzle (cont.)

cure was desired to prevent bond failure on cooling because of the thermal coefficient variations between steel and plastic components. The candidate adhesives included FM-86, Epon 948, and Epon 913. Before final selection of the adhesives, a program was conducted to evaluate the important properties of pot life, viscosity, and tensile shear strength that apply to large nozzle fabrication. Epon 913 was tentatively chosen because of previous successful use in similar applications of bonding inserts to steel sheels. Epon 913 has the following characteristics: a pot life of over 8 hr at 75°F, cure temperature of 180°F, minimum tensile shear of 3000 psi at room temperature, good adhesion to steel and plastic, 10% elongation, and a metal-to-metal peel strength of 18 lb/in.

Test results on the FM-86 adhesive film by Bloomingtondale Rubber Company indicated that the adhesive bond strength was essentially the same with or without the BR-86 primer. However, the primer was used along with the adhesive because it seals and protects the surface against moisture and corrosion and simplifies cleaning.

The FM-86 supported adhesive film was selected for bonding the inner and outer facings of the honeycomb sandwich to the aluminum core. This adhesive, which has been used in numerous similar applications and is currently used in the 624A Program nozzles has the desirable properties of low-temperature curing (180°F for 2 hr) and high shear strength (3600 psi tensile shear).

An epoxy-amide, micro-balloon-filled potting compound (Coril 615, a product of American Cyanamid Company) was used in potting the gaps between segments of the aluminum honeycomb core and between the core and forward and aft flanges. This material was selected because of its ease-of-handling, pot-life, low-density, strength, and caulking and edge-filling characteristics. The compressive yield strength of the material is 1700 psi minimum and the double shear strength is 3500 psi minimum.

IV, A, 260-SL Motor Nozzle (cont.)

An alternate fabrication method for the exit cone structural shell was evaluated. With this method, the structural shell is built from individually fabricated longitudinal segments. Each segment is a completely fabricated honeycomb sandwich with the inner and outer facings bonded to the honeycomb core and is preformed to fit the contour of the insert. This method had the advantage of both in-process and final inspections of each segment before acceptance for use. The segments are assembled and bonded to the insert and end attachment rings, thus completing the assembly. The disadvantages of this method is properly fitting and mating the plastic liner and adjacent segments.

IV, A, 260-SL Motor Nozzle (cont.)

Gen-Gard V-61 trowelable insulation was applied around the exit cone aft ring to provide thermal protection against exhaust gas radiation. This rubber insulation has been used successfully at Aerojet in several nozzle programs and has also been used to bond the internal insulation of solid rocket motors.

8. Fabrication

Wherever possible, available capabilities and current technology were used in establishing the fabrication techniques and processes for nozzle components. Using data obtained from such support efforts as tooling, quality control, and evaluation studies for the ablative plastic nozzle, well-defined, fully qualified and carefully controlled fabrication and processing techniques were specified on the fabrication control drawings and quality control specifications to ensure the quality and reliability of components.

The nozzle subcontractor conducted detailed studies on materials, fabrication techniques, processing techniques, and processing controls during the material and process evaluation studies program to ensure that the methods used during fabrication of the nozzle and exit cone would produce optimum parts at minimum cost. The material and process tasks that were performed and evaluated included; the debulking characteristics of selected tape wrapping materials, evaluation of joint designs and fabrication methods applicable to nozzle inserts and the exit-cone honeycomb structure, and determination of ablative-material cure cycles and bond integrity.

Fabrication in-process quality control and inspection records were to be completely documented and included in the Motor Log Book.

The selected fabrication procedure is as follows:



IV, A, 260-SL Motor Nozzle (cont.)

The entrance cap, nozzle throat, and throat-extension inserts are fabricated by wrapping and roller debulking the carbon cloth phenolic and silica cloth phenolic on a conical mandrel. The angle of the laminae measured from the nozzle center line is 72 to 87 degrees, 60 to 75 degrees, and 45 to 60 degrees for the entrance cap, nozzle throat, and throat-extension inserts, respectively. After the required insert thickness has been achieved the outside diameter is machined in the debulk ("B" staged) condition. Silica cloth is then wrapped on the machined surface with the laminae parallel to the wrapping surface. The inserts are molded at 1000-psi pressure and 300°F in a hydroclave. The cured parts then are machined and bonded to the nozzle shell. The internal contour of the nozzle is machined after the inserts have been bonded to the shell.

The exit cone insert is fabricated by wrapping both carbon-cloth and silica-cloth tape on a mandrel at a 3 to 18 degree angle measured from the nozzle center line, and machined to the proper thickness. Subsequently, silica cloth is overwrapped with the laminae parallel to the surface, and molded at vacuum-bag pressure.

The exit cone structural shell of honeycomb-sandwich construction can be readily fabricated by two methods. The method that was selected entailed building the honeycomb sandwich onto the machined ablative plastic insert in successive steps. The two layers of the inner facing are preformed and machined to fit the insert. These layers are then positioned to allow for maximum overlap, and bonded to the insert. The fore- and aft-end rings and aluminum core are fitted and bonded to the inner facing and to each other. The bonding of the outer facing and doubler completes the assembly. Both the inner and outer facings consist of continuous sheets (welded if necessary) for the entire axial length of the exit cone and structurally connect the fore and aft end rings. At each stage of the bonding process, nondestructive inspection ensures that the bond strength and bond surface are adequate.

IV, A, 260-SL Motor Nozzle (cont.)

An alternate fabrication method for the exit cone structural shell was evaluated. With this method, the structural shell is built from individually fabricated longitudinal segments. Each segment is a completely fabricated honeycomb sandwich with the inner and outer facings bonded to the honeycomb core and is preformed to fit the contour of the insert. This method had the advantage of both in-process and final inspections of each segment before acceptance for use. The segments are assembled and bonded to the insert and end attachment rings, thus completing the assembly. The disadvantages of this method is properly fitting and mating the plastic liner and adjacent segments.

B. 120-SS-1 MOTOR NOZZLE

1. Nozzle Geometry

The initial 30.3-in.-dia throat was a motor performance requirement established from interior ballistic design and performance parameters.

The 120-SS-1 motor nozzle was similar to the 260-SL motor nozzle. The following 120-SS-1 nozzle characteristics were selected from the 260-SL motor nozzle: (1) exit cone half-angle of 17.5 degrees, (2) sea level optimum expansion ratio of 6.0:1, and (3) the entrance radius of curvature equal to the throat radius.

Additionally, the selection of an entrance curvature geometrically similar to the 260-SL motor nozzle was based on studies of inlet contour conducted for the Minuteman Wing VI Program. These studies correlated the firing performance of geometrically-similar subscale nozzles with actual full-scale motor firings. The results of aerodynamic experiments conducted of nozzle entrance geometry indicated excellent correlation between cold-flow

IV, B, 120-SS-1 Motor Nozzle (cont.)

model data and the observed erosion characteristics in geometrically-similar nozzles. In particular, the correlation studies demonstrated the direct relationship between relative heat transfer rates obtained by quantitative aerodynamic measurements in nozzle entrances and the erosion distribution in corresponding regions.

2. Material Selection

The liner insert materials which were selected for the 120-in.-dia motor nozzle were identical to those selected for the 260-SL motor nozzle as discussed in Section III,A. Carbon cloth (MX-4926) was selected for the high ablation areas of the nozzle extending from 1.6 area ratio in the subsonic region to 3.5 area ratio in the supersonic region. MX-2646 and FM-5131 silica cloths were selected for use at entrance area ratios greater than 1.6 and in the exit cone region between area ratios of 3.5 and 6.0, respectively.

The ablative liners were overwrapped parallel to the mating surfaces with two silica cloth tapes (MX-2646 in the entrance insert and FM-5131 elsewhere) similar to the 260-SL motor nozzle.

The location of transition between carbon cloth and silica cloth was selected so that only a minimum of carbon cloth is used yet the ambient temperature material thickness (below the heat-affected zone) is sufficient for structural requirements. Transition in the nozzle entrance occurs at an area ratio of 1.6 where the carbon cloth recession depth is 0.20-in. and the 100°F depth is 0.84 in. The remaining material thickness of 1.75 in. is at ambient temperature. At the exit cone area ratio of 3.6 the silica cloth recession depth is 0.30 in., and 1.37 in. of ambient temperature material thickness remains. The material thickness at ambient temperature is calculated considering twice the recession rate.

## IV, B, 120-SS-1 Motor Nozzle (cont.)

3. Determination of Nozzle Material Thicknesses

The nozzle insert material thickness requirements were based on the amount of surface recession (using a margin of safety of 2.0 for design), char depth, heat-affected zone (100 to 500°F), and ambient temperature material below 100°F required for structural integrity and to meet fabrication requirements. Minimum margins of safety for the nozzle components are shown in Figure 19. Heat-transfer analysis was conducted to determine the temperature gradients at various stations along the nozzle. The analytical method used for the nozzle thermal stress analysis was identical to that used for the 260-SL motor nozzle. The calculated heat-transfer coefficients at the throat are shown in Figure 53.

Results of the 120-SS-1 nozzle heat-transfer analysis at various area ratios are presented in Figures 54 through 62. The thermal properties of the material are listed in Figure 33. The butadiene rubber in the entrance-cap region was not included in the analysis so that a conservative analysis of this critical region would result. The burnout dimensions at various area ratios are summarized in Figure 63. The variations in throat diameter with time are shown in Figure 64. The calculated burnout recession and char depth at the throat of 120-SS-1 are 0.36 and 0.60 in., respectively. The depth of heat penetration at the throat, as defined by the 100°F depth, was 0.87 in. Figure 64 indicates that the throat variations are approximately linear during web action time and increase very little during tailoff. The ablation throughout the nozzle follows these general characteristics.

The ablation depth of the carbon cloth decreases as the area ratio increases. At an area ratio of 1.2 upstream of the throat, the ablation, char, and 100°F depths at burnout were 0.32, 0.58, and 0.86 in., respectively. At an area ratio of 3.4 in the exit cone, the ablation, char, and 100°F depths in the MX-4926 were 0.07, 0.47, and 0.63 in., respectively.

IV, B, 120-SS-1 Motor Nozzle (cont.)

Because of the lower ablation temperature and heat of ablation of the MX-2646 silica cloth, the ablation depth is greater than the ablation depth of the MX-4926 carbon cloth for similar exposures. The ablation, char, and 100°F depth predicted for MX-2646 at an entrance cap area ratio of 2.26 were 0.64, 0.75, and 0.85 in., respectively. The exit cone ablation depth at an area ratio of 3.6 was 0.30 in., and decreased to 0.17 in. at an area ratio of 6.

Figures 54 through 62 present the predicted temperatures as a function of depth at 20, 40, 60, and 80 sec from ignition. As indicated in these figures, negligible heating of the silica cloth back-up material occurred.

The thermal stress and structural stress analyses of the liner components were similar to those used for 260-SL nozzle components. A designed safety factor of two on recession rate was used to compensate for the uncertainties in material properties. The structural analysis indicated that a minimum of 1.5 in. of ablative insert material is a conservative requirement for the throat section which has the maximum thermal gradient at the end of firing (Figure 65).

Results of the throat-insert thermal stresses vs material allowables are presented in Figures 66 and 67; these data indicate that the compressive stresses are below the allowables shown. Also, the tensile stresses are well below the tensile stress allowable of 3800 psi.

In addition to thermal gradient stress calculations, the nozzle throat insert was analyzed for structural adequacy due to ejection forces. A differential pressure load, which was calculated based on the design chamber pressure of 965 psi, was assumed to be acting to eject the throat

IV, B, 120-SS-1 Motor Nozzle (cont.)

insert. Although the bond strength between the insert and the nozzle stack was calculated to be sufficient to resist the ejection load, a mechanical stop was provided by the throat overwrap for added reliability. The stop was designed to be adequate in both bearing and interlaminar shear to resist the ejection load.

The throat-extension insert thickness was the same as the aft end of the throat insert because of nozzle geometry. Since both thermal gradient and internal pressure decrease along the insert, the resultant stresses in the throat extension insert were less than at the aft end of the throat insert. Sufficient material thickness remains at the 2:1 area ratio joint so that a mechanical retention of the throat extension insert can be provided. The mechanical retention prevents transfer of the ejection load to the exit cone insert and prevents ejection of the extension insert in case of exit cone malfunction.

The entrance-cap insert was analyzed for structural adequacy when subjected to chamber pressure which is the primary stress factor in this region; the thermal stresses were within allowable limits in the throat insert which is a more critical thermal stress region than the entrance insert. To be more conservative, the chamber design pressure of 965 psi and the material thickness below 500°F were used in the analysis. It was also assumed that the V-44 rubber does not contribute any strength. The meridional and hoop stresses at three stations of the entrance cap insert are shown in Figure 68. The stresses were based on the deflection of the nozzle shell.

The exit cone insert thickness was selected to provide a high margin of safety with respect to tensile stresses on the outer surface because of a lack of precise knowledge of material properties at elevated temperature. Stresses due to hoop pressure and thermal loads are well within the allowables as shown in Figures 69 through 71. To resist delamination, a minimum thickness of 0.50 in. ambient temperature ablative liner material was provided. Twice

IV, B, 120-SS-1 Motor Nozzle (cont.)

the predicted recession rate was considered in providing the 0.50 in. material, located at an area ratio of 3.6.

The silica-cloth overwrap thickness is 0.50 in. This thickness provides adequate insulation for the structural shell in the event delamination occurs in the ablation surface liner. The overwrap material also provides strength to the insert during handling and assembly.

4. Orientation of Laminates

The plastic inserts of the 120-in.-dia motor nozzle have the same angles of laminate orientation as proposed for the 260-in.-dia motor nozzle. The silica-cloth and carbon-cloth entrance sections are oriented 72 to 87 degrees to the nozzle center line. The carbon-cloth throat insert has 60 to 75 degrees to the nozzle center line and the throat-extension insert has lamination 45 to 60 degrees to the nozzle center line. The mating surface between the throat and throat-extension inserts is oriented parallel to the laminations of the throat insert so that the tendency of short-length cloth to delaminate and spall at the low area ratios is minimized.

The laminate orientation of the carbon-cloth and silica-cloth inserts of the exit cone is 3 to 18 degrees to the nozzle center line to facilitate fabrication and to provide mechanical locking of each laminate against delamination. It was anticipated that warp (straight) tape could be used to fabricate the inserts with this orientation because of the large diameters and shallow angle. Final selection of the tape (straight or bias cut) would be based on the fabrication capability to meet the orientation angle.

The silica cloth material that overwraps the ablation surface liners is oriented parallel to the bonding surfaces similar to the 260-SL nozzle.

IV, B, 120-SS-1 Motor Nozzle (cont.)

5. Structural Components

a. Nozzle Shell

A discussion of the 120-SS-1 nozzle shell is presented with the 260-SL nozzle shell discussion in Reference (1). However, a brief discussion is presented herein to provide a general understanding of the design. The nozzle shell material is 18% nickel maraging steel with 200,000 psi minimum and 235,000 psi maximum yield strength at 0.2% offset. The quality of the material was controlled in accordance with Aerojet specifications AGE-34316 and AGC-34315 for forgings and plates, respectively. These specifications were also used for the 260-in.-dia motor chamber and nozzle shell.

A reduction in strength of 5% throughout the nozzle shell was assumed to allow for weld efficiency combined with weld mismatch, resulting in 190,000 psi as the allowable stress. The maximum weld mismatch as specified by the drawings was 10% of the minimum thickness (90% continuous membrane) for all welds.

The nozzle shell design pressure was 965 psia, which had a 1.3 safety factor on the 120-SS-1 motor MEOP pressure. Results of the structural analysis of the nozzle shell are summarized in Figure 72. The complete stress analysis is presented in Reference (7).

The entrance configuration of the nozzle shell had a conical angle. This angle was for compatibility with the chamber joint and to permit inclusion of the mechanical stop for the throat insert.

The shell thickness was selected to minimize deflections of the nozzle inserts. The limiting deflection was selected to reduce the stress levels of the inserts to within allowable limits.



IV, B, 120-SS-1 Motor Nozzle (cont.)

The 7-degree taper angle was selected for support of the throat insert so that the insert is wedged in place against the ejection loads. The taper angle also served to center the insert and to obtain the proper bond line between the insert and the steel shell during assembly.

The forward attach joint was designed for compatibility with the chamber aft joint. The aft attach joint was designed for structural adequacy under static firing conditions.

The nozzle shell was not hydrostatically tested. The shell was designed to a high margin of safety and considered to be structurally adequate without hydrostatic test verification. The established processing schedule also demonstrated that mating of chamber and nozzle shell for hydro-test would have been impractical.

b. Exit Cone Shell

The selection of the exit cone structural shell for the 120-in.-motor was based on the 260-SL motor nozzle design. Therefore, 17-7 PH stainless steel was selected for the honeycomb facings. The selected strength level for the 17-7 PH steel is a minimum of 150,000 psi at 0.2% off-set yield with an ultimate tensile strength of 180,000 psi minimum. Likewise, aluminum was selected as the honeycomb core material. The aluminum honeycomb selected was No. 6.0-1/4-30P(3003) per MIL-G-7438C. The core is a non-permeated type.

Although a 0.018-in. sheet that is continuous in the hoop direction would have been structurally adequate for each of the inner and outer facings, two sheets were actually used for the inner facing to simplify fabrication and to eliminate the necessity for close tolerance control. The two sheets of the inner facing were overlapped in the complete circumferential

IV, B, 120-SS-1 Motor Nozzle (cont.)

direction to eliminate machining of the honeycomb core. The outer facing was a single sheet thickness with doublers at the splice joints of the sheet. The doubler width was selected to provide sufficient bond strength.

The 0.018-in. thickness was selected for the facing sheets based on the structural requirements due to internal pressure. The internal pressure was calculated using supersonic flow theory and the chamber design pressure of 965 psia which includes a 1.3 safety factor over the MEOP pressure. The margin of safety for the inner facing was 0.66 as shown in Reference (7).

There was no structural requirement for the 0.50-in. thickness and the density of the aluminum core; they were selected to provide a good structural bond between the core, facings, and the end rings and to provide structural rigidity during the handling and shipping of the exit cone assembly.

FM-86 supported adhesive film, which was also used for the 260-SL exit cone, was selected for bonding the inner and outer facings of the honeycomb sandwich to the aluminum core.

The honeycomb sandwich was analyzed for buckling stability, face dimpling, and shear in the aluminum core. Buckling in the honeycomb sandwich is due to the sum of the exit cone weight and the axial component of the internal pressure load. Shear in the aluminum core is due to the transfer of the axial load from the inner facing to the outer facing. The margins of safety for all three conditions were high.

The honeycomb facings were bonded to the forward and aft end attachment rings with sufficient length to provide adequate bond strength. A high margin of safety was used in all bond joints for added

IV, B, 120-SS-1 Motor Nozzle (cont.)

reliability because of the difficulty in nondestructive inspection of bonded joints. Self-tapping screws were provided as redundant fasteners for attaching the doubler and outer facing to the end rings to prevent possible peeling of the doubler bond.

The effects of discontinuities between the honeycomb sandwich and end rings were analyzed at a station adjacent to the forward ring. The assumed condition was conservative in that the ring is infinitely rigid with respect to the sandwich and the sandwich structure was considered a semi-infinite cylinder. The resultant margin of safety was high as shown in Reference (7). To reduce the effects of discontinuity, the cross-sectional areas of the end rings were gradually reduced for transition into the honeycomb sandwich structure.

The forward attachment ring was designed to transmit the total compressive load acting on the exit cone structural shell to the nozzle shell. The axial component of the compressive load is transferred by bearing between the flange faces and the radial component is transferred by the shear lip in the ring. The magnitude of these loads was small. An aft attachment ring was provided for handling the exit cone assembly during fabrication and assembly and for supporting the assembly during shipment. Analysis indicated that the aft attachment ring was capable of withstanding 3g axial and lateral acceleration during handling and shipping.

Both the forward and aft attachment rings were fabricated of normalized AISI 4130 steel, similar to those used in the 260-SL exit cone. The strength of this material is sufficient to meet the structural requirements.

The exit plane ring is provided to retain and to minimize movement between the liner and structural shell in the event of bond failure. Normalized AISI 4130 steel was used for this ring; the ring was segmented for ease of fabrication and assembly.

IV, B, 120-SS-1 Motor Nozzle (cont.)

6. Sealants and Adhesives

The sealants and adhesives selected for the 120-SS-1 nozzle were identical to those selected for the 260-SL nozzle to enable prior evaluation of these materials in the subscale nozzle.

Similarly, Gen-Gard V-61 trowelable insulation was applied around the exit cone aft ring to provide thermal protection against hot exhaust gas radiation.

7. Fabrication

Fabrication techniques used for the 120-SS-1 nozzle were selected to duplicate all materials, processes, quality control and inspections selected for the 260-SL nozzle as discussed in Section IV,A,8.

C. 44-SS MOTOR NOZZLE

1. Nozzle Geometry

The 44-SS motor nozzle was a reliable and relatively inexpensive nozzle used to evaluate motor performance and internal motor materials selected for the 260-in.-dia motor. Interior ballistic design and performance requirements resulted in the selection of the 13.1 in. throat diameter. The nozzle design specified a fixed-type nozzle and a 17.5-degree exit cone half-angle, the same as for the 260-SL nozzle. The 17.5 degree exit cone half angle was determined in previous programs to be an optimum compromise based on weight, cost, and fabricability.

IV, C, 44-SS Motor Nozzle (cont.)

The nozzle entrance radius of curvature was equal to the throat radius. This contour geometrically simulated the 260-in.-dia motor nozzle entrance curvature. Selection of an entrance curvature geometrically similar to the 260-in.-dia motor nozzle was based on studies of inlet contour conducted for the Minuteman Wing VI Program which correlated the performance of geometrically similar subscale nozzle firings with actual full-scale motor firings. The results of aerodynamic experiments of nozzle entrance geometry indicated excellent correlation between cold flow model data and the observed erosion characteristics in geometrically similar rocket motor nozzles. In particular, the correlation studies demonstrated the direct relationship between relative heat transfer rates obtained by quantitative aerodynamic measurements in nozzle entrances and the erosion distribution in corresponding regions.

Selection of the exit cone expansion ratio of 2.5:1 was based on the minimum exit cone length necessary for providing: (1) sufficient structural support for the throat insert, (2) sufficient nozzle expansion to satisfy interior ballistic requirements, and (3) the exit plane at a low erosion area to maintain a relatively constant exit area. The minimized exit cone length represented a saving in both material cost and fabrication time without jeopardizing the program objective.

2. Material Selection

A monolithic RVA or ATJ graphite throat was initially considered for the 44-in.-dia motor nozzle design. Results of the thermal stress analysis of a monolithic graphite throat showed negative margins of safety and indicated that the insert could not withstand the compressive and tensile thermal stresses that are induced during motor firing. Typical thermal stress results are shown in Figures 73 and 74 for ATJ, graphite. During other Aerojet programs,

## IV, C, 44-SS Motor Nozzle (cont.)

nozzles with similar negative margins of safety were fired with only marginal success. Evidence of cracking in the insert was often found in post fire inspection. The high level of confidence necessary to ensure success of program objectives could not be demonstrated with the use of monolithic graphite in the nozzle throat. The stress analysis further indicated that by segmenting the graphite radially into a minimum of six sections, the thermal stresses in the throat insert could be maintained within the material allowable strengths. Segmentation of the throat insert radially cannot be designed and used confidently without further development because of the uncertainty of gas erosion on continuous axial joints. The use of the segmentation method would have complicated fabrication and assembly and would have increased costs. Although traverse (doughnut) segmenting appeared more practical for fabrication and assembly and resistance to gas flow, the thermal stresses are not sufficiently reduced to be within allowable limits. Although the basic material cost of graphite is low, it was rejected for use on the basis of questionable reliability.

Selection of ablative plastic as the throat-insert material was based primarily on design reliability. Ablative plastic nozzles have been successfully used on numerous motor firings by Aerojet and others. The technology of ablative plastic parts is advancing rapidly. Experience has indicated that reliable and uniformly eroding parts can be obtained. The throat area change is negligible, using carbon cloth rather than solid graphite, and results in a chamber pressure reduction of less than 1% (1 to 3 psi).

Either a tape-wrapped or stacked-laminated method is satisfactory for fabricating nozzle inserts. Ablative plastic inserts can be pressure molded from chopped fabric, tape-wrapped laminates, or die-cut and stacked laminates. Although the material cost of chopped fabric is lower than

IV, C, 44-SS Motor Nozzle (cont.)

cloth fabric, the requirement of expensive dies and high pressures for molding chopped fabric greatly offsets the cost advantage. Tape-wrapped and stacked-laminated plastic nozzle parts have also demonstrated greater reliability and uniformity in erosion than chopped fabric plastic parts.

The liner insert materials which were selected for the 44-SS motor nozzles are identical to those selected for the 260-SL nozzle so that additional information with respect to fabrication and processing could be obtained prior to the initiation of 120-SS-1 and 260-SL nozzle fabrication. Phenolic-resin-impregnated carbon cloth (MX 4926 or FM 5072) was selected for the nozzle in the high ablation areas which include the throat insert and the short exit cone. Phenolic-resin-impregnated silica cloth (MX 2646, MX2600, or FM 5131) was selected for use at the nozzle entrance area ratios greater than 1.6 where conditions conducive to low surface recession are present. Silica cloth was used in the nozzle entrance insert because of its low cost and extensive use in similar applications. The exact type of carbon cloth and silica cloth was to have been selected after evaluation of candidate materials conducted by the nozzle subcontractor. The selection was to have been made without delay to the program schedule. The physical and mechanical properties of the candidate materials are presented in Figure 18. The program schedule did not permit complete evaluation of the candidate materials; therefore, the selection was based on the extensive use of materials for similar applications. The materials selected were MX 4926 for the throat and exit cone liner, MX 2646 for the entrance liner and overwrap, and FM 5131 for the throat and exit cone overwrap.

An effort was made to use FM 5072 as the exit cone liner material for the 44-SS-2 nozzle; however, the component delaminated severely following hydroclaving and no further attempt was made to use the material. The cause of the delaminations were not established. The component was

IV, C, 44-SS Motor Nozzle (cont.)

fabricated accordingly to procedures established for MX 4926, and it was apparent that those procedures were not applicable to FM 5072. The schedule did not permit the establishment of fabrication procedures specifically for FM 5072.

The location of transition between carbon cloth and silica cloth at the nozzle entrance was selected so that a minimum of carbon cloth would be used and yet ensure that the ambient-temperature material thickness (below the heat-affected zone) would be sufficient to meet structural requirements. Transition in the nozzle entrance occurs at an area ratio of 1.60, which is the same as for the 260-SL nozzle design. At that area ratio, the silica-cloth recession depth is 0.22 in., char depth is 0.33 in., and the 100°F depth is 0.43 in. Using a safety factor of two on the recession depth, an ambient-temperature material thickness of 1.48 in. remains.

Silica cloth was not selected for the short exit cone because of its high recession rates at low area ratios near the throat section. To meet objectives, it was desirable to maintain constant throat and exit areas for motor performance evaluation. A study was conducted by the TRW Electro-mechanical Division on the location of the transition between graphite cloth and silica cloth in an exit cone. This study indicated that the transition should occur at area ratios greater than 2.5.

The liner inserts were overwrapped parallel to the mating surfaces with silica cloth identical to that selected for the 260-SL nozzle; this provided a thermal barrier in event of delamination in the inserts and provided more rigidity during handling.



IV, C, 44-SS Motor Nozzle (cont.)

3. Determination of Material Thicknesses

The nozzle-insert material thickness requirements were based on the amount of surface recession (using a margin of safety of 2.0 for design), char depth, heat-affected zone (100 to 500°F) and ambient temperature material below 100°F required to maintain structural integrity and to meet fabrication requirements. A heat-transfer analysis was conducted to determine these gradients at various stations along the nozzle and at various times from motor ignition. The theory and method of the analysis was identical to that used for the 260-SL nozzle, as previously discussed.

Results of the 44-SS nozzle heat-transfer analysis at various area ratios are presented in Figures 75 through 81. The thermal properties of the materials used in the analysis are listed in Figure 33. The butadiene rubber in the nozzle entrance-cap region was not included in the analysis, so that a conservative analysis of this critical region could be obtained. The burnout dimension at various area ratios are summarized in Figure 82. The variation of throat diameter is approximately linear during web time as shown in Figure 83 and increases very little during tailoff. The ablation in other area ratios of the nozzle follows these general characteristics. The calculated burnout recession and char depth at the throat are 0.094 and 0.29 in., respectively. The depth of heat penetration at the throat, as defined by the 100°F depth, is 0.47 in.

The ablation depth of carbon cloth decreases with increasing area ratio. The ablation, char, and 100°F depths at burnout at an entrance area ratio of 1.50 are 0.067, 0.28, and 0.47 in., respectively. At an exit cone area ratio of 1.50, the ablation, char, and 100°F depths in the MX-4926 are 0.052, 0.28, and 0.47 in., respectively. The ablation depth at the exit plane is 0.025 in.

IV, C, 44-SS Motor Nozzle (cont.)

The ablative depth predicted for silica cloth entrance insert decreases from 0.22 in. at an area ratio of 1.65 to 0.096 in. at a 4.0 area ratio. Maximum heat penetration (100°F) is 0.43 in.

Figures 75 through 81 present the predicted temperatures as a function of depth at 10, 20, and 25 sec from ignition. These data indicate that the 0.300-in.-thick silica-cloth back-up material remains at ambient temperature.

Only the material at temperatures below 100°F was considered for structural requirements to assure full integrity of liner inserts. Although small insert thicknesses are sufficient to withstand internal pressure loads, the ambient-temperature material thickness required is primarily because of the thermal stresses induced by temperature differential in the char and heat affected zone. The magnitude of the thermal stress in the nozzle insert cannot be explicitly determined. The material strength and modulus of elasticity in the elevated temperature zone of the insert result in compression in the inner layers and tension in the outer layers of the insert. Unfortunately, mechanical and physical properties of the ablative plastics at elevated temperatures are limited and only estimated values can be used in the stress analysis.

The compressive stresses on the inner surface of the insert could exceed the allowable compressive strength of the material depending on the assumed material strength and modulus of elasticity. The consequence of an excessive compressive stress would be an increase in recession rate. A designed safety factor of 2.0 on recession rate was used to compensate for the uncertainties. The tensile stress on the outer surface also could vary depending upon the assumed material properties and results in a change of the insert thickness requirement. The thermal stress analysis indicated that a minimum of 1.6 in. of ambient temperature material is necessary (Figure 84) at the end of

IV, C, 44-SS Motor Nozzle (cont.)

firing for the throat section which has the maximum thermal gradient. Additional material thickness was necessary to satisfy fabrication processing requirements and because of the inherent nozzle contour design.

Results of the throat-insert thermal stresses vs material allowables (Figures 85 and 86), indicate that the compressive stresses are below the tensile allowables. Also the tensile stresses are well below the tensile allowable stress of 3800 psi.

Stresses in the exit cone liner due to hoop and thermal loads are presented in Figures 87 and 88, which indicate that the imposed compressive and tensile stresses do not exceed the material allowables.

In addition to thermal gradient stress calculation, the nozzle throat insert was analyzed for structural adequacy when subjected to ejection forces. A differential pressure load, in which the calculation was based on the design chamber pressure of 819 psi, was assumed to be acting to eject the throat insert. The bond strength between the insert and the nozzle stack was calculated to be sufficient to resist the ejection load. However, the ambient-material thickness was considered adequate only if a good bond existed between the throat insert and nozzle shell. Stress analysis data indicate that if the throat insert bond fails, high compressive hoop stresses will occur on the outer surface as the throat insert wedges against the shell stack. The compressive stresses could collapse and eject the insert. For this reason, a mechanical stop was provided by the throat overwrap to prevent wedging in the event of bond failure. The stop was designed to be adequate in both bearing and interlaminar shear to resist the ejection load.

Structural analyses were similarly conducted for the entrance and exit cone inserts. The analyses determined meridional and hoop stresses in the inserts, and bond shear stresses between the ablative insert and the steel shell. In all instances, the margins of safety were high.

IV, C, 44-SS Motor Nozzle) (cont.)

The silica-cloth overwrap thickness was 0.30 in. This thickness provided adequate insulation for the structural shell in the event delamination occurs in the ablation surface liner. The overwrap material also provided strength to the insert during handling and assembly.

4. Orientation of Laminates

The laminate orientation of the inserts was identical to that selected for the 260-SL nozzle. The silica-cloth entrance section is oriented 72 to 87 degrees to the nozzle center line. This orientation approaches 45 degrees to the gas flow to provide minimum surface recession. The carbon-cloth throat insert was laminated 60 to 75 degrees to the nozzle center line, and the exit cone insert was laminated 45 to 60 degrees to the nozzle center line to provide the best combinations of minimum surface recession, good fabrication, and minimum orientation. The mating joints of the three inserts necessarily had short-length laminates because of their changes in laminate orientation. However, the mating surfaces between inserts were oriented parallel to the laminations of the inserts. By the selection of these orientations, the areas of the short-length laminates were reduced and the tendency for them to delaminate was minimized.

The silica cloth that overwraps the ablative surfaces was oriented parallel to the bonding surfaces (similar to that used in the 260-SL nozzle) to provide maximum protection against gas passage to the steel shell in event of liner delamination.

IV, C, 44-SS Motor Nozzle (cont.)

5. Effect of Aft-End Ignition

A preliminary analysis of the effect of instantaneous increase in pressure at the exit cone due to aft-end ignition was conducted and found to have no consequential effect on ablation or thermal gradient through the insert. The igniter was designed so that the ignition gases do not impinge on the nozzle wall.

6. Structural Components

a. Nozzle Shell

The candidate materials for the 44-SS motor nozzle shell were AISI 4135, 4140, or 4340 steel heat treated to 150,000 psi minimum yield strength. These materials have been extensively used by Aerojet in several programs and their ease of fabrication is well established. AISI 4130 steel was initially considered but was rejected because previous experience has shown that it does not harden through thick sections thus causing nonuniform strength. The AISI 4135, 4140, and 4340 steels have better deep-hardening properties although the ease of fabrication is reduced slightly. The final selection of AISI 4340 steel was based on the cross-sectional thickness of the part, the hardening required through the section, and material availability.

The structural stress analysis of the nozzle shell made use of the classical methods of pressure vessel theory. The methods involving simultaneous equations for discontinuity stresses were solved by programmed methods using the IBM 7090 computer.

The nozzle shell design pressure is 819 psia, which has a 1.5 safety factor on the motor MEOP. The following criteria were used in the stress analysis:

IV, C, 44-SS Motor Nozzle (cont.)

(1) Internal Pressure:

Average pressure, psi	462
MEOP (limit load), psi	546
Design yield load, psi (F.S. x MEOP)	819 where: F.S. = factor of safety = 2.0

(2) Motor Thrust:

Average thrust, lbf	86,800
Maximum nominal thrust, lbf	97,200
Design yield thrust, lbf (F.S. x max nominal thrust)	145,800

(3) Material Properties:

AISI 4340 - metal parts	
$F_{ty}$ , psi	150,000
E, psi	29,000,000

Figure 89 shows the pertinent geometry of the nozzle shell structure and the locations at which stresses were computed.

The analysis was based, conservatively, on a hydrostatic test loading with the aft-end fully plugged at exit plane and a design pressure of 819 psi. The hydrostatic test pressure was 600 psi, which was 1.1 MEOP.

IV, C, 44-SS Motor Nozzle (cont.)

Figure 90 summarizes the structural analysis and the margins of safety for the nozzle shell. The data indicate that the shell had adequate margins of safety. The minimum margin of safety of 0.300 occurred at location 57 on Figure 89. The closure-chamber bolt joint had a margin of safety of 0.567.

The configuration of the nozzle shell was dependent on the nozzle insert contour and thickness requirements, structural requirements, ease of fabrication. The forward flange configuration was identical to the flange of the second-stage Minuteman Wing I nozzle shell for compatibility with the chamber. The entrance section which joined the forward flange with the throat stack was a 45-degree conical section and provided support for the entrance liner insert and rubber insulation.

The throat stack had a shallow 7-degree conical configuration to provide support for the insert and permit minimum use of insert material. The throat stack had a mechanical step to provide an axial stop for the throat insert when subjected to ejection loads in the event of bond failure between the shell and liner.

b. Exit Cone Shell

The exit cone shell had an approximate 15.5-degree slope angle. This angle was selected based on the requirements of a 17.5-degree expansion cone half-angle and on the insert material thickness. The exit cone section and aft flange were designed to withstand hydrostatic test loads based on the 600-psig proof pressure and the attachment of a hydrostatic test plug at the aft flange. The plug attachment at the exit plane enabled the use of a simple, economical, disc-shaped hydrotest plug. Attachment of the test plug at other nozzle locations would have required a more complicated and expensive

IV, C, 44-SS Motor Nozzle (cont.)

device. The aft flange was designed so that the aft retainer ring could be recessed within the liner insert for heat-transfer protection from the exhaust gases.

The exit-plane retainer ring provided a mechanical stop as a redundancy in the event the bond between the exit cone liner and shell failed. The retainer-ring material was normalized AISI 4130 steel which is readily available, economical, and easily fabricated. Attachment of the retainer ring to the shell was accomplished with 42 0.5-in.-dia bolts which were preloaded to a torque value of  $350 \pm 25$  in.-lbf.

7. Nozzle Sealant and Adhesives

The sealants and adhesives used on the 44-SS nozzle were identical to those selected for the 260-SL nozzle. The gaps at the forward and aft joints of the throat insert were provided to permit thermal growth and to alleviate mating problems of the inserts. A silicone rubber sealant (Aerojet specification AGC-34076, Class 5) was selected as the gap filler. The sealant extrudes easily when squeezed, while maintaining a flame-end gas seal. The surface of the rubber compound will char when exposed to flame; however, its ablation depth was predicted to be only 0.125 to 0.25 in. below the adjacent ablation surfaces.

A minimum number of O-rings was provided at ablative insert joint interfaces to prevent gas from propagating behind the insert. Buna-N rubber (per MIL-R-6855 at a Shore A hardness of 60) was selected for use as the O-ring material. Epon 948 or 948.2 was selected as the bonding agent for the entrance-cap rubber insulation because of its long duration aging characteristics.



IV, C, 44-SS Motor Nozzle (cont.)

An adhesive with desirable properties of low cure temperature, high shear strength, and high elongation was to be selected for bonding the ablative inserts to the steel nozzle shell. The capability of low-temperature cure was desired to prevent bond failure on cooling because of the thermal coefficient variations between the steel and the plastic components. A program to evaluate the pot life, viscosity, and tensile shear of various adhesives prior to final selection for use in the 260-SL-1 nozzle was not completed in time for the 44-SS motor program. The candidate adhesives evaluated were FM-86, Epon 948, and Epon 913. However, the results of the evaluations were not available; therefore, Epon 913 was used. Epon 913 has the following characteristics: pot life of over 8 hr at 75°F, cure temperature of 180°F, a minimum tensile shear of 3000 psi at room temperature, good adhesion to steel and plastic, 10% elongation, and a metal-to-metal peel strength at 18 lb/in.

The selected bondline thicknesses were considered adequate and were the minimum thicknesses obtainable with practical fabrication tolerances. The liner bondline thicknesses, based on tolerance clearances, were 0.005 to 0.025 in. along the nozzle stack and exit cone surfaces, 0.006 to 0.060 in. along the entrance surface and 0.002 to 0.008 in. at the retainer ring surfaces. The rubber insulation had a bondline thickness of 0.030 to 0.125 in. Bonding of the retainer ring provided a gas seal and results in a rigid integral exit cone structure.

The bondline thicknesses for the 260-SL nozzle were determined from the results of a dimensional tolerance analysis conducted by the 260-SL nozzle subcontractor. The variation of tensile shear strength with bondline thickness was also determined. The results of this bond thickness evaluation indicated that the selected bondline thicknesses were adequate.

IV, C, 44-SS Motor Nozzle (cont.)

Although a degradation of shear strength was expected with an increase in bondline thickness, structural analysis calculations indicated that sufficient bond area was available even when based on a conservative bondline thickness.

Gen-Gard V-61 trowelable insulation was used around the exit cone retainer ring (similar to the 260-SL nozzle) to insulate the ring from the exhaust-gas plume radiation.

V. DESIGN CHANGES FROM THE ORIGINAL DESIGN

A. 260-SL NOZZLE

Certain design changes were made following the initial release of the design and fabrication control drawings for the nozzle and exit cone assemblies. Most of the changes were made from recommendations of the subcontractor to facilitate fabrication. Each recommended change was analyzed for conformance to the design quality of the end product prior to acceptance for incorporation. These changes were also incorporated into the 120-SS-1 design and were demonstrated to be acceptable. A summary of these changes follows:

1. The bond tolerances between the ablative inserts and the steel shell and between the ablative inserts and the honeycomb components were increased to simplify assembly of the components and yet ensure structural adequacy with a minimum 1.3 safety factor. The tolerances were established from process evaluation data of bondline thickness versus tensile shear strength.

2. The laminate orientation of the exit cone liner was changed from 3 to 18 degrees to parallel-to-nozzle center line. The revised orientation permitted the use of the less expensive straight (warp) tape, which also provides a higher debulk during tape wrapping and faster and better tape control. Parallel-wrapped exit cones were successfully used in related nozzle programs.

3. An adhesive film, Epon 75-25, which was used for bonding the honeycomb sandwich components, was selected as an alternate to FM-86. Epon 75-25 adhesive was demonstrated to have the same mechanical properties and cure cycle requirements as FM-86, but provided a longer bench life (72 vs 12 hr minimum) allowing adequate time for layup of large structures.

V, A, 260-SL Nozzle (cont.)

4. An interference fit was initially designed between the nozzle assembly and exit cone assembly flanges to resist an anticipated high shear stress due to internal pressure. A subsequent stress analysis indicated that the shear stress is low (1,300 psi) and that the interference fit was unnecessary. Therefore, the interference fit was eliminated to permit ease of assembly.

5. A coating of epoxy primer with a minimum thickness of 0.002 in. (Aerojet specification AGC-34345, Type II) was applied on the exposed ablative plastic surfaces after completion of the nozzle and exit cone assemblies. The epoxy primer was used to prevent moisture absorption by the ablative materials which are hygroscopic in nature.

6. The depth of the V-groove of both the forward- and aft-attachment rings to the honeycomb structure was reduced from 1.75 to 1.00 in. to facilitate fabrication. This revised design still provided a gradual transfer of structural loads from the steel rings into the honeycomb structure.

7. The allowable tensile yield strength of the forward and aft exit cone rings was reduced from 70,000 to 55,000 psi to permit the use of normalized AISI 4130 steel which was the specified material and met the lower strength limit through the entire thickness. The lower strength limit still provides a greater safety factor than 1.3.

8. Alternative methods of surface protection were specified for the exit-cone end rings and the honeycomb facings. Priming of the end rings could be omitted provided the rings were bonded with adhesive within 8 hr after cleaning, and the surface was inspected for cleanliness prior to bonding. Priming of the 17-7PH stainless steel facings could be omitted with proper protection after cleaning.

V, A, 260-SL Nozzle (cont.)

In addition to the above changes, four design revisions were made which only affected the 260-SL nozzle and exit cone assemblies; these were not tested in motor 120-SS-1.

These revisions are:

1. The laminate orientation of the 260-SL throat extension was changed from the 45- to 60-degree position to a position parallel to the nozzle center line following the rejection of a discrepant 120-SS throat extension that was oriented 45 to 60 degrees and the successful use of parallel-to-nozzle center line components in the UTC 120 nozzle and the Lockheed 156 nozzle. A parallel-to-center-line throat extension was subsequently fabricated and used successfully in the 120-SS-1 nozzle. However, as a result of delaminations observed in the first 260-SL-1 throat extension, it was decided to revert to an oriented wrap which provides a mechanical stop in the event of a complete circumferential delamination and failure of the insert to shell bond. Therefore, the discrepant parallel-to-center-line 260-SL-1 throat extension was replaced with a new throat extension wrapped 20 to 35 degrees to nozzle center line.

2. The outside diameter of the nozzle entrance insert was reduced from 128.50 to 128.13 in. to be within the fabrication capability of the existing hydroclave.

3. The length of the exit cone aft flange ring was increased from 3.86 to 5.68 in. to ensure structural adequacy during the ignition motor deployment condition of a 4-degree cant angle between the ignition motor and nozzle center lines, which results in a nozzle side force of 20,000 lbf.

V, A, 260-SL Nozzle (cont.)

4. The aft attachment joint diameter of the steel shell was increased from  $\frac{111.017}{111.092}$  to  $\frac{112.583}{112.568}$  in. to ensure structural adequacy when subjected to bending moment loads during hydrostatic test. The shear lip diameter of the exit cone forward ring was increased correspondingly to be compatible with the new interface diameter on the steel shell.

Postfiring evaluation of the 120-SS-1 motor performance resulted in four changes that were incorporated in the 260-SL nozzle and exit cone designs as follows:

1. The rubber entrance insulation of the 120-SS-1 nozzle eroded 66% higher than predicted. Therefore, the thickness of the 260-SL-1 nozzle entrance rubber insulation was increased approximately 2 in. The additional thickness ensured that the total insulation thickness would be at least twice that required.

2. The silica MX-2646 entrance insert of the 120-SS-1 nozzle eroded greater than predicted. Therefore, the more erosion-resistant carbon MX-4926 entrance insert was extended forward so that the interface between the MX-4926 and MX-2646 was increased from an area ratio of 1.6:1 to 2.0:1.

3. Test results indicated that the erosion of the 120-SS-1 exit cone liner did not exceed the amount predicted at any location. It was determined that the less expensive silica FM-5131 could be used further upstream and still provide at least twice the insulation required. Therefore, the interface between the silica FM-5131 and the carbon MX-4926 was moved forward from an area ratio of 3.5:1 to 3.0:1. At the 3.0:1 area ratio, the predicted erosion depth of the silica is 0.46 in. as compared to 0.37 in. for carbon.

4. Some unbonding of the aft end of the exterior honeycomb facing occurred from exhaust-plume heating during the 120-SS-1 motor tailoff. To

V, A, 260-SL Nozzle (cont.)

prevent this unbonding on the 260-SL-1 nozzle, a layer of cork sheet (Aerojet specification AGC-34338) was bonded around the aft 2 ft of the exterior of the nozzle exit cone.

B. 120-SS-1 NOZZLE

Design changes similar to those made for the 260-SL nozzle were made on the 120-SS-1 design and fabrication control drawings of the nozzle and exit cone assemblies since their initial release. The first eight design changes discussed for the 260-SL nozzle (Section V,A) were also incorporated in the 120-SS-1 nozzle. This enabled evaluation of the changes prior to this incorporation into the 260-SL-1 nozzle.

Also, as discussed in Section V,A, the laminate orientation of the 120-SS-1 throat extension was changed from the 45- to 60-degree position to parallel to the nozzle center line which enabled the use of the less expensive and better controlled straight tape.

C. 44-SS MOTOR NOZZLES

As a result of a fabrication discrepancy (Section VIII,D,5), the exit cone insert of the 44-SS-1 nozzle was too short. To enable use of the component, the throat insert was lengthened, and the joint between the throat and exit cone inserts was redesigned as shown in Figure 91.

A design change was made on the 44-SS-3 motor nozzle to determine whether the throat-insert gouging which occurred in the 44-SS-1 and -2 motor nozzles was due to material and fabrication anomalies or due to phenomena related to aft-end ignition. The gouging of both the 44-SS-1 and -2 motor nozzles occurred in a section which had been fabricated using a die-cut molded

V, C, 44-SS Motor Nozzles (cont.)

process. This section of the nozzle was replaced with a tape-wrapped portion in the third motor nozzle (Figure 8) similar to that used in the 120-SS-1 and 260-SL nozzles.

Changes associated with all three 44-SS nozzles were:

1. The O-ring lubricant was changed from MIL-I-8660 to MIL-G-4343 which was being used on other Aerojet programs.
2. Dimensional tolerances were generally enlarged to facilitate fabrication and assembly.
3. The nozzle shell aft flange was thickened to withstand hydrostatic loads when using a hydrostatic test plug at the aft flange. This necessitated changing the aft retainer ring bolts from AN8-14A to AN8-13A and the nuts from MS21045-8 to NAS1022-N8.



VI. MATERIALS AND PROCESS EVALUATION

The 260-in.-dia motor program requirement to fabricate the large ablative nozzle using state-of-the-art processing methods required defining in detail the materials and processing technology to be used. The experience obtained in the use of fabrication specifications for the procurement of the Minuteman and Polaris nozzles was combined with other Aerojet materials and processing technology to develop the evaluation tasks presented herein.

The process evaluation Subtasks I and III represent the first attempt to correlate ablative material properties and characteristics with such fabrication methods as tape wrapping, hydroclave and autoclave curing, and nylon tension-wrap molding.

Subtask II was instituted to develop adhesive bonding technology for both the assembly of the ablative components into the nozzle shell and the assembly of the stainless steel skins, steel attachment flange, and honeycomb core to the exit cone.

Subtask IV presented a process demonstration of fabricating a half-length sample of a 120-in.-dia nozzle-throat section and was instituted to correlate full-scale processing technology with the criteria developed in the performance of the process evaluation studies.

The criteria developed in Subtasks I, II, III, and IV were supplemented by production experience obtained in the fabrication of the 44-SS, 120-SS-1, and the 260-SL nozzles as indicated in the sections describing fabrication methods and problem areas.

VI, Materials and Process Evaluation (cont.)

A. SUBTASK I - WRAPPING CHARACTERISTICS OF SELECTED  
ABLATIVE TAPE-WRAPPING MATERIALS

1. Introduction

The objective of Subtask I was to define those properties and characteristics of the selected ablative materials most closely related to the tape wrapping phase of the fabrication procedure, in order to establish basic parameters for tape wrapping the 260-SL nozzles.

The materials and process evaluation studies performed in this subtask were as follows:

- a. Raw material testing.
- b. Development of debulking test equipment.
- c. Establishment of maximum allowable roller pressures.
- d. Evaluation of methods for determining degree of resin advancement.
- e. Evaluation of the effect of staging time and temperature on the interlaminar shear strength of components.
- f. Evaluation of tape-wrapping characteristics vs staging time.
- g. Evaluation of tape wrapping OD to ID ratio.

Three preimpregnated (prepreg) materials were evaluated: MX-4926, a carbon-fabric-reinforced phenolic; MX-2646, a silica-fabric-reinforced polyamide-modified phenolic; and FM-5131, a silica-fabric-reinforced modified phenolic.

VI, A, Subtask I - Wrapping Characteristics of Selected  
Ablative Tape-Wrapping Materials (cont.)

2. Program

a. Raw Material Testing

The materials procured for evaluation were tested to establish the as-received raw material properties for comparison with property changes which might occur during performance of the subtask tests.

The properties obtained were: (1) volatile content, (2) resin solids, (3) degree of polymerization, (4) infrared polymerization index, (5) gel time, (6) viscosity index, (7) Chang index, and (8) laminate flow.

The materials were initially purchased in accordance with Aerojet specifications (Figure 92). Specified values of infrared polymerization index (IRPI) were 1.3 to 1.5 based on suppliers' standards. The material with these IRPI values were not responsive to staging time tests and additional material was purchased with IRPI values of 1.0 maximum.

b. Development of Debulking Test Equipment

It was desired to simulate the compaction that occurs during tape wrapping using reasonably simple and inexpensive equipment and techniques so that measurements could be obtained of the effects of tape temperature, roller pressure, and wrapping speed on the density of the pre-formed ablative plastic.

c. Establishment of Maximum Allowable Roller Pressures

A study was conducted to determine the optimum roller pressure during tape wrapping of the selected ablative materials which would

VI, A, Subtask I - Wrapping Characteristics of Selected  
Ablative Tape-Wrapping Materials (cont.)

provide the highest laminate strength without abrading or macerating the tape. This was accomplished by correlating roller pressure with the tensile strength of the material.

Two-ply laminates were fabricated of the selected prepreg materials. The plies were preheated on an aluminum plate and rolled together in the debulk test stand developed to accomplish the objectives described in Section 2,b above. The preheat and roller temperatures were maintained at 150°F. Laminates were rolled at pressures of 75, 150, 300, 450, and 600 lb/in. of width.

The laminated specimens were removed after rolling from the aluminum sheet and the resin was extracted from the reinforcement separating the plies by a solvent; dimethyl formamide (DMF) solvent was used for MX-2646 and FM-5131 and acetone was used for MX-4926. One-in.-wide strips were cut from the two plies of extracted reinforcement and were tensile tested to failure using an Instron tester at a crosshead speed of 0.1 in./min.

d. Evaluation of Methods for Determining Degree  
of Resin Advancement

A study was initiated to compare the various methods used to determine the degree of resin polymerization (advancement); the objective was to establish in-process controls for time and temperature exposure of the selected ablative materials during tape wrapping, preforming and pressure curing.

Individual plies of the selected ablative materials were suspended in an air recirculating oven for the times and temperatures noted below:

VI, A, Subtask I - Wrapping Characteristics of Selected  
Ablative Tape-Wrapping Materials (cont.)

<u>Temperature, °F</u>	<u>Time at Temperature, min</u>					
150	120	180	240	-	-	-
175	60	90	180	240	300	360
200	30	60	120	180	240	-
225	25	30	60	120	180	-

After exposure, the resin in the prepreg material was evaluated for advancement by obtaining the following data: gel time, acetone extraction, Chang index, IRPI, viscosity index, and specific gravity.

Gel time is the time required for the resin in the laminate to advance to the point where it will adhere to a pointed probe and form a filament when the probe is withdrawn.

Acetone extraction is a method of removing uncured resin from the impregnated cloth by dissolving the uncured resin in acetone. The tests were conducted in accordance with the procedures described in Appendix A.

Chang index is a variation of the acetone extraction test whereby the impregnated material is immersed in acetone and distilled water is titrated into the solution until the solution becomes cloudy. The tests were conducted in accordance with the procedure described in Appendix A.

The IRPI is obtained using infrared light to determine the percentage of resin dissolved or extracted with acetone. The procedure is described in Appendix A.

Viscosity index is determined by dissolving the resin in dimethyl formamide (DMF), passing a light beam through the solution and measuring the refractive index, measuring the viscosity of the solution with

VI, A, Subtask I - Wrapping Characteristics of Selected  
Ablative Tape-Wrapping Materials (cont.)

a Ubbelohde viscosimeter, and finally correlating viscosity and refractive index with established values for various degrees of resin advancement. The procedure is described in Appendix A.

The effect of the staging time and temperature on the final cured density of specific gravity of the impregnated materials was evaluated. The selected materials were staged in accordance with the time and temperature schedule discussed above and final cured in a hydroclave at 1000 psi and 300°F. The specific gravity of the cured specimens was determined in accordance with the procedures of Federal Test Method Standard 406, Method 5011.

e. Evaluation of Effect of Staging Time and  
Temperature on Interlaminar Shear Strength

The objective of this evaluation was to determine the effect of staging time and temperature on the interlaminar shear strength of cured plastic components.

Panels were fabricated from the selected ablative materials that had been staged in an air recirculating oven for the same time and temperature schedule shown in Section 2,d above. After staging, the materials were placed between heated press platens and cured for 1 hr at 300°F and 200 psi. The final panel thickness after molding was approximately 0.400 in.

After molding, specimens from each of the panels were prepared and tested for evaluation of the interlaminar shear strength in accordance with Federal Test Method Standard 406, Method 1042, except that the distance between saw cuts was 0.25 in. and the specimen was 0.400 in. thick.

VI, A, Subtask I - Wrapping Characteristics of Selected  
Ablative Tape-Wrapping Materials (cont.)

f. Evaluation of Tape Wrapping Characteristics  
vs Staging Time

A study was made to establish a correlation between characteristics of the wrapped, preformed ablative material and the degree of resin advancement. The characteristics evaluated were: ply thickness, spring-back, roller indentation, hardness, task, deformation, and percent debulk.

Test cylinders of the selected ablative materials were wrapped on the debulk test stand (Section 2,b above). The 3-in.-ID cylinders were 4-in. long. Prior to wrapping, the materials were staged for periods of 0 to 7 hr at 175°F (a temperature selected as a result of the work described in Section 2,e above and selected as the maximum in-process temperature).

The test cylinders were made as follows:

Lengths of 4-in.-wide tape of the appropriate material were looped loosely in an air recirculating oven and heated for the requisite time at 175°F. The tape was removed from the oven, cooled to room temperature, and one end attached to the center roll (mandrel) of the test stand. The top roll had previously been heated to 175°F, while the bottom roll was cooled with tap water. One complete wrap was made on the mandrel before 200 lb/in. of width pressure was applied to the top roll, and heat was applied to the tape by means of quartz lamps. The tape temperature was regulated by an Infrascopes shielded from extraneous radiation by a black tube extending from the tape to the Infrascopes. Dial thickness gages were mounted to obtain roller separation and laminate thickness. As the tape ran out, the pressure was released and the mandrel was removed from the stand. The mandrels were chilled for 5 min in a deep-freeze chamber to facilitate removal of the wrapped tape.

VI, A, Subtask I - Wrapping Characteristics of Selected  
Ablative Tape-Wrapping Materials (cont.)

All test specimens of a given material were wrapped as nearly as possible to the conditions noted below:

<u>Material</u>	<u>Tape Temperature, °F</u>	<u>Tape Temperature, °F</u>	<u>Roll Pressure, lb/in. of width</u>	<u>Roll Speed, ft/min</u>
MX-4926	200 - 220	135 - 140	200	3.16
MX-2646	200 - 220	125 - 150	200	3.16
FM-5131	180 - 220	120 - 125	200	3.16

## (1) Ply Thickness

The ply thickness of staged material was measured during wrapping and compared to the ply thickness of instaged material.

## (2) Springback

Springback was determined by comparing the cylinder OD measured immediately after wrapping with the OD measured 24 hr later.

## (3) Indentation

Indentation is a measure of the resilience of the material and is determined while tape wrapping by comparing the cylinder radius in contact with the roller with the cylinder radius after wrapping. The radial difference is measured by two dial indicators mounted on the debulk stand (Figure 93).

## (4) Hardness

The hardness of the as-wrapped cylinders was measured with a Shore D hardness tester to determine the effects of stage time.



VI, A, Subtask I - Wrapping Characteristics of Selected  
Ablative Tape-Wrapping Materials (cont.)

(5) Percent Debulk

Roller debulk was determined by comparing the thicknesses of multiple plies of the staged materials immediately after rolling to thicknesses of multiple laminates of the unstaged materials that were cured between press platens for 1 hr at 300°F and 1000 psi. The percent of debulk is the ratio of the pressed ply thickness to the as-wrapped ply thickness.

(6) Tack

Tack was determined by measuring the lap shear strength of specimens of the selected materials prepared as follows: two strips of prepreg material, 4-in. long and 1-in. wide, were overlapped 1 in., placed on an aluminum plate, and heated in a press at contact pressure for 2 min at the desired tacking temperature. After heating, the aluminum sheet and the prepreg material were removed from the press, immediately placed under an air ram with a 1-in.-dia foot which is forced against the two plies of prepreg material. The foot was left in contact with the specimen until it had cooled to room temperature.

(7) Deformation of Preimpregnated Materials

In wrapping bias-cut tapes at orientation non-parallel to the center line, the tape must be capable of deforming under moderate loads and at temperatures below the level of rapid resin advancement.

A specially designed test fixture was built to measure the deformation of a bias-cut tape specimen under the combined effects of temperature and load. The fixture (Figure 94) was heated in an air-circulating oven maintained at the testing temperature. The tape specimen was inserted into the jaws of the fixture and heat was applied for 2 min; a solenoid

VI, A, Subtask I - Wrapping Characteristics of Selected  
Ablative Tape-Wrapping Materials (cont.)

was then activated to release pins holding a weight attached to the specimen. At the time the solenoid was activated, an electric timer was started and continued to operate until the specimen stretched 0.060 in.

(8) Correlation of Tape-Wrap Characteristics of Staged  
Materials with Indexes of Resin Advancement

A correlation of the various tape-wrap characteristics were correlated with the various indexes of resin advancement for the staged materials to determine the overall interrelation of the above parameters. A composite plot of the data was made as a function of staging.

g. Evaluation of Tape Wrap OD to ID Ratio

To wrap tape material at orientations non-parallel to the mandrel center line, the tape must be capable of deforming to conform to the mandrel surface. For this reason, bias-cut tapes are required. Various widths of bias-cut tapes were evaluated to determine the minimum tape wrap radius or OD to ID ratio. The tapes were hand-formed to the minimum curvature without wrinkling. The results of this test enabled proper selection of tape width.

3. Results

a. Raw Material Testing

The properties of the as-received raw materials purchased with 1.3 to 1.5 IRPI index values are shown in Figure 95. Also shown in Figure 95 are the properties of raw material purchased with 1.0 IRPI maximum.

VI, A, Subtask I - Wrapping Characteristics of Selected  
Ablative Tape-Wrapping Materials (cont.)

b. Development of Debulking Test Equipment

It was initially planned to develop a technique for fabricating flat panels instead of cylindrical specimens, which require autoclave or hydroclave curing, thereby reducing fabrication and testing time. The flat panels were cured between heated press platens. The method proved unsuccessful because each ply had a tendency to adhere to the heated pressure roller and to be rolled to a slight curvature. Although an aluminum plate was added to support the plies during rolling, the curvature was not completely eliminated. Accordingly, this approach was discontinued and the specimens for testing were produced as cylinders (Figure 96) in which the straight or bias-cut tape was wrapped parallel to the surface of the mandrel. The roller stand (Figure 93) was constructed to simulate the conditions occurring during the actual tape wrapping operations. The top roll was electrically heated and thermostatically controlled. The center roll served as a mandrel for wrapping cylindrical specimens and was removable. These two rolls were mounted in blocks which were free to slide vertically so that they could be forced against the bottom roller by air cylinders mounted at the top of the stand. The bottom roll was water-cooled.

The preimpregnated fabric tape was preheated by passing it through a bank of four quartz-tube infrared heaters, each manually operated. The temperature of the incoming tape material was measured by an infrared radiation pyrometer (Infrascope) protected from stray radiation by a 1-in.-dia black tube mounted between the lens of the pyrometer and the hot tape.

As finally developed, the tape-wrapping stand was equipped for complete control and measurement of tape temperature, roller pressure, and wrapping speed.

VI, A, Subtask I - Wrapping Characteristics of Selected  
Ablative Tape-Wrapping Materials (cont.)

c. Establishment of Maximum Allowable Roller Pressure

Figures 97, 98 and 99 show the results of the breaking-strength tests performed on the resin-extracted fabric tapes which had been previously rolled at various pressures. Degradation which occurred in the fabric at low pressures was caused by abrasion of the fabric due to slippage of the rollers; degradation at high roller pressures was caused by crushing. The optimum roller pressures were 400 lb/in. width for MX-4926, 300 lb/in. width for MX-2646, and 200 lb/in. width for FM-5131.

d. Evaluation of Methods for Determining Degree  
of Resin Advancement

The results obtained with the various methods of determining resin advancement are discussed below. Figure 100 lists the properties of the as-received preimpregnated fabrics.

(1) Gel Time

Gelation-temperature relationships for MX-4926 and FM-5131 are shown in Figure 101. Gel time was excessive at temperatures below 200°F. Since the temperatures encountered in the wrapping and preforming phases of fabrication were below 200°F, gel time did not provide an accurate prediction of resin achievement.

(2) Acetone Extraction

The results obtained of the acetone extraction of MX-4926, FM-5131, and MX-2646 are shown in Figures 102, 103, and 104, respectively. The resin contents of the as-received materials are also indicated.

VI, A, Subtask I - Wrapping Characteristics of Selected  
Ablative Tape-Wrapping Materials (cont.)

The resin system in MX-4926 is completely soluble in acetone because the percentage of extractables in the unstaged material is essentially equal to the resin content reported for the as-received material. However, the resin systems in MX-2646 and FM-5131 are not completely soluble. Approximately two-thirds of the resin was extracted from the unstaged FM-5131 and only half of the resin was extracted from the unstaged MX-2646.

At staging temperatures of 150 and 175°F, no change in percent acetone extraction was observed in MX-4926 for 6-hr staging and in FM-5131 for 4.5-hr staging; the percent acetone extraction in MX-2646 decreased gradually with staging time. At temperatures of 200°F and above, the percent acetone extraction of all three materials decreased rapidly with staging.

The results indicate that acetone extraction may be used for measuring resin advancement in MX-4926 and FM-5131. Because the acetone extraction in MX-2646 changes with staging, the results may not be used independently but may be correlated with such parameters as density and interlaminar shear.

(3) Chang Index

The Chang index test was satisfactory only for the MX-4926 solution which indicated a sharp transition from a clear to cloudy appearance. However, the MX-2646 and FM-5131 solutions became cloudy immediately upon the addition of water due to the presence of resin modifiers which made measurements of the Chang index impossible.

Chang index appears to be very sensitive for measuring the initiation of resin advancement in the unmodified phenolic polymer (MX-4926). Chang index values for MX-4926 are shown in Figure 105.

VI, A, Subtask I - Wrapping Characteristics of Selected  
Ablative Tape-Wrapping Materials (cont.)

(4) Infrared Polymerization Index (IRPI)

IRPI values obtained for MX-4926 are shown in Figure 106. Like the Chang index, IRPI is obtainable for relatively short staging times (4 to 6 hr maximum). After longer staging times, sufficient resin can not be extracted to yield satisfactory measurements.

The IRPI values obtained for FM-5131 are shown in Figure 107. The scatter of the data preclude the use of the IRPI data for this material without additional investigation.

The IRPI method could not be used for MX-2646 because sufficient quantities of resin could not be extracted to conclude the test.

(5) Viscosity Index

The viscosity index results obtained with MX-4926 and FM-5131 are shown in Figures 108 and 109. The scatter and insufficient quantity of the data made it difficult to establish a reliable correlation of viscosity index with resin advancement. Viscosity index could not be obtained for MX-2646 because sufficient quantities of resin could not be extracted.

(6) Specific Gravity

The specific gravity values obtained for MX-4926, FM-5131, and MX-2646 are shown in Figures 110, 111, and 112, respectively.

Staging at 150 and 175°F had little effect on the ability of the three selected materials to achieve full density at the normal

VI, A, Subtask I - Wrapping Characteristics of Selected  
Ablative Tape-Wrapping Materials (cont.)

hydroclave pressure of 1000 psi; full density was achieved at very short staging time (less than 1 hr) at 200 and 225°F.

The influence of staging time and temperature was further verified by measurements of the ply thickness of the laminates. The relationship of ply thickness vs staging condition is shown in Figures 113, 114 and 115 for the three materials.

e. Evaluation of Effect of Staging Time and Temperature  
on Interlaminar Shear Strength of Composites

The results of the interlaminar shear tests of the three selected materials staged for various times and temperatures are shown in Figures 116, 117 and 118. The results indicate that high interlaminar shear strength may be obtained by maintaining a maximum temperature of 175°F for a 6-hr maximum duration prior to final cure for all three materials.

f. Evaluation of Tape-Wrapping Characteristics  
vs Staging Time

(1) Ply Thickness

A comparison of the laminate thickness of unstaged material to the laminate thickness of wrapped staged material is shown in Figures 119, 120 and 121. The average increase in ply thickness of the maximum staged materials to the unstaged materials was 8.3% for MX-4926, 6.25% for MX-2646, and 2.5% for FM-5131. The maximum staging times for these tests were: MX-4926, 2.25 hr; MX-2646, 7.0 hr; and FM-5131, 7.0 hr. Staging up to 2.25 hr at 175°F had no effect on the ply thickness of MX-4926 and MX-2646.

VI, A, Subtask I - Wrapping Characteristics of Selected  
Ablative Tape-Wrapping Materials (cont.)

(2) Springback

Springback data for the materials are shown in Figures 122 through 124. The springback of the unstaged material decreased rapidly between 0 and 1-hr staging time and remained constant at staging greater than 1 hr, up to the point where the plies do not tack. The MX-2646 had a higher springback than the FM-5131 and the MX-4926.

(3) Indentation

The measurements of roller indentation are shown in Figures 125, 126, and 127. Considerable scatter is indicated, but the maximum indentation occurred with the maximum staging time.

(4) Hardness

Shore D hardness measurements are presented in Figure 128. The hardness of the wrapped cylinders increased as the staging time increased, as expected.

(5) Percent Debulk

Percent debulk of MX-4926 and MX-2646 as a function of staging time at 175°F is shown in Figure 129; the data indicate a decrease in percent debulk with increased staging. The results obtained for FM-5131 were erroneous and are not presented.

(6) Tack

The limiting time and temperature envelopes within which tack was obtained in the three materials staged at 200°F are shown in



VI, A, Subtask I - Wrapping Characteristics of Selected  
Ablative Tape-Wrapping Materials (cont.)

Figures 130, 131 and 132. Tack values for MX-4926 at 175°F are also shown in Figure 130. These data constitute the first attempt to establish tack limitations as a function of staging time, staging temperature, and wrapping temperature.

(7) Deformation of Prepreg Materials

Figure 133 is a plot of the deformation or the time required for MX-4926 bias-cut specimens staged at 175°F to stretch 0.060 in. when tested at various temperatures. As indicated, the deformation decreased (required more time to stretch) with staging and increased with oven or tape-wrapping temperature.

(8) Correlation of Tape-Wrapping Characteristics of  
Staged Materials with Indexes of Resin Advancement

The composite data of the tape-wrapping characteristics and indexes for measuring resin advancement are presented in Figures 134 through 139. Correlation of the various parameters are thus obtainable and can be used to establish criteria for optimum tape wrapping of the materials.

g. Evaluation of Tape Wrapping OD to ID Ratio

The recommended maximum outside to inside tape-wrapping diameter vs tape width is shown in Figure 140. Higher OD to ID ratios than that recommended results in the tape wrinkling and nonconforming to the mandrel surface.

4. Conclusions and Recommendations

The wrapping characteristics of MX-4926, MX-2646 and FM-5131 were established. Roller-debulking test equipment was developed which permitted evaluation of the tape-wrapping parameters. The effects of staging time

VI, A, Subtask I - Wrapping Characteristics of Selected  
Ablative Tape-Wrapping Materials (cont.)

and temperature were determined and methods of determining resin advancement were compared. The relationship of the various material properties and characteristics as a function of staging were established. Detailed conclusions of the studies are as follows:

a. Optimum roller pressures established for MX-4926, MX-2646 and FM-5131 are 400, 300 and 200 lb/in. of width, respectively.

b. Conclusions of the various methods of determining degree of resin advancement are:

(1) Gel time does not provide an accurate prediction of resin advancement.

(2) Acetone extraction may be used accurately for determining resin advancement of MX-4926 and FM-5131, but not for MX-2646 which is insoluble in acetone.

(3) Chang index may be used to measure resin advancement of unmodified carbon-phenolic polymer (MX-4926) but not for the resins with modifiers (MX-2646 and FM-5131).

(4) IRPI is suitable for measuring resin advancement in MX-4926 but not for MX-2646. Data for FM-5131 were inconclusive.

(5) Viscosity index data were erratic. Indications are that viscosity index may be used for MX-4926 and FM-5131 but not for MX-2646.

(6) Staging temperatures should be 175°F or less to ensure full density of the final cured part.

VI, A, Subtask I - Wrapping Characteristics of Selected  
Ablative Tape-Wrapping Materials (cont.)

c. Staging should be limited to 175°F maximum for 6 hr maximum to ensure high interlaminar shear strength.

d. The effects of staging on tape-wrapping characteristics were:

(1) Staging up to 2.5 hr at 175°F had no effect on ply thickness of the wrapped component. Additional staging reduced roller debulking, i.e., the wrapped ply thickness increased with staging in excess of 2.5 hr.

(2) Springback decreased rapidly between 0 and 1 hr staging and remained constant beyond 1-hr staging.

(3) Roller indentation generally increased with staging. Additional test data are required.

(4) The Shore D hardness of wrapped laminates increased with staging.

(5) Percent debulk decreased with staging. Additional test data are required for FM-5131.

(6) The relationship of stage temperature and time were established for various tacking temperatures. This is the first known attempt to obtain such a correlation.

(7) The ability of the material to deform or stretch under tension loads decreased with staging and increased with tape-wrapping temperature. Staging up to 3.5 hr is tolerable at a 175°F tape-wrapping temperature.

VI, A, Subtask I - Wrapping Characteristics of Selected  
Ablative Tape-Wrapping Materials (cont.)

(8) Correlation of tape-wrapping characteristics with indexes of resin advancement were obtained as a function of stage time and temperature. The data enables selection of criteria for obtaining optimum tape-wrapped components.

e. The tape-wrapping OD to ID relationship was established as a function of tape width and flat-pattern ID and OD as shown in Figure 140.

VI, Materials and Process Evaluation (cont.)

B. SUBTASK II - EVALUATION OF ADHESIVES, JOINT DESIGNS,  
AND FABRICATION METHODS

1. Introduction

The 260-SL nozzle design required the use of adhesives to bond the ablative plastic inserts to the steel nozzle shell and to the honeycomb exit cone structure. Whereas the plastic inserts were bonded into the finished nozzle shell, the exit cone honeycomb structure was built up over the exit cone plastic liner. The latter process involved a series of layups wherein the inner honeycomb skin, the honeycomb core, and the other honeycomb skin were individually bonded in a series of vacuum bonding operations. To ensure the nozzle design integrity, Subtask II of the nozzle evaluation program was conducted to verify the selection of adhesive and potting materials and establish bonding and honeycomb sandwich processing parameters.

2. Program

a. Establishment and Verification of Materials and  
Processing for the 260-SL Honeycomb Structure

(1) Optimization of Cure Cycle for Adhesive

Initially, flatwise tensile tests, which were conducted in accordance with ASTM Standard C-297-55, were used to determine the optimum cure cycle for the bonding of the honeycomb at 50 to 100 psi. The specimens were taken from honeycomb sandwiches fabricated from 17-7 PH stainless-steel cover skins, Condition TH-1050, bonded to aluminum alloy 3003 core, Code No. 6.0-1/4-30P. A minimum of three specimens was tested for each condition of time and temperature. The various bonding materials and cure cycles evaluated are shown in Figure 141. Subsequent tests were conducted to determine

VI, B, Subtask II - Evaluation of Adhesives, Joint Designs,  
and Fabrication Methods (cont.)

optimum cure cycles when bonding was conducted under vacuum. Two adhesives were evaluated: FM 86, which was considered the best of the initial group evaluated; and Epon 75-25 adhesive, which has a longer pot life.

(2) Effect of Multiple Heat Cycles on Bond Strength

Flatwise tensile tests were used to determine the effect of additional heat input on the strength of cured adhesive. Two adhesives were evaluated, Epon 75-25 and FM 86. Two sets of honeycomb panels of each adhesive were bonded at 180°F and the panels were exposed to two and three cycles, respectively, consisting of exposure to 180°F for 3 hr followed by cooling to room temperature and holding at room temperature for 2 hr.

(3) Mechanical Properties of Honeycomb

Sandwich panels were vacuum-bonded with FM 86 adhesive and submitted to tests to measure the flatwise tensile strength, the plate shear strength, the flatwise compressive strength, and the ultimate flexural strength. A minimum of 12 specimens were tested for each property determination. The stainless steel skins were cleaned in accordance with Aerojet specification AGC-13842 prior to bonding. Flatwise tensile strength tests were repeated using Epon 75-25 adhesive.

(4) Adhesive Pot Life

Both FM 86 and Epon 75-25 adhesives were kept refrigerated while the panels were prepared for bonding, and then were allowed to warm to 70°F. Successive panels were then bonded with warm adhesive that was held at room temperature for various lengths of time prior to bonding. The pot life was considered to be the longest time that the adhesive could be held at room temperature without a 20% decrease in flatwise tensile strength.

VI, B, Subtask II - Evaluation of Adhesives, Joint Designs,  
and Fabrication Methods (cont.)

(5) Effect of Heat-Up Rate During Bonding

A series of vacuum bonded panels were fabricated in which the time to reach the curing temperature of the adhesive was varied from 1 to 4 hr. Both FM 86 and Epon 75-25 adhesives were evaluated. A minimum of three flatwise specimens was prepared and tested from each panel.

(6) Storage Life of Honeycomb Skins After Cleaning

Panels were fabricated from 17-7 PH stainless steel skins, cleaned in accordance with Aerojet specification AGC-13842, and then stored in sealed polyethylene film for as long as 11 days prior to bonding. Flatwise tensile specimens were prepared from the FM 86 bonded panels; the useful storage life was considered to be the time at which the strength decreased 20% below that obtained with panels bonded on the same day they were cleaned.

b. Bond Strength Between Exit-Cone Attachment  
Ring and Honeycomb Structure

Three flat specimens were prepared to evaluate the strength of the joint. The specimens simulated the joint between the nozzle exit cone attachment ring and the honeycomb structure, and had double-lap shear joints of 17-7 PH stainless steel skins, bonded to 0.50-in.-thick loading blocks as shown in Figure 142. One skin was bonded with FM-86 adhesive, the other skin with Epon 913 adhesive. The bonded area on each block was 4 sq in.

VI, B, Subtask II - Evaluation of Adhesives, Joint Designs,  
and Fabrication Methods (cont.)

c. Adhesive and Potting Material Design Parameters

(1) Selection of Adhesive for the Plastic-to-Steel  
Bond

The requirements for this adhesive were a reasonably long working life to accommodate the assembly of the skins to the exit cone liner, a curing temperature of less than 180°F, high strength, and sufficient elasticity to adjust to the differences in thermal expansion between the metal and plastic. A survey was made of available candidate adhesives, and Epon 913 and Epon 933 were selected for evaluation of their lap shear strengths, block shear strengths, compressive strengths, and tensile strengths and elongations.

(2) Potting Material Selection

The selection of potting compound to be used between honeycomb core sections and in the attachment ring grooves was based on ease of handling, pot life, density, strength, caulking, and edge-filling characteristics. Materials considered were Epon 912 and Corfil 615.

(3) Rubber-to-Nozzle Adhesive Selection

Epon 948 adhesive was selected to bond the rubber insulation to the inlet section. The selection was based on prior Aerojet experience with this material. Adhesive bond strength of Epon 948 to Gen Gard V-44 was determined.

(4) Exit Liner Gap Filling Compound Selection

Selection of the compound used to fill the gaps between the plastic sections of the exit cone liners was based on the basis



VI, B, Subtask II - Evaluation of Adhesives, Joint Designs,  
and Fabrication Methods (cont.)

of ease of handling, pot life, sufficient flexibility to accommodate thermal expansion, and resistance to burnout and blow-out. Aerojet specification AGC-34076C was used for the acceptance standard.

d. Evaluation of Metal to Plastic Glue-Line Thickness

Lap shear specimens were used to evaluate the effect of adhesive bond thickness. The specimens were taken from panels of 17-7 PH stainless steel bonded with a 1-in. overlap using Epon 913 adhesive. Five panels were fabricated, in which the adhesive bond thickness was controlled at 0.006, 0.033, 0.037, 0.120, and 0.205 in. Six lap shear specimens were tested from each panel.

e. Thermal Stress and Distortion Between the  
Honeycomb Skin and Ablative Liner

Three panels were fabricated by bonding 17-7 PH stainless steel sheet to FM-5131 silica cloth using Epon 913 adhesive. Two panels were 20 by 2 in. and one was 20 by 8 in. (Figure 143). The smaller panels were used for uniaxial stress measurements; the larger were used for biaxial stress measurements. All panels were measured for flatness before and after bonding.

Prior to bonding, the FM-5131 panels were fabricated by laying strips of fabric at an angle of 22.5 degrees to the flat surfaces, as shown in Figure 144, and cured in a hydroclave. Flexural specimens were prepared from the FM-5131 panels and tested parallel and normal to the 24-in. dimension to determine flexural strength and modulus. Thermal expansion properties were measured in the direction parallel to the 20-in. dimension.

VI, B, Subtask II - Evaluation of Adhesives, Joint Designs,  
and Fabrication Methods (cont.)

f. Evaluation of Bond Joint Between the Steel  
Shell and Ablative Liner

Using the tooling procured for the fabrication of the 120-in. subscale nozzle throat insert, a ring was tape wrapped and cured using the identical materials and procedures that were used to fabricate the 120-in.-dia throat section. The ring length was approximately half that of the actual 120-SS-1 throat. A steel ring was fabricated duplicating the size, material, and fabrication method of the 120-in. nozzle shell. The metal shell and plastic components were bonded with Epon 913 (cured at 180°F for 3 hr), after which the interfaces between metal and plastic were machined and visually examined for bond integrity.

3. Results

a. Establishment and Verification of Materials and  
Processing for the 260-SL Honeycomb Structure

Of the candidate adhesives that were initially evaluated, FM-86 had the best combination of high tensile strength for low cure temperature for the bonding of the honeycomb structure (Figure 145); however, it had a limited pot life of 12 hr. During the course of the evaluation program, Epon 75-25 adhesive, which has a pot life of 48 to 72 hr, was evaluated and selected for use in the 260-SL nozzles. The results of tests conducted on FM 86 and Epon 75-25 are discussed below:

(1) Optimization of Cure Cycle for Adhesives

The Epon 75-25 adhesive produced flatwise tensile strengths in honeycomb panels of approximately 700 psi (Figure 146) when bonded with vacuum pressure of 25 to 27 in. of Hg as compared to an average

VI, B, Subtask II - Evaluation of Adhesives, Joint Designs,  
and Fabrication Methods (cont.)

flatwise tensile strength of 435 psi when using FM 86 adhesive (Figure 145). Figure 146 also shows the results obtained with honeycomb panels bonded with Epon 75-25 adhesive that was exposed to 75°F for periods up to 72 hr prior to bonding; the 72-hr exposure had no adverse effect on the tensile strength. The decrease in tensile strength after 24-hr exposure was found to be caused by excessive flow of the adhesive up the core cells, and resulted in poor fillets. Additional Epon 75-25 panels, bonded after 24-hr exposure at 77°F using a vacuum of 21.5 in. of Hg, were evaluated to determine whether the decreased vacuum would lower the adhesive flow. Figure 147 indicates that increased strength was obtained at the decreased vacuum pressure.

The individual layup time of the 260-SL nozzle sandwich structure was estimated to take a minimum of 5 hr; therefore, a panel that was vacuum bonded (25-27 Hg) with Epon 75-25 adhesive, aged at 75°F for 5 hr prior to bonding, was evaluated. The resulting flatwise tensile strengths were in excess of 875 psi. Based on these results, Epon 75-25 was selected for use in the 120-SS-1 and 260-SL nozzles. The layup time of the 120-SS-1 exit cone was actually 9 hr; however, the results of trepan specimens taken from the bonded honeycomb structure of the 120-SS-1 exit cone (Figure 148) indicate that satisfactory bonding was obtained.

(2) Effect of Multiple Heat Cycles on Bond Strength

The results of tests performed on honeycomb panel vacuum-bonded with FM-86 adhesive (Figure 149) indicated that multiple heat cycles did not cause a reduction in bond strength. The fabrication of the 120-SS-1 honeycomb sandwich involved layup and cure of each layer of the structure. With the curing of each new layer, the inner layers received another heat cycle. The results of tests performed on the trepan specimens taken from the 120-SS-1 exit cone support structure (Figure 148) indicate that Epon 75-25 is similarly unaffected by multiple heat cycles.

VI, B, Subtask II - Evaluation of Adhesives, Joint Designs,  
and Fabrication Methods (cont.)

(3) Mechanical Properties of Honeycomb

The mechanical properties of panels vacuum bonded with FM-86 adhesive are shown in Figure 145. Epon 75-25 adhesive had a higher flatwise tensile strength of approximately 700 psi (Figure 146) as compared to the 435 psi obtained for FM-86. Because flatwise tensile strength was considered to be the most important mechanical property, tests of additional properties of Epon 75-25 were not conducted.

(4) Adhesive Pot Life

The maximum working life of FM-86 adhesive was determined to be 12 hr (Figure 150). The average flatwise tensile strength of specimens bonded after 14 hr exposure to 70°F decreased almost 50% from the values obtained with specimens exposed for 12 hr. In contrast, the Epon 75-25 retained its bond strength after a 72-hr exposure (Figure 146).

(5) Effect of Heat-Up Rate During Bonding

The effect of heat-up rate on the flatwise tensile strength of panels vacuum bonded with FM-86 and Epon 75-25 adhesives are shown in Figure 147; the data indicate FM-86 is not affected by heat-up time, whereas the tensile strength of Epon 75-25 fluctuates widely with heat-up time. However, the minimum tensile strength of Epon 75-25 is considered adequate.

(6) Storage Life of Honeycomb Skins After Cleaning

Panels stored up to 11 days after cleaning, and subsequently bonded with FM-86 adhesive, exhibited no decrease in flatwise tensile strength.

VI, B, Subtask II - Evaluation of Adhesives, Joint Designs,  
and Fabrication Methods (cont.)

b. Bond Strength Between Exit-Cone Attachment Ring  
and Honeycomb Structure

The lap shear strengths of the bonded joints were found to be 2985 psi. In the 260-SL exit cone assembly, there are three skins in the exit cone attachment ring, consisting of two inner skins and one outer skin. Assuming an average tensile strength of 200,000 psi for the 17-7 PH stainless steel, the three 0.018-in.-thick skins would have a tensile strength of 10,800 lb/in. of sandwich width. With an average lap shear strength at the joints of approximately 3000 psi, a 4-in. total bonded contact length per inch of sandwich width would cause failure to occur in the skins. Because there are two skins in contact with the attachment ring, a 2-in. contact length for each skin was deemed sufficient to cause skin failure (Figure 151).

c. Adhesive and Potting Material Design Parameters

(1) Selection of Adhesive for the Plastic-to-Steel  
Bond

The mechanical properties of the two candidate adhesives are shown in Figure 152. The specimens were cut from castings of the adhesives. Because these materials are viscous, a large number of air bubbles were caused by mixing. This resulted in some erratic data and generally lower values than are usually obtained for epoxy compounds. Although the Epon 933 showed a slight superiority over the Epon 913, it was considered that the extensive experience obtained with the use of Epon 913 during other nozzle programs outweighed its slightly lower mechanical properties; therefore, Epon 913 was selected for use on the program.

Tensile lap shear tests were performed on specimens of FM-5131 silica cloth bonded to 17-7 PH stainless steel with Epon 913. Failure occurred in the FM-5131; the test results are shown in Figure 153.

VI, B, Subtask II - Evaluation of Adhesives, Joint Designs,  
and Fabrication Methods (cont.)

Since the Epon 913 is capable of attaining lap shear strengths as high as 3000 psi (Figure 154) and the interlaminar shear strength of FM-5131 is about 2000 psi (results of Subtask I), it appeared that the bond strength would exceed the cohesive strength of the FM-5131.

Fuller No. 162-Y-22 primer was applied to the steel surfaces for protection during storage, and the Epon 913 adhesive was bonded to the primer. Figure 154 shows the results of lap shear tests conducted on specimens of 17-7 PH stainless steel primed with the 162-Y-22 material. The data indicate a reduction of approximately 7% in bond strength; however, the values were consistent, and the average is representative of the strength attainable with Epon 913 adhesive.

(2) Potting Material Selection

No comparative tests were conducted on Epon 912 and Corfil 615. Corfil 615 was selected as the potting material because of extensive fabricating experience obtained in its use at TRW on other programs.

(3) Rubber-to-Nozzle Adhesive Selection

Epon 948 was selected for bonding the Gen-Gard V-44 rubber to the nozzle shell. Data on peel strength are shown in Figure 155, and were developed by Goodyear. The optimum cure time is 3 to 7 days at 80°F. The surface preparation prior to bonding, as recommended by Goodyear, is as follows:

(a) Degrease rubber surface with isopropyl alcohol and abrade with 80-grit abrasive cloth. Degrease again with isopropyl alcohol.

(b) Clean metal with methyl ethyl ketone.

VI, B, Subtask II - Evaluation of Adhesives, Joint Designs,  
and Fabrication Methods (cont.)

(c) Apply a skin coat of adhesive to rubber surface and approximately 0.0625-in.-thick coat to metal surface.

(4) Exit Liner Gap Filling Compound Selection

Aerojet specification AGC-34076C was selected as the acceptance standard for the gap-filling compound. No qualification testing was necessary.

d. Evaluation of Metal-to-Plastic Glue-Line Thickness

The results of tests on lap shear specimens of 17-7 PH stainless steel bonded with Epon 913 adhesive of varying bond thicknesses are shown in Figure 156. All of the specimens in which the thickness of the adhesive was 0.033 in. or less failed by fracture of the steel; 5 of the 7 specimens with an adhesive thickness of 0.037 in. also failed in the steel. Lap shear strength of approximately 2700 psi was obtained in the 0.006 and 0.033-in.-thick adhesive bond specimens. Since the interlaminar shear strength of the FM-5131 silica cloth is approximately 2000 psi, failures of the Epon 913 bond are considered to be unlikely for bond thicknesses of 0.033 in. or less. However, larger bond thicknesses can be used depending on the nozzle component bond strength requirement.

e. Thermal Stresses and Distortion Between the  
Honeycomb Skin and Ablative Liner

After bonding, panels 1 and 2 (Figure 143) showed a slight curvature concave toward the steel side. After bonding, the wide panel (panel 3, Figure 143), was concave toward the plastic side. The depths of curvature,  $h$  (Figure 157) are shown in Figure 159. As shown in Figure 157, the radius of curvature of the test panel can be computed with the equation:

VI, B, Subtask II - Evaluation of Adhesives, Joint Designs,  
and Fabrication Methods (cont.)

$$r = \frac{L^2 + h^2}{2h}$$

where  $r$  = radius of curvature

$L$  = half the specimen length

$h$  = height of arc (depth of curvature)

The composite specimen was reduced to an equivalent steel section as shown in Figure 158. That portion of the equivalent steel section which represents the plastic has an equivalent width,  $b_1$ , as follows:

$$b_1 = b \left( \frac{E_p}{E_s} \right)$$

where  $E_p$  = modulus of elasticity of plastic

$E_s$  = modulus of elasticity of steel

The thickness of the bond was included in the thickness of the plastic. The following modulus and thermal expansion properties were used:

17-7 PH steel

$$E_s = 30.0 \times 10^6 \text{ psi}$$

$$\alpha_s = 6.3 \times 10^{-6} \text{ in./in./}^\circ\text{F}$$

Plastic

$$E_p = 2.11 \times 10^6 \text{ psi}$$

$$\alpha_{p1} = 7.2 \times 10^{-6} \text{ in./in./}^\circ\text{F parallel to long laminate dimension}$$

$$\alpha_{p2} = 4.6 \times 10^{-6} \text{ in./in./}^\circ\text{F perpendicular to long laminate dimension}$$



VI, B, Subtask II - Evaluation of Adhesives, Joint Designs,  
and Fabrication Methods (cont.)

The center of gravity and moment of inertia of the equivalent section were then computed. For the dimensions shown:

$$Y_1 = 0.0604 \text{ in.}$$

$$Y_2 = 0.2136 \text{ in.}$$

$$I = 0.924 \times 10^{-4} \text{ in.}$$

The bending moment in the panel is related to the radius of curvature by the equation:

$$\frac{1}{r} = \frac{M}{EI}$$

The tensile bending stress in the extreme fiber in the steel is equal to:

$$\sigma_s = \frac{MY_1}{I}$$

Substituting:

$$\sigma_s = \frac{E_s Y_1}{r}$$

For the plastic, the compressive bending stress is equal to:

$$\sigma_p = \frac{E_p}{E_s} \cdot \frac{E_s Y_2}{r} = \frac{E_p Y_2}{r}$$

The results of the bending stress computations for each of the panels are shown in Figure 159. The bending stresses developed during the bonding process in both steel and plastic are low. This indicates that there was very little differential growth at the time the bond set.

VI, B, Subtask II - Evaluation of Adhesives, Joint Designs,  
and Fabrication Methods (cont.)

Of interest is the fact that two test panels, during cure, became concave toward the steel side. Since the steel has a lower coefficient of thermal expansion than that of the plastic, in the direction parallel to the long dimension, the panel should be curved the other way. The cause for the reverse curvature has not been determined. However, it is believed that the cause is related to the anisotropic properties of the plastic component. The two coefficients of thermal expansion of the plastic, in the directions parallel and perpendicular to the long laminate direction, bracket the thermal expansion coefficient of the steel. Additionally, the higher thermal conductivity of the steel would cause the steel to heat up and expand first, and possibly cure the adhesive, before the plastic completely heated and expanded.

f. Evaluation of Bond Joint Between the Steel Shell  
and Ablative Liner

Visual examination of the interface between the steel nozzle shell and the FM-5131 silica cloth indicated that there was no separation of the Epon 913 bond between the two materials.

4. Conclusions and Recommendations

Pertinent conclusions obtained from Subtask II of the nozzle process evaluation program are as follows:

a. Neither FM-86 nor Epon 75-25 metal adhesives are deleteriously affected by the application of multiple heat cycles subsequent to cure.

b. Acceptable mechanical properties are obtained in honeycomb structures bonded with either FM-86 or Epon 75-25 metal adhesives.

VI, B, Subtask II - Evaluation of Adhesives, Joint Designs,  
and Fabrication Methods (cont.)

- c. Epon 75-25 metal adhesive has a useful pot life of 72 hr at room temperature. There is an anomalous decrease in bond strength after 24 hr exposure which should be verified by further testing.
- d. FM-86 metal adhesive is unaffected by heat-up time during curing. The bond strength of Epon 75-25 varied with various heat-up times. The Epon 75-25 bond strength at a heat-up time of 2 hr was less than that obtained with shorter and longer heat-up times.
- e. Stainless-steel honeycomb skins may be cleaned and stored in polyethylene bags for as long as 11 days prior to bonding without a decrease in the bond strength.
- f. Fuller 162-Y-22 primer applied to metal surfaces does not appreciably reduce the bond strength of Epon 913 adhesive.
- g. Bonding of the 260-SL exit cone attachment ring to the honeycomb skins may be accomplished using a 2-in. overlap.
- h. Epon 913 and Epon 933 were both acceptable for bonding metal components to ablative plastics; Epon 913 was selected for use because of extensive experience obtained in its use during other programs.
- i. The bond on Epon 913 decreases sharply at thicknesses greater than 0.033 in. However, the strength at thicknesses as great as 0.12 in. is 1120 psi which is adequate for the 260-SL nozzle.
- j. Thermal stresses and distortion between bonded metal to ablative plastic components are very low.

VI, Materials and Process Evaluation (cont.)

C. SUBTASK III - DEVELOPMENT OF CURE CYCLES FOR THE  
260-SL PROGRAM ABLATIVE NOZZLES

1. Introduction

The cure cycles used prior to the program subtasks were based on apparent success or failure in molding of small nozzle components; therefore, a technology had not been developed for preforming and curing the large nozzle components up to 6-in. thick. Since random success of components for the 260-SL nozzle could not be tolerated, the development of adequate cure cycles was necessary. This required the determination of a relationship between the elements (pressure, temperature, and time) of a cure cycle in relation to: (1) the heating response of the pressure vessel to be used, (2) thermal diffusivity of the ablative plastic during polymerization, (3) resin advancement, and (4) thermal conductivity of pressure bags, bleeder cloth, and steel mandrels. Considering the above parameters, a preliminary cure cycle was determined. The preliminary cure cycle was subsequently modified, using data obtained from laboratory test, and the cure cycles were determined for use in molding the 260-SL nozzles.

The studies conducted in the accomplishment of this subtask were as follows:

- a. Determination of the properties of the prepreg ablative materials.
- b. Preliminary determination of cure cycle.
- c. Determination of curing rate of MX-4926 ablative material.
- d. Densification and heat transfer characteristics of thick ablative laminates.
- e. Theoretical heat transfer analysis.
- f. Analysis of stresses created during cure.
- g. Determination of final predicted preform and cure cycles.

VI, C, Subtask III - Development of Cure Cycles for the  
260-SL Program Ablative Nozzles (cont.)

2. Program

a. Determination of Raw Material Properties of  
Ablative Materials

The purpose of this task was to establish acceptability of the MX-4926 and FM-5131 raw materials purchased for use in this subtask. The property tests performed for acceptance were as follows:

<u>Property</u>	<u>Specification</u>
Resin Solids	Tap-Dap-103A
Volatiles	Tap-Dap-102A
Degree of Polymerization	Tap-Dap-104A
Acetone Extraction	ASTM-D-494
Material Thickness	---
Infrared Index	Fiberite Method I-3
Gel Time	(See Subtask I)
Flow	Tap-Dap-105A
Tack	Tap-Dap-115A
Formability (Drape)	Tap-Dap-114

b. Preliminary Determination of a Cure Cycle

The purpose of this study was to assume a typical molding cycle used during bag preforming and curing of ablative components, separate the cycle into zones, and establish studies and tests necessary for evaluating the preliminary cure cycle.

VI, C, Subtask III - Development of Cure Cycles for the 260-SL Program  
Ablative Nozzles (cont.)

c. Determination of Curing Rate of MX-4926 Ablative  
Material

The object of this evaluation was to determine resin advancement (degree of cure) of MX-4926 vs exposure time at  $300^{\circ} \pm 10^{\circ}\text{F}$  by performing acetone-extraction and volatile-content tests at various increments of exposure time.

This evaluation refined the data obtained in Subtask I and provided a basis for comparison of acetone-extraction values with those obtained in other studies of this subtask.

The test consisted of subjecting 4-ply (4 by 4 in. square) specimens, wrapped in cellophane, to a platen pressure of 50 psi and  $300^{\circ}\text{F}$  temperature for durations of 1, 2, 5, 10, 20, and 30 min. Approximately 10 grains of shavings from each specimen were used to obtain acetone extraction and volatile content.

d. Densification and Heat Transfer Characteristics of  
Thick Ablative Laminates

The objective of this test was to determine the time and temperature conditions required to achieve optimum densification of MX-4926 and FM-5131 tape-wrapped structures under a 1000 psi pressure at preforming temperatures of 150 to  $180^{\circ}\text{F}$  and curing temperatures of 250 to  $300^{\circ}\text{F}$ . From the data obtained from this test, several material curing parameters were obtained as follows:

(1) Heat transfer properties of uncured material up to  $180^{\circ}\text{F}$  and transient thermal characteristics during cure at 250 to  $300^{\circ}\text{F}$ .

VI, C, Subtask III - Development of Cure Cycles for the 260-SL Program  
Ablative Nozzles (cont.)

(2) Density obtainable at various preform and/or curing temperatures.

(3) Polymerization characteristics as a function of time and temperature.

(4) Development of data necessary to establish hydroclave curing cycles as a refinement to the preliminary cure cycle.

The test procedure used involved preforming and curing a cylindrical layup of die-cut ablative material, 4-in. in dia and 280 plies in thickness, by the application of heat from one surface only and perpendicular to the laminations. Thermocouples were inserted between laminates to monitor heat transfer through the specimen. The test method and special compression mold is described in detail in Appendix B. The following tests were performed on specimens taken at various locations in the component: specific gravity, acetone extraction, volatile content, DMF extraction, and degree of polymerization. The test methods are described in Appendix A.

e. Theoretical Heat-Transfer Analysis

The object of this evaluation was to establish a theoretical heat-transfer analysis for determination of cure cycles for thick ablative components during preforming and temperatures of up to 300°F for final cure. The thermal analysis was based on the temperature gradient through the material. This data was obtained by embedding thermocouples at various depths in the ablative material. This permitted the calculation of the diffusivity of the ablative material during resin advancement. Additionally, the heat exposure to the material is dependent on the maximum heat capacity of the hydroclave which was calculated using data from thermocouples within the 130-in. TRW hydroclave.

VI, C, Subtask III - Development of Cure Cycles for the 260-SL Program  
Ablative Nozzles (cont.)

f. Analysis of Stresses Created During Cure

The objective of this study was to determine the magnitude of stresses developed in ablative plastics in curing at 300°F and subsequent cooling to ambient temperature. The study evaluated four processing conditions which produce internal stresses in the ablative part as follows:

- (1) Internal thermal stresses due to temperature gradients within the part.
- (2) Interaction of steel mandrel and ablative plastic material due to differential thermal expansion of the two materials during preforming and cure.
- (3) Interaction of mandrel and ablative plastic material due to shrinkage of the plastic during polymerization of the resin.
- (4) Interaction of mandrel and material due to hydroclave pressure.

g. Determination of Final Predicted Cure Cycles

The results of the above subtasks were used in the development of analytical preform and cure cycles which would be verified in the fabrication of the half-length 120-SS-1 throat described in Subtask IV.



VI, C, Subtask III - Development of Cure Cycles for the 260-SL Program  
Ablative Nozzles (cont.)

3. Results

a. Determination of Raw Material Properties of the  
Ablative Materials

The raw material properties of the MX-4926 and FM-5131 materials employed in this subtask were determined and are presented in Figure 160. The properties met specification requirements.

b. Determination of a Preliminary Cure Cycle

The determination of a preliminary cure cycle was based on previous experience obtained in the cure of small nozzle parts. The cycle was separated in A, B, C, D and E zones for evaluation (Figure 161).

(1) Zone A (Initial Heat-up Cycle)

The start of this cycle from ambient to the predicted maximum of  $165 \pm 10^{\circ}\text{F}$  is dependent on the heat capacity of the hydroclave or autoclave, temperature differential within the bagged tapewrap component, and the maximum temperature required without incurring excessive resin advancement as discussed in Subtasks I and II. The above relationships were determined in subsequent studies. The initial pressure of 200-psi hydroclave water pressure was selected to proof test the bag, thermocouple fittings, and vacuum line piping for leakage, and allow entrapped air and/or volatiles to be removed by the vacuum system. The pressure was increased in Zone A to 1000 psi when the center of the tape-wrapped component reached  $155 \pm 5^{\circ}\text{F}$ .

VI, C, Subtask III - Development of Cure Cycles for the 260-SL Program  
Ablative Nozzles (cont.)

(2) Zone B (Heat-up Cycle)

This cycle was predicted to accomplish 90 to 100% debulk of the tape-wrapped laminate as the temperature of the laminate center increases to  $165 \pm 10^{\circ}\text{F}$ . The time required to accomplish total debulk was determined from the results of resin advancement, and debulk evaluation studies in Subtask I and the total time allowed would determine the start of the initial cure cycle (Zone C). Thermal analysis was used for this determination.

(3) Zone C (Preliminary Cure Cycle)

The temperature rise from  $165 \pm 10^{\circ}\text{F}$  to final cure at  $300 \pm 10^{\circ}\text{F}$  was required to be controlled to a surface-to-center temperature differential ( $\Delta T$ ) of  $10^{\circ}\text{F}$  to enable uniform polymerization (resin advancement). The time required to effect a controlled preliminary cure cycle was predicted by thermal analysis.

(4) Zone D (Final Cure Cycle)

The final cure cycle starts after the surface of the laminate reaches  $310^{\circ} \pm 10^{\circ}\text{F}$  and the center reaches  $290^{\circ}\text{F}$ . Subsequently, 2 hr were arbitrarily added to the cure cycle to ensure complete polymerization. The time for the center portion of the component to reach  $290^{\circ}\text{F}$  was predicted by thermal analysis.

(5) Zone E (Cool-Down Cycle)

During cool-down, the temperature should be decreased while maintaining full molding pressure to minimize internal thermal stresses. A study is required of the differences in thermal contraction of

VI, C, Subtask III - Development of Cure Cycles for the 260-SL Program  
Ablative Nozzles (cont.)

the mandrel and the component during cool-down. The rate of cool-down would also be determined and is related to the cooling capacity of the hydroclave or autoclave.

c. Determination of Curing Rate of MX-4926 Ablative Material

The degree of polymerization\* and volatile content vs exposure time at 300°F for MX-4926 are presented in Figure 162. The data indicate that significant advancement occurs in 3 min, advancement is 94.6% within 5 min, and 99% after 10 min at 300°F.

d. Densification and Heat-Transfer Characteristics of  
Thick, Ablative, Laminate-Section Laminates

The results of the densification and heat transfer tests of MX-4926, and FM-5131 are presented as follows:

(1) Specimen 1 (MX-4926)

Specimen 1 was subjected to 180°F for 278 hr. The test of this laminate was complicated by several discrepancies in the temperature-recorder readings. The problem was attributed to failure of the 38 gage thermocouple wire in the laminate. Larger wire was used in subsequent tests.

The data obtained, shown in Figure 163, was retained for comparison with subsequent test data.

---

\*Degree of Polymerization, % =  $100 - \frac{\text{Percent Acetone Soluble Material} \times 100}{\text{Percent of Resin Solids}}$

VI, C, Subtask III - Development of Cure Cycles for the 260-SL Program  
Ablative Nozzles (cont.)

(2) Specimen 2 (MX-4926)

This test subjected 280 plies of MX-4926 to a 180°F temperature until densification ceased. The laminate was cooled and Segment A was removed and its specific gravity was determined to be 1.425 in comparison to an ultimate molded specific gravity of 1.44. Segment A was then repositioned and the entire laminate was exposed to 300°F for 4.66 hr. The results of this test show attainment of 1.44 for Segment A decreasing through the laminate to 1.38 for Segment D. Acetone extraction was 0.40% for Segment A, increasing to 18.72% for Segment D. The properties of the specimen after 300°F cure are shown in Figure 164.

The temperature gradients throughout the test specimen are shown in Figure 165.

(3) Specimen 3 (FM-5131)

The laminate was composed of 80 die-cut plies which resulted in a molded thickness of 2.11 in. A temperature of 180°F was planned for the hot side of the laminate; however, the temperature reached 210°F within 5 min and was reduced to 180°F for the balance of the heating cycle. The properties of Specimen 3 are shown in Figure 166.

The specific gravity of the laminate varied from 1.63 to 1.65, or approximately 92% of ultimate density.

The acetone extractables, indicating resin advancement, varied from 23.20% for Segment A to 26.65% for Segment D as compared to the as received preimpregnated resin content of 34.9%.

VI, C, Subtask III - Development of Cure Cycles for the 260-SL Program  
Ablative Nozzles (cont.)

The temperature gradients throughout the test specimen are shown in Figure 167. A malfunction in the control of heat input was noted during the initial 100 min of the cycle which required retest of the preform cycle (Specimen 4).

(4) Specimen 4 (FM-5131)

Specimen 4, composed of 80 plies of FM-5131, was subjected for 50 min to 180°F and for 165 min to 800°F, similar to the cure cycles predicted for molding of the 120-SS-1 half-length throat and the large rocket components. The properties of Specimen 4 are shown in Figure 168.

The specific gravity of the specimen was 1.70 for Segment A and decreased to 1.66 for Segment D.

The resin advancement, as measured by acetone extraction, was 1.60% for Segment A, and increased to 17.10% for Segment D.

The temperature gradients throughout the test specimen are shown in Figure 169. The data indicate evidence of an exothermic reaction between 60 and 80 min. Since the specimen was heated at the outer-face of Segment A, Segment D was the coldest portion of a thick laminate or typical of the center of a nozzle ablative component.

e. Theoretical Heat Transfer Analysis

(1) The mathematical heat transfer model developed for determination of cure cycles for ablative components is presented in the following discussion. The mathematical model is based on the heat conduction equation (1) below:

VI, C, Subtask III - Development of Cure Cycles for the 260-SL Program  
Ablative Nozzles (cont.)

$$\frac{d}{dr} \left( K \frac{dT}{dr} \right) + \frac{K}{r} \frac{dT}{dr} = \rho C_p \frac{dT}{dt} \quad \text{Eq. (1)}$$

where:     K     = thermal conductivity  
            r     = radius  
            ρ     = density  
            C<sub>p</sub>    = specific heat  
            T     = temperature  
            t     = time  
            α     = thermal diffusivity =  $\frac{K}{\rho C_p}$

In a modified form, equation (1) can be written as:

$$\left( \frac{1}{r} + \frac{1}{K} \frac{dK}{dr} \right) \frac{dT}{dr} + \frac{d^2 T}{dr^2} = \frac{1}{\alpha} \frac{dT}{dt} \quad \text{Eq. (2)}$$

If the temperature gradients  $\frac{dT}{dr}$ ,  $\frac{d^2 T}{dr^2}$  and  $\frac{dT}{dt}$  are known, i.e., by thermocouple data in various depths of the material under consideration, then manipulation of equation (2) permits the calculation of α. For ease of calculation the above mathematical model was programmed on a 7070 IBM computer.

The thermal diffusivity values of the ablative materials at various temperatures during preforming and cure are shown in Figures 170 and 171. There is considerable scatter in the data which required fairing of the resulting curves. The diffusivity of MX-4926 decreases from 0.080 sq ft/in. at 70°F to 0.025 sq ft/in. at 100°F, remaining constant between 100 and 140°F.

VI, C, Subtask III - Development of Cure Cycles for the 260-SL Program  
Ablative Nozzles (cont.)

The diffusivity of FM-5131 has a fairly constant value of 0.010 sq ft/in. between 80 and 200°F, increases rapidly to 0.025 sq ft/in. at 240°F, and decreases slightly to 0.020 sq ft/in. at 280°F. This abrupt change in diffusivity between 200 and 240°F indicates a possible existence of an exotherm in the material during the cure cycle.

The hydroclave maximum heat capacity can be expressed by equation (3) below:

$$T = T_{s_{av}} \frac{(K-1)}{K} + \frac{T_o}{K} \quad \text{Eq. (3)}$$

where:  $T_{s_{av}}$  = average temperature of steam in hydroclave heat exchanger  
 $T_o$  = starting temperature of water in hydroclave  
 $T$  = hydroclave water temperature at any time

$$K = e^{\frac{\theta_m}{W}} \left[ \frac{\left( \frac{UA}{C_{p m}} \right)}{e^{\frac{UA}{C_{p m}}} - 1} \right]$$

$m$  = water circulation rate

$$W = W_{H_2O} + W_{steel} \left( \frac{C_{p steel}}{C_{p H_2O}} \right) \sum_{i=1}^i \left( \frac{W_i C_{pi}}{C_{p H_2O}} \right)$$

$W$  = weight

$A$  = effective heat-transfer area in hydroclave heat exchanger

$U$  = overall heat-transfer coefficient in hydroclave heat exchanger

VI, C, Subtask III - Development of Cure Cycles for the 260-SL Program  
Ablative Nozzles (cont.)

Thermal properties of the ablative plastic composites were determined on the basis of these mathematical relationships and recorded thermocouple data from the close-die thick laminates. Equation (3) was used in predicting the heat-up characteristics of the 130-in. hydroclave and autoclave cycles. These predictions are plotted as smooth solid-line curves and compared with experimental data points in Figure 172.

f. Analysis of Stresses Created During Cure

The analysis of the stresses created during cure consisted of a relatively simplified and cursory evaluation of an exit cone insert. Detailed analyses could not be conducted due to lack of material property data at various temperatures and during various stages of polymerization. The simplification of the analysis rendered the results inconclusive. Additional analysis in conjunction with experimental work is recommended.

g. Determination of Final Predicted Preform and Cure Cycles

The final predicted preform and cure cycles were determined from data obtained from Subtasks I and II and previous studies in this subtask. Parameters utilized included ablative material characteristics, processing methods, and hydroclave heating response. The analytical preform cure cycles, as determined for the 120-SS-1 half-length throat, are shown in Figures 173 and 174. The cycles were separated into zones representing phases in the cycles which are discussed below.



VI, C, Subtask III - Development of Cure Cycles for the 260-SL Program  
Ablative Nozzles (cont.)

(1) Preform Cycle

(a) Zone A - Initial Phase of Preform Cycle

The maximum allowable temperature in the initial phase of the preform cycle Zone A, was determined in Subtasks I and II to be 180°F for all the ablative materials. The time required to reach 180°F is 1.5 hr as determined from the thermal analysis, employing the heat capacity of the hydroclave and the temperature differential for the specific bagged component.

(b) Zone B - Preform Zone

Zone B is that portion of the cycle where the component surface is maintained at 180°F while the interior temperature of the component is increased to 165°F min. The time required was 3.5 hr, which does not advance the resin appreciably.

A thermal diffusivity of 0.01 sq ft/hr for MX-4926 was used in the thermal analysis rather than the 0.025 sq ft/hr value calculated in the computer program. The lower diffusivity value was used to permit a longer preform cycle to ensure obtaining maximum debulk.

(c) Zone C - Preform Cool-Down Zone

The component temperature is reduced to 100°F within 3 hr in the cool-down portion of the preform cycle while maintaining the 1000-psi hydroclave pressure. This cool-down rate permitted the component to be cooled without incurring high internal stresses.

VI, C, Subtask III - Development of Cure Cycles for the 260-SL Program  
Ablative Nozzles (cont.)

(2) Cure Cycle

(a) Zones A and B - Heat-up Zone

Zones A and B of the cure cycle are identical to Zones A and B of the preform cycle. This portion of the cycle raises the temperature of the component to 180°F prior to final curing.

(b) Zone C - Initial Cure Zone

The initial cure cycle consists of raising the temperature of the component from heat-up condition to 300 to 310°F.

(c) Zone D - Final Cure Zone

During final cure, the component temperature is maintained at 300 to 310°F for 1.66 hr to achieve complete cure.

(d) Zone E - Cool-Down Zone

During cool-down the component temperature was reduced at a rate of 30°F/hr while maintaining full cure pressure. The component temperature reduces to 150°F in approximately 4.5 hr.

4. Conclusions

The conclusions obtained from the studies conducted in Subtask III are as follows:

VI, C, Subtask III - Development of Cure Cycles for the 260-SL Program  
Ablative Nozzles (cont.)

a. Material properties and curing characteristics of MX-4926, FM-5131, and MX-2646 were determined and reconfirmed to the data obtained in previous studies.

b. Cure cycle parameters were developed for large ablative components made with MX-4926, MX-2646, and FM-5131.

c. Preform and cure cycles were determined and verified for the 120-SS-1 half-length throat insert.

d. Cure cycles for all nozzle components in the program were developed by the above proven methods.

D. SUBTASK IV - DEMONSTRATION OF HALF-LENGTH 120-SS-1 THROAT  
FABRICATION

1. Introduction

The purpose of this subtask was to tape wrap, cure, and destructively test a throat module of the same size and material as that planned for the 120-SS-1 nozzle except that its length was half that of the 120-SS-1 throat. This throat sample enabled the evaluation of wrapping problems that occur in wrapping a highly oriented, thick-walled cylinder of high OD to ID ratio with bias tape. Previously, these factors made difficult the achievement of high debulk, proper orientation, and a satisfactory, wrinkle-free nozzle component.

Further, Subtask III provided data to define the pertinent material characteristics necessary to accurately predict the preforming and final curing behavior of the materials used. Tests of the instrumented throat provided data for a comparison between the predicted cure schedule, developed

VI, D, Subtask IV - Demonstration of Half-Length 120-SS-1 Throat  
Fabrication (cont.)

by a computer using data provided by Task III, and the actual behavior of the component during the cure process.

Once the component was cured, physical tests were conducted to obtain data for the determination of realistic value ranges, and a practice bonding of the component to a sample section of the nozzle shell was accomplished.

Another objective was the radiographic examination of deliberately located defects in the completed component. However, this objective was deleted from the 260-SL program and was conducted under a separate Rocket Propulsion Laboratory (RPL) program.

2. Program

The half-length throat was wrapped on a 144-in. Betts vertical turret lathe (Figure 175). A fabrication sketch is shown in Figure 176.

The composite molding was constructed of two materials. The inner ablative wrap was MX-4926, and the outer insulative wrap was FM-5131. The raw material properties of MX-4926 and FM-5131 are shown in Figure 177.

An experimental chute used to feed the tape onto the mandrel (Figure 178) was not satisfactory. A three-roller, feed-tensioning device was tried, but did not accept the sewn tape splices smoothly and also caused an excessive width reduction in the bias tape just prior to the debulk roller. As a result, the bulk of the part was made by manually feeding the tape under the single debulking roller. Heat guns were used during wrapping as shown in Figure 179.

VI, D, Subtask IV - Demonstration of Half-Length 120-SS-1 Throat  
Fabrication (cont.)

Both cylindrical and conical single debulk rollers were tried, using a constant wrapping speed of approximately 6 ft/min. The conical roller (Figure 180) was used more successfully in minimizing wrinkles which, however, were not completely eliminated. A typical wrinkle is shown in Figure 181.

The MX-4926 tape was wrapped onto a mandrel. The predicted wrapping parameters are shown in Figure 182. Wrapping was followed by a hydroclave preform cycle. The predicted preform cycle is shown in Figure 173. This preform cycle did not cure the material but brought it to maximum density. The MX-4926 was overwrapped with FM-5131 and then fully cured in the hydroclave. The predicted final cure cycle is shown in Figure 174. The thicknesses of the MX-4926 and FM-5131 materials were 3.5 and 1.25 in., respectively. The half-length throat was adequately instrumented so that complete temperature profiles were obtained throughout the thickness of the laminate. It was possible to substantiate the thermal analysis derived from laboratory experiments with these data. It was not possible to determine thermal properties in a heat flow direction parallel to the plies of the laminate in the closed-die tests; however, it was possible to adjust the thermal properties to compensate for fiber orientation effects.

Data on tape temperature, part length, and laminate orientation were obtained during wrapping in which the calculations on debulk, neck-down, tape wander, etc. were based.

During the wrapping of the MX-4926, a number of defects was intentionally introduced. The object was to evaluate nondestructive detection systems against these known defects. Figure 183 shows the area of placement of one of the defects, a resin-rich area. Figures 184 and 185 show areas of placement of all other defects. The quadrant containing the defects was later inspected radiographically under a separate RPL program.

VI, D, Subtask IV - Demonstration of Half-Length 120-SS-1 Throat  
Fabrication (cont.)

After final curing, the part was finish-machined, primed, and bonded to the steel shell with Epon 913. The shell had been previously primed with Fuller 162-Y-22. The bond was cured at  $145 \pm 10^{\circ}\text{F}$  for 7 hr; the temperature then was reduced to  $110^{\circ}\text{F}$  and held constant for 2 hr, and finally cooled to ambient temperature.

3. Results

A comparison between the predicted wrapping parameter ranges and those actually achieved in wrapping the MX-4926 are shown in Figure 182. As indicated, some deviation occurred. This was the result of operator adjustments necessary to accommodate changes in material wrapping quality, shifts in heat buildup, and variations in environmental conditions.

The ply debulk achieved during wrapping is shown in Figure 186. These data were calculated from measurements taken during wrapping. Differential height readings were taken at points 1 in. from the OD of the mandrel. Calculations for ply thickness were corrected for the 15-degree angle so that actual ply thickness is reported.

The percent debulk was calculated as follows:

$$\% \text{ Debulk} = \frac{\text{Thickness of ply at 1000 psi}}{\text{Thickness of ply obtained}} \times 100$$

A molded 1000-psi thickness of 0.013 in. was used throughout the demonstration.

The actual ply thickness ranged from 0.023 to 0.015 in. corresponding to a debulk ranging from 57 to 87%. Original planning predicted that a debulked thickness of 0.017 in. would be accomplished. No correlation was observed between the material characteristics, tape width, or use of cylindrical or conical roller and high debulk percentages.

VI, D, Subtask IV - Demonstration of Half-Length 120-SS-1 Throat  
Fabrication (cont.)

Two serious problems encountered were tape wandering and neck-down. Neck-down was caused by deformation of the bias tape as it was distorted to conform to the configuration of the mandrel. The wandering was caused by the difficulty of feeding the material so that the inner edge was aligned with the mandrel OD.

During the wrapping of MX-4926, measurements were made of wrapped-tape width and the departure of the tape from the planned position in contact with the mandrel. Figure 187 shows the distribution of the distances between the 5-in. tape and mandrel. Fifty % of the distances were less than 0.2 in. from the mandrel and 90% of the distances were less than 0.5 in. The tape climbed the mandrel as much as 0.1 in. in three instances. This is indicated on the negative portion of the ordinate.

Distribution of wrapped widths and percent reduction (neck-down) during application of the 4- and 5-in. tape is shown in Figure 188. The neck-down of the 4- and 5-in. tapes was similar, ranging from 12 to 30%.

The actual preform cycle on the 120-SS-1 half-length throat is given in Figure 189. The component temperatures achieved the preform temperature range much faster than predicted (Figure 173). The coldest part reached 170°F in 150 min compared with the predicted time of 300 min. Therefore, it was possible to start the cool-down of the preform cycle after 200 min rather than at the predicted 500 min. The hydroclave water temperature reached preform temperature in 115 min; the predicted time was 80 min. However, a significant portion of this deviation was due to the low inlet water temperature (42°F) rather than the 78°F temperature value used in the heat-transfer analysis. Another factor contributing to the discrepancy was the conservative thermal diffusivity figures used in the computer program.

VI, D, Subtask IV - Demonstration of Half-Length 120-SS-1 Throat  
Fabrication (cont.)

It should be noted that the temperature record (Figure 189) indicates an exotherm taking place in the component. This exotherm resulted in an approximate 15°F temperature rise above the preform temperature for the hottest section of the component. This exotherm in a part of 5 in. in cross-sectional thickness is not considered serious and, in fact, actually is of some value as it helps to shorten the hydroclave cycle.

Also, no attempt was made to advance the cure of the resin. The plan was to achieve full debulk with as little resin advancement as possible.

After the preforming of the MX-4926, ring and machining chip samples were collected for analysis. The ring was removed from the extreme aft end. The following results were obtained from the analysis:

Specific gravity (water immersion)	1.32, 1.39, 1.44
Acetone extractables (ASTM-494), %	32.4, 32.3
Volatiles (20 min at 325°F), %	3.30, 3.29, 3.65, 3.20

As indicated, almost no resin advancement determined by acetone extraction was obtained. The specific gravity results vary quite widely, and were probably caused by the difficulty of determining the specific gravity by water immersion of a piece of the preform. Water absorption must be avoided, and the irregular surface leads to specimen buoyancy because of attached air bubbles. Another method, which determines the component volume by dimensional measurement before and after preforming and weighs the amount of material used, will be used in future tests.



VI, D, Subtask IV - Demonstration of Half-Length 120-SS-1 Throat  
Fabrication (cont.)

A steel end ring was used on the top of the wrapped cylinder during cure in the hydroclave. A length measurement before and after cure indicated a reduction in length of 2.200 in. With a total length of 10.188 in., a longitudinal debulk of 21.5% occurs in the hydroclave. This value does not include the radial debulk achieved. It was also apparent that length measurements after several days of storage did not indicate any longitudinal springback.

Because of neck-down and tape wander, the OD of the MX-4926 material was undersize on the ends after machining. As a result, 0.800 in. of FM-5131 had to be added to each end.

The predicted and actual FM-5131 tape-wrapping parameters are shown in Figure 190. The roller pressures used were high as compared to values obtained in Subtask I which indicated that a maximum of 300 lb/in. width at 120°F and a maximum of 200 lb/in. width at 150°F should be used. The use of roller pressure is dependent on the size of the roller "footprint", i.e., the total area of contact between the roller and the wrapping mass. The roller had a larger footprint; therefore, more pressure was required to obtain tack.

The ply thickness and the percent debulk (based on a 1000-psi pressure and a thickness of 0.026 in.) obtained when wrapping the FM-5131 tape is shown in Figure 191.

After overwrapping, the entire composite was final-cured. The actual cure cycle is given in Figure 192. The correlation between the actual cure cycle and that predicted (Figure 174) was excellent. An exotherm probably accounts for the deviation occurring after 250 min. The only other deviation from the predicted cure cycle was that approximately 70 min longer than estimated was required for the hydroclave temperature to reach 310°F. However, because of the exotherm, the coldest part of the component reached

VI, D, Subtask IV - Demonstration of Half-Length 120-SS-1 Throat  
Fabrication (cont.)

300°F in 450 min compared to the predicted 490 min. The deviation in heat-up time could be attributed to the quality of the steam passing through the heat exchanger, differing slightly from the value used in the calculations for the predicted cycle.

Radial measurements taken after cure indicate that a diametral debulk of about 21.5% occurred in the FM-5131 overwrap during cure assuming that the MX-4926 substrate did not undergo additional debulk.

Rings were machined from both ends of the cylinder and tested. A summary of the test results is shown in Figure 193. Although much difficulty was encountered in determining ply orientation in machining the specimens, the results were quite uniform from end to end and around the circumference. The high shear values are attributed to ply misorientation in the specimens. The physical test results indicate a strong, sound, well-cured component.

The center of the throat module that had been bonded into the steel shell was sectioned for examination. When the first radial cuts were made the ring closed, indicating internal stresses.

Figure 194 shows the bonded steel shell broken away from the OD of the plastic. About 75% of the fractured bond face is represented by a failure in the FM-5131 laminate; the other 25% of the fractured face indicates a cohesive failure within the adhesive layer itself. These observations indicate a properly prepared and cured joint.

Figures 195 through 197 show three cross sections of the half-length throat at 120-degree stations. The small, separate section shown in Figure 196 was removed to accomplish a better polish. The irregular line at the left of Figure 197 is in the MX-4926 cloth segment and is the result of a separation induced by placing a sheet of Mylar film in the cloth during tape

VI, D, Subtask IV - Demonstration of Half-Length 120-SS-1 Throat  
Fabrication (cont.)

wrapping to illustrate its orientation. As indicated by the three sections, the as-wrapped orientation of the plies was not maintained during cure. Additional debulking experienced during cure caused this orientation change. Orientation measurements of the MX-4926 cloth near the FM-5131 interface (Figure 196) show an orientation of 73.5 degrees from the center line, which is within the specification limits of 67.5 to 75 degrees to the center line.

Due to difficulty of polishing the MX-4926 cloth pieces, Figures 195 through 197 do not show a series of small interlaminar cracks which exist in the carbon component near the silica-carbon interface. These cracks do not extend through to the ID; the ID section is free of cracks. The cause of these cracks is not known, although they may have been caused by the restraint offered by the FM-5131 cloth to the edges of the MX-4926 laminae during cooling after cure. This is possible because of the large difference in coefficients of thermal expansion between the materials and between the axes of anisotropy of the MX-4926 laminate. The thermal expansion coefficient of a laminate, measured perpendicularly to the plies, may be over 10 times that value measured along the axis parallel to the wrap threads.

Another unexplained phenomenon is the presence of tiny black areas shown on the surface of the sectioned part as illustrated in Figure 198. When examined under the microscope and probed with a sharp instrument, these tiny spots deform in the manner of a tar-like substance. These are not considered to be uncured resin, because the acetone extraction tests indicate satisfactory cure. One possible explanation might be that they are small local concentrations of resin filler material.

Another interesting phenomenon can be observed in the cross-sectional views magnified 10X or greater (Figures 198 through 202). Throughout the entire section, flattened plies can be seen, with almost rectangular

VI, D, Subtask IV - Demonstration of Half-Length 120-SS-1 Throat  
Fabrication (cont.)

fiber bundles, and little or no ply intermingling. When compared to other more normal areas of this part and others, the fiber bundles appears to have been ruptured. The exact cause of this and its significance is not known.

In Figure 198, two circles show a normal area and one exhibits the flattened plies. Figures 199 and 200 show the flattened plies at higher magnifications. Figures 201 and 202 show normal sections of the throat at the same high magnifications.

4. Conclusions and Recommendations

Construction of the half-length throat fulfilled its major objectives as follows:

a. Difficulties encountered while tape wrapping bias-cut MX-4926 tape with a high OD or ID ratio were determined.

b. Corroboration of the data developed to define material behavior through cure. The final cure of the half-length throat was successfully predicted within very narrow limits. The use of these data with the computer program enabled short, precise, safe schedules for subsequent hydro-clave preform and cure operations.

c. Practical physical property limits were established for these materials in the finished part. The interlaminar shear values were high because of orientation difficulty, but other property values were acceptable. The repetitive shear testing permitted much to be learned about this type of specimen.

VI, D, Subtask IV - Demonstration of Half-Length 120-SS-1 Throat  
Fabrication (cont.)

d. Recorded data and observations made indicate that additional work is required in the following areas of bias tape wrapping:

(1) A device is required to pre-stretch the bias tape to the required curvature.

(2) Analytical work is required to exactly define the acceptable maximum OD to ID ratio for each material.

(3) A device is required to ensure accurate placement of the tape on the wrapped mass as the material is applied.

(4) Additional work is required to increase the debulk achieved and ensure uniform debulk throughout the part. This can be accomplished in part through continuing efforts in material characterization in relation to a particular wrapping system; however, to be completely effective, this depends on the development of a stable, optimized mechanical wrapping system.

VII. SPECIFICATIONS

A. MATERIAL SPECIFICATIONS

Specifications were prepared by Aerojet to provide quality control of materials used in the fabrication of the nozzle and exit-cone assemblies. The specifications defined in detail the physical and mechanical properties of both the B-staged and the cure materials. Qualification tests and sampling plans were defined for the following properties: resin solids, volatiles, laminate flow, tack, drape, specific gravity, flexural strength, tensile strength, interlaminar shear, thermal conductivity, fabricability index, storage, and shelf life. Proper conformance to the specifications ensured uniform and well defined basic materials. Each material was qualified to the requirements defined in the specification and was tested for acceptance prior to use based on a rigid sampling plan defined in the specification. The disposition of material that did not conform to the specification requirements was accomplished by Material Review Board action.

The specifications used for the ablative plastic materials were: AGC-34306, Type I, Molding Tape, Carbon Fabric, Impregnated Phenolic Resin, for MX 4926 carbon cloth and phenolic; and AGC-34312, Molding Tape, Silica Fabric, Impregnated, Phenolic Resin, Types I and II, for MX-2646 and FM-5131 silica cloth and phenolics, respectively.

Adhesive and sealant material specifications used were:

AGC-34076, Compound, Sealing, Silicone Rubber Base,  
Thixotropic

AGC-34151, Adhesive, Epoxy Paste with Amine Curing Agents

AGC-34323, Adhesive Film, Supported, Structural Bonding

AGC-34335, Potting Insulation, Epoxy Polysulfide,  
Acrylonitrile Butadiene Copolymer, Ambient Curing

AGC-34345 Primer, Epoxy Resin, Corrosion Inhibitive

VII, A, Material Specifications (cont.)

Material specifications which were used to control the external insulation system for the exit-cone assembly included the following:

- AGC-34238 Cork, Sheet
- AGC-34310 Adhesive, Cork Bonding
- AGC-34305 Coating, Protective, Cork
- AGC-34308 Potting Compound, Epoxy, Cork Filled
- AGC-10758 Resin, Epoxy, Epichlorohydrin-Bisphenol A Type  
Low and Medium Viscosity

All other materials were in accordance with military specifications as specified on the drawings.

B. IN-PROCESS SPECIFICATIONS

Three basic Aerojet process specifications were used in the fabrication and assembly of the nozzle and exit-cone assemblies. Specification AGC-36413, Nozzle Components, Tape Wrapped, Phenolic Fabric, Process Control of, defined the in-process and quality control measures used during tape wrapping of the nozzle plastic components. The process control specification was used with the fabrication drawing and specified the in-process controls and the physical and mechanical property requirements applicable to raw material and the final component, tests to verify the required properties, acceptance criteria, and log book records of the entire process. The in-process controls were defined in a manufacturing outline that included the following:

1. Tape temperature and roller pressure.
2. Predicted as-wrapped profile before and after debulk or cure.
3. Description of equipment used in debulk and cure cycles.
4. Location of thermocouples in the billet.
5. Predetermined debulk and cure cycles.

VII, B, In-Process Specifications (cont.)

6. Summaries of actual pressure and temperature cycles during each operation.
7. Tape-wrap feed velocity.
8. Test specimen location and orientation.
9. Description of the manufacturing sequence.

The physical and mechanical properties controlled and verified included specific gravity, microtensile strength, acetone extraction, volatile content, and interlaminar shear.

Final qualification of the component consisted of visual and radiographical examinations for flaws, delamination, and inclusions. The specification required that the supplier provide product engineering drawings and a manufacturing outline for Aerojet review prior to initiation of fabrication. After completion of fabrication, physical and mechanical properties of the component were required to be within acceptance limits of the specification.

The specifications for assembly of the nozzle and exit cone are AGC-36422, Nozzle Assembly, Process Control of, and AGC-36400, Exit Cone Assembly, Process Control of, respectively. These specifications defined the adhesive and sealant materials that were used and the surface preparation requirements for bonding. The supplier was required to describe the bonding process which was submitted to Aerojet for review prior to assembly bonding. Integrity of the bond was determined by ultrasonic inspection and by destructive testing of sample specimens. The assemblies were leak tested after completion of bond cure cycles in accordance with Aerojet procedures. The supplier was required to provide a log book for each assembly. The log book contained raw material test data, pressure and temperature variation vs time during each cycle cure, manufacturing procedure data, physical and mechanical property test data, inspection records, and all Supplier Discrepancy Action Reports.



VII, B, In-Process Specifications (cont.)

Second tier Aerojet process Specifications are referenced in the three basic process specifications. These specifications defined the method for surface preparation, leak detection, primer application, and adhesive cure associated with the nozzle and exit-cone assembly. These specifications were:

- AGC-13842 Bonding, Surface Preparation
- AGC-36072 Priming, Corrosion Inhibitive
- AGC-36180 Adhesive, Curing of
- AGC-36425 Leak Detection, Methods of
- AGC-36434 Chamber Surface, Cleaning and Priming
- AGC-36433 Epoxy Adhesive, Use and Care of
- AGC-36394 Cork, External Insulation, Installation of

## VIII. FABRICATION

Fabrication of the ablative components and assembly of the nozzle were performed by TRW. The nozzle shell and rubber insulation were fabricated by Sun Shipbuilding and Goodyear, respectively, and are discussed in separate phase reports.

### A. 260-SL-1 NOZZLE

#### 1. Nozzle Plastic Components

The nozzle plastic components were fabricated in accordance with procedures that met the design and quality control requirements defined in the design and fabrication control drawing No. 600260 and process specification AGC-36413. On the basis of these requirements, a detail fabrication plan for each component was established by the subcontractor and defined in a manufacturing outline, fabrication drawings, and specifications. In-process tests and inspections were conducted in accordance with the drawing and specification requirements as discussed in Section IX.

The fabrication plan was essentially the same for the entrance, throat, and throat-extension inserts of the nozzle. The ablative surface of the liner was tape wrapped on a mandrel to the necessary laminate orientation angle. Tape wrapping of the entrance insert is shown in Figure 203. The liner was vacuum bagged and preformed in a hydroclave at a temperature of 180°F and 1000 psi pressure. The preformed liner was then machined on the outside diameter and overwrapped parallel-to-part with silica cloth tape to the required thickness. The composite insert was vacuum bagged (Figure 204) and final cured in a hydroclave at a temperature of 300°F and 1000-psi pressure. The cured composite was machined on the outside diameter and ends to mate with the nozzle shell and adjacent components.

VIII, A, 260 SL-1 Nozzle (cont.)

Deviations from the above fabrication procedures and discrepancies from the design requirements are delineated as follows for each plastic component:

a. Entrance Insert

The design OD at the forward end of the insert exceeded the diameter that the hydroclave could process. A reduction of 0.3 in. radially was necessary. This area was subsequently filled and built to the initial configuration with glass roving impregnated with room-temperature-curing epoxy resin.

A machining error resulted in a 0.5-in. undercut over a 1-in. length on the outer surface of the preform at the 90-in. dia. The undercut was filled by parallel wrapping MX-4926 carbon cloth tape which was cured with the overwrap material.

A vacuum-bag leakage occurred during the preform cycle after 40 min at 1000 psi and 180°F. Physical property tests indicated normal volatile content and degree of advancement at both ends. The part was subsequently overwrapped and cured in an autoclave at 325 psi and 300°F.

The carbon-liner-to-silica-liner interface was shown by X-ray to be delaminated. No adverse effects were expected and no corrective action was necessary.

b. Throat Insert

The throat insert used on motor 260-SL-1 was the second component built. The initial insert was rejected because of high volatile

VIII, A, 260 SL-1 Nozzle (cont.)

content after a vacuum-bag failure during a hydroclave preform cycle. Subsequent drying and postcuring cycles were not effective in reducing the volatile content sufficiently.

During the preform cycle of the replacement throat insert, a vacuum bag leakage occurred after 2.25 hr, at which time the throat insert had reached a temperature of 172°F and 500 psi pressure. Physical property tests indicated normal volatile content and minimum degree of advancement. This component was subsequently preformed in an autoclave at 325 psi and 180°F, overwrapped with silica cloth, and final cured in an autoclave at 300°F.

A delamination was detected radiographically at a station 3 in. aft of the insert lip, extending 340 degrees circumferentially and radially from the ID to the overwrap. Also detected were several small delaminations located 4.5 to 7 in. aft of the insert lip and extending 30 to 45 degrees circumferentially and radially from the center of the liner to the overwrap. The overwrap was designed to prevent gas passage, and the delaminations were not considered to be detrimental to nozzle performance.

c. Throat Extension Insert

The initially fabricated throat extension insert was wrapped parallel to the nozzle center line. A circumferential delamination developed at the forward face of the insert after assembly to the shell. The delamination was located at the 75.25-in. diameter and extended the length of the laminate. Attempts to repair the delamination by injecting room-temperature-curing epoxy resin were unsuccessful. Since the laminate orientation was parallel to the nozzle center line, no mechanical restraint of the defective part was available in the event of insert-to-shell bond

VIII, A, 260 SL-1 Nozzle (cont.)

failure. The component was rejected and removed from the shell. A short ring section was also fabricated for possible replacement of the delamination portion but was not used.

The replacement throat-extension insert was tape wrapped with a 25 to 35 degree laminate orientation to the nozzle center line. The component was preformed and final cured under pressure in an autoclave.

Tag-end test specimens of the silica overwrap were not obtained from the aft test ring because of insufficient material.

2. Nozzle Assembly

The assembly of the inserts to the steel shell was in accordance with a procedure that conformed to the design and quality control requirements defined by design and fabrication control drawing No. 600260 and process specification AGC-36422. In this procedure, the plastic inserts were assembled to the nozzle shell in the following sequence: throat extension, throat, and entrance insert. After completion of assembly of the inserts, the internal contour was machined. The V-44 rubber insulation was then bonded in place with Epon 948 adhesive and vacuum-bag cured at ambient temperature. The forward face of the V-44 insulation was final-machined to the design configuration as shown in Figure 205.

Each insert to be assembled to the shell was dry-fitted, and shim thickness gages were used to determine the bondline thickness (Figure 206). O-rings were lubricated in accordance with MIL-L-4343 and installed in the O-ring groove. PR-1910 silicone rubber sealant was applied to the tapered interface gap between inserts. The insert and shell mating surfaces were coated with Epon 913 adhesive, assembled and positioned as the dry fit.

VIII, A, 260 SL-1 Nozzle (cont.)

The assembly was cured at room temperature for 72 hr. A deviation from this procedure was made because of the use of a replacement throat-extension insert. After bonding the initial throat-extension insert to the shell, a delamination was observed on the forward face of the insert. After attempts to repair the delamination failed, a replacement insert was fabricated. While the replacement part was being fabricated, assembly of the throat and entrance inserts to the shell was accomplished. The throat-extension insert was then removed by machining. The bonding surface was cleaned, inspected, and primed with Skydrol primer. The replacement throat-extension insert was final-machined and bonded to the shell by the normal procedure. PR-1910 was then injected into the joint between the throat insert and throat-extension insert. Following final inspection of the nozzle assembly, the internal surface of the plastic liner was sprayed with Skydrol 162Y22 primer.

Discrepancies observed during assembly of the plastic inserts were as follows:

The gap between the throat insert lip and the shell ranged from 0.003 to 0.011 in. instead of the required 0.000 to 0.006 in. Epon 913 was used on the forward face of the throat extension as part of the throat insert. The additional gap was acceptable.

Ultrasonic inspection of the throat insert-to-shell bond revealed two areas of unbondedness of 9 and 5.1%, respectively instead of 5% maximum. The total unbonded area was less than 1% of the total area. The discrepancy was acceptable.

VIII, A, 260 SL-1 Nozzle (cont.)

The Skydrol shell primer thickness was 0.0010 instead of 0.0004 to 0.0007-in. thick. This resulted in a 0.019 to 0.031 in. gap between the forward end of the extension insert and the throat insert instead of 0.000 to 0.006 in. The gap was filled with PR-1910 and was acceptable.

The samples of the extension insert-to-shell bond had lap shear values from 120 to 1800 psi (989 psi average), instead of 2300 psi minimum. The bond occurs in a low stress area and bond values were acceptable.

The bond gap of rubber shell was 0.026 to 0.096 in. instead of 0.002 to 0.050 in. The bond gap of rubber to plastic was 0.085 to 0.239 in. instead of 0.002 to 0.080 in. The gaps were filled with Epon 948 and were acceptable.

Minimum test values of shell-to-rubber bond with Epon 948 were 1000 psi instead of 1400 psi minimum. The discrepancy was acceptable.

The insulation step joint was 0.010 to 0.048 in. below the shell flange instead of 0.000 to 0.010 in. above the flange. The clearance was accepted.

Removal of the V-44 blocks from the face of insulation resulted in a gouge 3.5-in. long by 0.125-in. deep in one location. The gouge was repaired by Goodyear.

3. Exit Cone Plastic Liner

The exit cone plastic liner was fabricated in accordance with procedures that met the design and quality control requirements defined in the design and fabrication control drawing No. 600265 and process

VIII, A, 260 SL-1 Nozzle (cont.)

specification AGC-36413. On the basis of these requirements, a detail fabrication plan was established by the subcontractor. The fabrication plan was to tape wrap both MX-4926 and FM-5131 inner wrap materials parallel to the nozzle center line (Figure 207). The outside diameter was machined and the FM-5131 silica cloth tape was overwrapped parallel to part. The composite was tension wrapped with nylon tape, which applied an 85-psi pressure to the part initially. Longitudinal metal strips were used to prevent axial slippage of the nylon tape (Figure 208). The composite was then vacuum bagged and cured at 300°F temperature.

Discrepancies observed in the component were as follows:

The raw material flow and volatile content as obtained from a 90-day storage retest were somewhat out of tolerance. It was determined that sufficient tack was achieved at low (225°F) temperature to provide a satisfactory liner. The part was accepted.

Ultrasonic inspection revealed a delamination after cure, extending 1.65 in. below the surface of the forward end, through to the inner surface and 360-degrees circumferentially. A repair of the delamination was made by machining a 90-degree 0.100-in.-wide V-groove at the forward face of the delamination. The groove was filled with Epon 919, vacuum bagged, and cured. Subsequent inspection revealed that the epoxy did not penetrate beyond the forward groove of the delamination. It was decided to bond the exit cone assembly to the nozzle assembly instead of using a silicone rubber sealant in the gap. The delaminated piece would be held in place by the forward face since the ejection force in this zone is less than the bond shear strength. Gluing the gap between the exit cone and throat extension inserts eliminated the thermal expansion gap originally included in the design for relief of stresses



VIII, A, 260 SL-1 Nozzle (cont.)

induced during thermal growth. Although lack of the expansion gap could cause additional internal stresses, the joint is at a relatively low temperature and pressure region, and the effect from thermal expansion was considered to be slight. A second delamination extended from the inner surface at a plane 7 in. aft of the forward end and extending outward 1.5 to 3.0 in. and 360-degrees circumferentially. Repair was effected by injecting Epon 919 partially into the separation. No adverse effects from the defect was expected.

The specific gravity of MX-4926 carbon cloth was 1.37 compared with the minimum requirement of 1.38. This deviation was accepted because of its high interlaminar shear strength (2200 psi).

4. Exit Cone Assembly

The assembly of the exit cone honeycomb structure to the plastic liner was in accordance with procedures that conform to the design and quality control requirements defined by design and fabrication control drawing and process specification AGC-36400. The assembly consisted mainly of three bond cycles that successively built up the structural shell on the liner. Each bond cycle consisted of vacuum-bag curing at  $185 \pm 10^{\circ}\text{F}$  for 4 hr at 20 to 25 in. of Hg.

a. The first cycle bonded the liner doublers to the liner with Epon 913 epoxy adhesive.

b. The second cycle bonded the inner facing, aft ring, and honeycomb to the inner doubler and liner. Epon 913 adhesive was used for bonding

VIII, A, 260 SL-1 Nozzle (cont.)

the aft ring to the liner, while Epon 75-25 adhesive film was used for bonding the inner facing and honeycomb core. Prior to assembly, the cavities of the aft and forward rings were filled with Corfil 615 and cured at ambient temperature for 4 hr.

c. The third cycle bonded the forward ring, outer facing, and outer doublers in place. The O-ring was installed in the groove of the liner. Epon 913 adhesive was used for bonding the forward ring to the liner, and Epon 75-25 adhesive film was used for bonding the outer facing and outer doublers. After bonding, screws were installed to attach the outer doublers to the forward and aft rings.

Bondline thicknesses were determined for each component of the honeycomb structure during assembly. Adhesive bond strength was determined either from test panels of representative bondline thickness for each component or from trepan test results. The bond strength between the honeycomb core and the inner and outer facings was determined by a trepan test conducted after the second and third bond cycles. A minimum of one test was performed on each core segment. After test, the trepan test hole was repaired by filling the cavity with Epon 913 resin and bonding a 5-in.-dia doubler over the cavity.

Bondline defects, such as voids and delaminations, were determined by ultrasonic method after the second and third bond cycles.

The completed exit cone assembly was leak tested to assure that no gas flow existed in the bondline between the plastic liner and honeycomb structure, and within the bondlines of the honeycomb structure.

The five segments of the retainer ring were bonded to the aft ring with Epon 913 adhesive. The 190 bolts and nuts were assembled.

VIII, A, 260 SL-1 Nozzle (cont.)

Cork-sheet insulation was bonded to the aft 2 ft of the exit cone external surface with Armstrong J-1156A adhesive and E-30 catalyst. Vacuum-bag cure at ambient temperature for 12 hr was used. Vinyl primer was sprayed on the cork sheet.

A trial assembly of the nozzle and exit cone was conducted prior to shipment (Figure 209). The interface gap and the mating contour were within design tolerance.

The internal surface of the exit cone plastic liner was sprayed with Skydrol 162Y22 primer to a 0.002-in. minimum thickness and cured at ambient temperature for 6 hr.

Discrepancies detected during exit cone assembly are as follows:

- (1) The edges of the inner doublers did not lay flat in bonding due to inadequate vacuum pressure and exceeded the 0.005-in. minimum straightness requirements. This was repaired by grinding.
- (2) The thickness of aft flange was 0.294 to 0.343 in. instead of  $0.265 \pm 0.015$  in. Added thickness does not affect performance. The bolt length is compatible with flange thickness.
- (3) The aft flange did not seat during cure. The length between the forward and aft flanges was 117.340 in. instead of 117.580 to 117.380 in. This condition was acceptable.
- (4) The 36 1/4-in.-dia holes in aft ring (flange) were redrilled to 3/8 in. in diameter to accommodate handling ring bolts.

VIII, A, 260 SL-1 Nozzle (cont.)

(5) One hole of the forward flange was tapered (0.9595/0.958 in.) instead of being 0.926/0.946 in. in diameter. Sufficient strength remained to provide adequate coupling to nozzle.

(6) Two delaminations occurred in the forward portion of the liner after assembly and were repaired. No effect on performance was expected.

B. 260-SL-2 NOZZLE

1. Nozzle Plastic Components

The fabrication plans for the entrance, throat, and throat extension inserts of the nozzle were similar to those used for the 260-SL-1 nozzle, with one exception. As a result of vacuum bag leakage during hydroclaving of 260-SL-1 inserts, the 260-SL-2 inserts were vacuum-bagged and final-cured in an autoclave cycle at 300°F and 300-psi pressure.

Deviations from the scheduled fabrication procedures and discrepancies from the design requirements for each plastic component are delineated below.

a. Entrance Insert

The entrance cap liner was preformed at approximately 180°F for approximately 3 hr longer than the cycle specified. In subsequent test values for the fully cured part the physical properties were verified to be within specification limits.

VIII, A, 260 SL-1 Nozzle (cont.)

After machining the outside diameter of the preformed liner, undersized discrepant areas were observed in three circumferential regions. One discrepancy (0.030 to 0.200 in. deep by 0.125 to 1.00 in. wide) was located in the silica cloth and phenolic material adjacent to the forward end. The other two regions were in the carbon cloth material; one was located near the silica-cloth to carbon-cloth interface, and the other approximately 10 in. aft of the interface. The discrepancies in the two carbon cloth regions were 0.005 to 0.140 in. deep by 0.200 to 0.450 in. wide. These grooves were sanded to roughen the glazed surfaces, and each side of the groove was feathered to an angle of 15 degrees to the main surface. The grooves were subsequently filled with silica cloth and phenolic overwrap material during overwrapping of the liner.

The surface at the 128.13-in. diameter of the final cured insert was undersize by a maximum of 0.25 in. The undersized area was filled with additional Epon 913 adhesive during bonding of the insert to the nozzle shell.

A series of radiographic and ultrasonic inspections showed one delamination and five resin defect indications. The delamination was located midway axially in the silica cloth and phenolic liner and adjacent to the overwrap interface. One resin defect was in the silica cloth liner near the interface to the carbon cloth. Nondestructive test data indicated that these defects were all of less severity than the delamination indications observed in the 260-SL-1 nozzle throat insert.

b. Throat Insert

No discrepancies were observed in the final-cured throat insert.

c. Throat Extension Insert

The depth of the O-ring groove was 0.177 to 0.193 in. for approximately 90 degrees of the circumferential length; this depth was 0.007 in.

VIII, B, 260-SL-2 Nozzle (cont.)

over maximum dimensions. Compression of the O-ring is still within design limits, and areas forward and aft of the O-ring were sealed with Epon 913 adhesive.

No silica cloth material was available for property determinations from the aft test ring, because the as-wrapped liner was held to the maximum possible length to assure sufficient bagging surface during preform and cure without blocking the vacuum ports on the mandrel.

All results were within specification limits except for volatile content of the silica-cloth overwrap. The average volatile content was 3.29%, as compared with the specification limit of 3% maximum. This discrepancy was acceptable because the overwrap is used primarily as an insulator. Components with volatile contents of 3.0 to 3.5% were used in the 120-SS-1 and 260-SL-1 motor nozzles with no apparent effect on performance.

d. Exit Cone Liner

The fabrication sequence for the exit cone plastic liner of 260-SL-2 was similar to that used for 260-SL-1. Discrepancies were as follows:

There was insufficient material in the silica overwrap of the aft test ring for interlaminar shear and microtensile test specimens; therefore, properties were determined only from the forward test ring.

The volatile percentage, which was 3.29% maximum, exceeding the specified 3.0% maximum. This deviation was accepted since previous components from the 120-SS-1 and 260-SL-1 motor nozzles performed as designed with comparable volatile content.

VIII, B, 260-SL-2 Nozzle (cont.)

2. Nozzle Assembly

The nozzle assembly procedure of 260-SL-2 was similar to that used for 260-SL-1. Discrepancies were as follows:

The insulation bond strength did not meet the minimum requirement, however, the values obtained were greater than those obtained on the 120-SS-1 and 260-SL-1 motor nozzles, and were acceptable.

Slight deviations from specification tolerances in the gap dimensions occurred between the throat insert and nozzle shell and between the entrance and throat inserts, were minor and were acceptable. Also, a gap deviation occurred between the rubber insulation and entrance insert. However, a greater disparity occurred in the 260-SL-1 nozzle without degrading performance; therefore, the deviation in the 260-SL-2 nozzle was accepted.

3. Exit Cone Assembly

The exit-cone honeycomb structure of 260-SL-2 was fabricated similar to that of 260-SL-1. Discrepancies were as follows:

The thickness of the forward flange was changed from the specified dimension of 0.500 to 0.520 in. to a dimension of 0.486 to 0.509 in. and the aft-flange thickness was also changed from 0.250 to .280 in. to a dimension of 0.279 to 0.297 in. to compensate for variation in the inner doubler material and bondline thickness.

The tensile shear strengths of test specimens were less than the specified minimum; however, the values are in excess of the functional design requirements. The trepan test results on the actual assembly were above requirements and are a truer representation of the bond strengths.

VIII, B, 260-SL-2 Nozzle (cont.)

Ultrasonic inspection of the exit cone liner ID after assembly revealed intermittent delaminations at the forward end extending up to 50% of the circumference and 1/8 to 1/4 in. beneath the ID. The delaminations were injected with Epon 913 and cured at room temperature.

A sling failure caused the leak-test fixture to drop onto the exit cone assembly during post-leak-test disassembly operations. The resulting damage consisted of three 0.5-in.-square by 0.050-in.-deep gouges in the front face of the forward flange; five indentations (up to 0.125 in. deep) on the outer doublers; and two 5-in.-square gouged areas in the cork insulation. The forward flange gouges were blended and dye-penetrant inspection indicated that the flange was acceptable. The damaged areas of the doublers were ultrasonically inspected, and unbonding was indicated between the outer doubler and the facing. The unbonded and damaged portions of the doublers were removed and replaced with new doubler pieces which were bonded with Epon 913. Subsequent ultrasonic inspection indicated no unbonding in the repaired areas. The damaged areas of the cork were removed and replaced with new cork.

The boom of a lift truck came in contact with the exit cone, causing minor indentations to two outer facings which were 0.045 to 0.070 in. deep and created an unbonded area of approximately 1 sq in. in a doubler scallop. The areas surrounding the indentations were ultrasonically inspected, found to be sound, and accepted for use in motor 260-SL-2.

C. 120-SS-1 NOZZLE

The 120-SS-1 nozzle was fabricated prior to the 260-SL-1 nozzle and used the same planned fabrication procedures previously described for the larger nozzle. Fabrication of the 120-SS-1 nozzle successfully demonstrated the various procedures and techniques. As a result of the 120-SS-1 nozzle



VIII, C, 120-SS-1 Nozzle (cont.)

fabrication, only minor refinements were made to the 260-SL nozzle fabrication procedure to improve process reliability. Photographs of various phases of the 120-SS-1 nozzle fabrications are shown in Figures 210 through 214.

Fabrication was performed in accordance with Aerojet drawing No. 600264 for the nozzle assembly and Aerojet drawing No. 600246 for the exit cone assembly. Specifications were identical to those described for the 260-SL nozzles. Deviations from the procedures that resulted in processing or component discrepancies are discussed below.

1. Entrance Insert

A debulking of 45 to 75% was obtained in roller tape wrapping, as compared to the objective of 80% debulking. The lower amount of debulking was approved because of the increased debulking attained in the 1000-psi hydroclave preforming and final cure.

Because of a machining error, the outside conical surface of the overwrap was grooved to a depth of 0.887 in. The overwrap was removed from the area of the groove; tape was applied parallel to the surface and the component was again hydroclave cured. Subsequent machining resulted in a repetition of the machining error of a V-groove, 0.30-in. deep at the 42.8 in. diameter. This groove was repaired by filling it with Epon 828 epoxy resin and glass roving.

Minor water leakage occurred during the hydroclave preform cycle at 200 psi; the part was not wetted. The part was rebagged and successfully hydroclave preformed.

A machine error caused a 1.674 in. undercut in the overwrap at the 56.766 diameter. The component was repaired by machining off the overwrap

VIII, C, 120-SS-1 Nozzle (cont.)

at a 15-degree taper forward of the diameter in error, overwrapping parallel to surface with MX-2646, final hydroclave curing, and final machining.

2. Throat Insert

A thermocouple wire embedded in the outside of the throat inlet was accepted as being noncritical.

A loss in vacuum on the hydroclave bag during preforming occurred due to a line breakage. The hydroclave conditions were 840-psi pressure and 185°F at the occurrence. This discrepancy was accepted as noncritical.

3. Throat Extension Insert

The first throat extension insert became wetted primarily in the aft end due to a bag failure during preforming. An extended cure cycle was unsuccessful in reducing the volatile content of the part. An extended post-cure cycle reduced the volatiles to slightly above 3%; however, specific gravity of the aft end of the part was reduced from 1.41 to 1.32 (or 93% of the original specific gravity). Additionally, the laminate orientation at the aft end was quite variable with a chevron effect. The disorientation was attributed to difficulty in supporting the oriented wrap on the divergent conical surface, resulting in buckling under hydroclave pressure.

To maintain schedule, the first extension insert was bonded into the shell prior to final receipt of tag-end property tests and final assessment of the component. Subsequently, the component was rejected and machined from the shell.

The second throat extension insert was tape wrapped parallel to nozzle center line instead of the 45- to 60-degree orientation used on the

VIII, C, 120-SS-1 Nozzle (cont.)

first extension. The change to the parallel orientation was due to the difficulty in obtaining the proper orientation in the first 45- to 60-degree oriented part and the current success of parallel oriented parts in other large solid motor nozzles.

The second throat extension was fabricated per requirements except for one finished part discrepancy. Radiographic inspection showed a resin-rich area starting from the forward end of the part and 0.10 in. from the overwrap, extending approximately 4-3/4-in. long and 180 degrees circumferentially. This variation was accepted on the basis that it would not affect performance of the part. The defect was well within the carbon insert, and the resin-rich area would not be exposed to chamber gases.

In-process discrepancies were minor and did not affect the finished part. Of note, was the 83 to 85% debulk achieved during roller wrapping instead of the desired 93 to 94% of specific gravity. The lower debulk attained in tape wrapping was compensated by the 1000-psi hydroclave pre-forming pressure cycle.

4. Exit Cone Insert

Slippage of the tape during wrapping resulted in wrinkles and creases in the forward inner surface of the MX-4926 wrap. The creases were filled with epoxy-powdered carbon-fabric putty.

The 120-SS-1 exit cone insert was preformed, overwrapped, and final cured. The preform operation was eliminated in fabricating the 260-SL-1 exit cone insert; the 260 part was innerwrapped and overwrapped followed by a single final cure cycle.

VIII, C, 120-SS-1 Nozzle (cont.)

During preforming, 193 to 200°F temperatures were attained instead of the 187°F maximum specified. The discrepancy was accepted as not affecting the part. Also, the vacuum pressure in the bag enclosing the nylon overwrap was inadvertently lost during final cure. The part was accepted with the attainment of 93 to 95% debulking.

5. Nozzle Assembly

The bond gap between the rubber insulation and entrance insert was 0.014 to 0.070 in. instead of the 0.05 in. maximum. This condition was accepted.

As a result of a slight mismatch between the nozzle and exit cone liner, the final contour aft of the throat diameter was decreased by approximately 0.080 in. radially to match the exit cone liner. This was achieved by machining a 0.171-in.-long flat surface at the throat, which moved the downstream nozzle contour aft.

6. Exit Cone Assembly

The forward attachment flange slipped during adhesive bonding, resulting in a nonparallelism to the aft flange of 0.078 to 0.083 in., as compared to a drawing tolerance of 0.020 in. This discrepancy was acceptable.

The outer stainless-steel skin was 0.30 to 0.55 in. short at the aft flange. This discrepancy was acceptable.

The inside diameter of the exit cone liner at the forward end was machined undersize from 0.100 to 0.120 in. as a result of discrepancies in the forward flange, which caused the exit cone liner position to shift with respect to the flange.

Several other minor dimensional discrepancies were accepted.

VIII, C, 120-SS-1 Nozzle (cont.)

7. Nozzle and Exit Cone Assembly

The interface gap between the exit cone and nozzle assemblies was 0.030 to 0.050 in. instead of the required 0.040 to 0.070 in.

D. 44-SS NOZZLES

1. Ablative Plastic Components

Fabrication of the ablative plastic components and assembly of the nozzle was performed by TRW. Whenever possible available capabilities and current technology was used in the fabrication techniques and processes for the ablative plastic components. Results of the 260-motor nozzle supporting efforts on tooling, quality control, and evaluation studies were used to assist in the fabrication of the 44-SS nozzle components. Fabrication in-process quality control and inspection records were completely documented for inclusion into the Motor Log Book.

The ablative components of the nozzle were fabricated in three conical sections, consisting of the entrance insert, throat insert, and the exit cone insert.

The MX-2646 entrance insert was fabricated by a combination of two processes: (1) tape wrapping and roller debulking bias-cut silica cloth on both ends of the insert; and (2) layup of precut 120-degree segments under the roller in the center portion of the insert. Selection of tape wrapping or precut layup was based on the OD/ID ratio of the tape. Tape wrapping was used up to a maximum OD/ID ratio of 1.3. The orientation of the laminae was approximately 80 degrees. The combination tape-wrapped and die-cut layup component was bagged, instrumented and preform cured in a hydroclave at a temperature of 180°F and a pressure of 1000 psig. Following the preform cure,

VIII, D, 44-SS Nozzles (cont.)

the outer contour was machined and overwrapped parallel to surface with MX-2646 bias tape (approximately 58 degrees to center line). The component was rebagged, instrumented, and fully cured in a hydroclave at a temperature of 300°F and a pressure of 1000 psig. A sample ring was removed, and the part was final-machined. The part was then removed from the mandrel and radiographically inspected. Test specimens were made from the test ring, and tests were performed to determine specific gravity, volatile content, resin solids, acetone extraction, tensile strength and interlaminar shear strength.

The exit cone insert was tape wrapped 52.5 degrees (nominal) to the nozzle center line with MX-4926. The part was then preformed at a temperature of 180°F and a pressure of 1000 psig, machined on the outer diameter, overwrapped parallel to surface (17.5 degrees to the center line) with FM-5131 and final cured at a temperature of 300°F and a pressure of 1000 psig. Test ring samples were obtained and tested as described for the entrance insert.

The throat insert of the 44-SS-1 and -2 nozzles was fabricated by laying up precut 90-degree segments of MX-4926 in a die-mold. The loaded die was heated in an oven to a temperature of 180°F, then installed in a press and preformed at a pressure of 1000 psig. Following preform, the outside diameter was machined and overwrapped parallel to surface with FM-5131. The component was hydroclave-cured at a temperature of 300°F and a pressure of 1000 psig, radiographically inspected, final machined, and tests were performed on test specimens.

The throat insert of the 44-SS-3 nozzle consisted of a diecast molded carbon section for the forward 5-1/4 in. and a tape-wrapped carbon section for the aft 2-1/2 in. Details of the fabrication of 44-SS-3 throat insert, are presented in Section VIII,D,5,c.

VIII, D, 44-SS Nozzles (cont.)

2. Nozzle Shell

Fabrication of the nozzle shell was performed by Aerojet, Downey. The shell was made from a single forging. The forging was rough-machined, heat-treated, and final-machined, from AISI 4340, heat-treated to a 150,000 to 170,000 psi tensile yield strength. The stock material was ultrasonically inspected in accordance with Aerojet specification 36163. The shell was radiographically inspected before and after heat treatment in accordance with Aerojet specification 36065, using Aerojet specification 13860, Table I, Class I standard of quality. The shell was magnetic particle inspected before and after hydrostatic test, which was conducted in accordance with Aerojet specification 36140/7, using a spare second stage Minuteman Wing I chamber and a closure plate over the shell exit plane as shown in Figure 214. Hydrostatic test pressure was  $600 \pm 5$  psig.

The exterior of the shell was protected with zinc chromate primer. The internal surfaces were primed with FM-47, Type II primer.

3. Retainer Ring

The exit cone retainer ring was machined by TRW from AISI 4130 normalized steel plate. The surfaces in contact with the nozzle shell and exit cone insert were primed with FM-47 epoxy primer, while the remaining surfaces were primed with zinc chromate. The as-received steel stock was ultrasonically inspected, and the final part was magnetic particle inspected.

4. Assembly and Final Processing

Nozzle assembly was accomplished in the following manner:

VIII, D, 44-SS Nozzles (cont.)

a. The inserts were dry-stacked into the nozzle shell to obtain the required bondline thickness. Silicone rubber sealant was placed between the inserts; the inserts were then bonded into place with Epon 913 epoxy and cured at 180°F for 4 hr.

b. The inner contours of the inserts were final machined.

c. The assembly was leak checked in accordance with Aerojet specification AGC-36425.

d. The entrance-cap rubber insulation was dry-stacked in the nozzle, bonded in place with Epon 948.2 epoxy, and cured at 140°F under 20 in. of Hg vacuum for 24 hr.

e. The forward step joint of the rubber insulation was machined and the insulation plaster mold removed.

f. The exit cone retainer ring was bonded in place with Epon 913 epoxy.

5. Discrepancies

a. 44-SS-1

The MX-4926 broadgoods used in the nozzle inserts were initially rejected by TRW due to deviations in flow, tack, resins solids, and volatile content. It was subsequently determined that differences in interpretation of acceptance test procedures existed between the supplier and TRW. The material was eventually accepted and used satisfactorily in the nozzle inserts of the 44-SS-1 and -2 nozzles.



VIII, D, 44-SS Nozzles (cont.)

The outside contour of the entrance insert preform was undersize (0.100 in. deep) in six small areas (1 to 5 in. in length). The undersized areas were built up with similar material prior to overwrapping. The cured entrance insert chipped slightly at the interface joint between the entrance and throat inserts during final machining. The discrepancy was corrected during nozzle assembly by filling the gap and chipped area with silicone rubber.

The exit cone insert had insufficient tape width in the as-wrapped condition; subsequent debulk resulted in minor undersized areas in the outer contour. These areas were built up with FM-5131 silica cloth and overwrapped. A bag leakage also occurred during preforming, resulting in a volatile content of 7.88%. An extended postcure heating cycle reduced the volatile content to 2.55%, which was acceptable. During final machining, the exit cone insert was machined 0.775 in. too short. To use the exit cone insert, the throat insert was accordingly lengthened and a new throat-to-exit-cone joint was designed as shown in Figure 91.

The final cured throat insert was slightly high in resin solids, 38.6% as opposed to the maximum required 37.0%. The component was acceptable.

The FM-47 primer was observed by the nozzle assembler (TRW) to be flaking off the shell, and was removed and replaced by Fuller epoxy 162Y22. Discrepancies in the internal dimensions of the shells were also detected at TRW. This necessitated the outside contour of the nozzle plastic inserts to be match-machined to fit the nozzle shell contour.

VIII, D, 44-SS Nozzles (cont.)

Minor discrepancies in surface flatness and ID of the retainer ring were observed but were considered acceptable for use.

A leak check was conducted following bonding and machining of the inserts in the shell. A small leak was detected between the entrance cap and shell. The leak path was blocked when the rubber insulation was bonded in place.

Small bondline gaps were detected between the rubber insulation and the steel shell. These were repaired by injection of Epon 948 epoxy into the gaps. Several 1/4-in.-deep gouges occurred in the rubber insulation during removal of the rubber pads, which were used to position the plaster mold. The gouges were repaired in accordance with standard procedures. Revisions were made in the pad removal for subsequent nozzles.

b. 44-SS-2

Discrepancies in the raw plastic materials were identical to those discussed for 44-SS-1 nozzle.

The tape width of the entrance insert was insufficient, such that the outer contour of the preform was undersize (0.010 to 0.100 in. deep) in several areas. These areas were filled with additional silica material prior to overwrap.

Throat insert No. 2 was rejected due to several circumferential delaminations. The delamination resulted from improper removal of the preform from the mandrel. Repair of the delaminations was attempted by reheating and applying pressure. After the second preform, no delaminations were observed. The part was machined, overwrapped, final-cured, and machined.

VIII, D, 44-SS Nozzles (cont.)

The part was wetted during final cure due to bag failure. The delaminations were observed again in the X-ray results, and the part was rejected. Throat insert No. 3 was successfully fabricated and used.

A leak check was conducted after bonding and machining the inserts in the shell. A leak was detected between the entrance insert and the shell. Repair was accomplished by applying a vacuum and drawing Epon 913 into the leak path.

Nozzle shell and retainer ring discrepancies discussed for the 44-SS-1 nozzle were also applicable for the 44-SS-2 nozzle.

The bondline of the rubber insulation was 0.017/0.115 in. instead of the required 0.030/0.120 in; the disposition was to use the part in its existing condition. The forward edge of the rubber insulation was undersize by 0.030 in. over a 2-in. circumferential arc. The component was used in its existing condition since the undersized area is filled with sealant upon nozzle-to-chamber assembly.

c. 44-SS-3

The entrance insert had a slight deviation in volatile content, 2.0 to 2.18% instead of the 2.0% maximum. The component was acceptable.

Exit cone insert No. 3 was made from FM-5072 carbon cloth and phenolic. The component was rejected due to several circumferential delaminations observed following removal of the part from the mandrel. The processing techniques established for MX-4926 were used for the FM-5072 material; apparently, different processing techniques are required. Due to the program schedule, no further attempts were made to use FM-5072. Exit cone insert No. 4 was made successfully with MX-4926.

VIII, D, 44-SS Nozzles (cont.)

Throat insert No. 4 was rejected due to circumferential delaminations which were detected after preforming; repair of the delaminations using a second preform cycle was unsuccessful, and the part separated into three cylinders. A check of the degree of polymerization revealed the part to be 86% advanced and the component was rejected. In a final attempt to bond the segments and hydroclave cure, bag leakage occurred.

The raw materials of throat insert No. 5 were slightly high in volatile content and resin solids; however, they were used, based on successful use of similar material properties in the 44-SS-1 and -2 nozzles.

Following preforming, throat insert No. 5 was observed to have a circumferential delamination 5-1/4 in. aft of the forward face. The component was separated at the delamination, rebonded with epoxy, and cured at a temperature of 120°F for 14 hr. The rebonded component was machined, overwrapped, and hydroclave-cured. Radiographic inspection revealed a low density area 3 in. from the forward end, extending 1-5/8 in. inward from the ID and circumferentially from 27 to 315 degrees (9 in.). Alcohol penetrant did not penetrate the low density area, and the component was considered acceptable.

Subsequently, the throat insert of the 44-SS-3 nozzle was redesigned to determine the cause of the unpredicted circumferential gouging that occurred in the MX-4926 throat insert downstream of the geometric throat area of both the 44-SS-1 and -2 nozzles. The existing throat insert No. 5 was used by machining off the silica overwrap and the carbon cloth aft of the repaired bond line (5-1/4 in. aft). The aft carbon section was replaced with a tape-wrapped portion. The aft carbon-cloth section was tape-wrapped and roller-debulked, preformed at a temperature of 180°F and a pressure of 1000 psig, and machined for overwrapping and mating with the forward die-cut

VIII, D, 44-SS Nozzles (cont.)

molded section. The two carbon sections were bonded together with an ambient curing epoxy (ERL 2774), and overwrapped parallel to the surface with FM-5131 bias cut tape. The component was cured at a temperature of 300°F and a pressure of 1000 psig. Based on previous tape-wrapped components, it was considered that 1.3 was the maximum OD/ID tape wrap ratio. Because of the 1.3 ratio, it was anticipated that the outer contour of the throat insert would have a 17-degree conical section with a reverse slope from the 7-degree aft conical section, as shown in Figure 215. It was subsequently determined that a higher OD/ID ratio could be wrapped, and a wider tape was used for the aft portion of the throat insert. The final tape-wrapped configuration, also shown in Figure 215, has a continuous 7-degree slope.

Nozzle shell and retainer ring discrepancies discussed for the 44-SS-2 nozzle were also applicable to the 44-SS-3 nozzle.

The rubber entrance insulation was undersized by 0.057 in. radially over a 5-in. circumferential arc at the forward edge. The component was accepted since this area is filled with silicone rubber during assembly of the nozzle to chamber. Additionally, the rubber insulation had several repaired areas 0.10 in. deep, which were considered as marginally bonded. However, the component was accepted because the insulation thickness is excessively large in the repaired areas as evidenced by the postfired insulation thickness of the 44-SS-1 and -2 nozzles.

IX. IN-PROCESS TESTING AND INSPECTION

A. 260-SL NOZZLE

The in-process and quality control measures that were used in the fabrication of the tape wrapped ablative plastic components are defined by Aerojet specification AGC-36413. Specific gravity, acetone extractables and volatile content were obtained for each component after preforming. Also, mechanical and physical properties were determined for each billet after final cure. The end rings of each billet were sectioned into test specimens and tested in compliance with specification requirements. Each cured billet was tested for specific gravity, acetone extractables, interlaminar shear volatile content, and microtensile strength. Test specimen data for the 260-SL-1 nozzle entrance, throat, throat extension, and exit cone inserts are shown in Figures 216 through 219. Test specimen data for the inserts of 260-SL-2 are shown in Figures 220 through 223. Properties were determined for both the ablation surface liner and the overwrap materials. The property values were within specification limits except for very slight exceptions.

Nondestructive tests were also performed on each billet for examination of flaws, delaminations, and inclusions. Primarily, the components were inspected radiographically after OD machining and removal from the wrapping mandrel. The entrance and throat inserts were inspected completely, while the throat extension insert and exit cone liner were inspected at six and five equally spaced radial locations, respectively. Additional exposures were made to determine the full extent of defects. Inspection of delamination-type defects were augmented with ultrasonic inspection and alcohol penetrant inspection. A summary of defects observed from nondestructive testing of the 260-SL-1 nozzle components is shown in Figure 224. The entrance insert was the only component of 260-SL-2 in which discrepancies were detected. A discussion of the defects is presented in Section VIII. The defects that exceeded the allowable limit were recorded on supplier discrepancy action reports for material review board disposition.

IX, A, 260-SL Nozzle (cont.)

The quality control measures used in the assembly of the ablative plastic inserts into the steel shell are defined by Aerojet specification AGC-36422. Adhesive bond strength was determined from test panels of representative bondline thickness, processed simultaneously with the assembly for each bonding cycle. Bonds of plastic insert to steel, rubber insulation to plastic insert, and rubber insulation to steel were simulated. Each panel was sectioned into test specimens, which were tested for lap tensile shear strength in accordance with Standard Federal Test Method, Standard No. 175, Method 1033. Ultrasonic inspection was used to determine bondline defects such as voids and delaminations. The total surface area of the shell was scanned, and areas indicating substandard bonds were fully explored to define the full extent of the defect. Areas, in which the percent of void or other defect exceeded the allowable limits, and specimen test values that did not meet minimum requirements were recorded in Supplier's Discrepancy Action Report for Material Review Board disposition. A summary of the ultrasonic inspection and panel specimen test results for the 260-SL-1 and -2 nozzle assemblies are shown in Figures 225 and 226, respectively. Bond strength and bond area results were satisfactory.

A leak test of the bonded nozzle assembly was conducted as a further inspection of the bond between the steel shell and the plastic inserts to assure no gas flow path within the bondline. A halogen leak detector was used; the unit is sensitive to a leakage change of 1 oz of halogen a year. The leak detection medium used with the halogen leak detector was Freon gas pressurized to 50 psi with nitrogen gas. Leak-check tooling was installed at the entrance-insert-to-throat-insert joint and at the throat-insert-to-extension-insert joint, the Freon was introduced at the throat insert joints and all other plastic insert interface joints, and plastic-to-steel bond interfaces were checked for leakage. No leakage was detected in the nozzle assembly.

IX, A, 260-SL Nozzle (cont.)

The quality control measures employed in the assembly of the honeycomb structural shell to the exit cone ablative-plastic overwrap are defined by Aerojet specification AGC-36400. The bond integrity was determined from both test specimens and ultrasonic inspection. Adhesive bond panels were prepared for representative bondline thicknesses of the bonds between the plastic overwrap and honeycomb inner facing, the forward and aft flanges, and the plastic overwrap and the honeycomb outer facing and outer doubler sheet. Each panel was sectioned into test specimens, which were tested for lap tensile shear strength in accordance with Standard Federal Test Method, Standard No. 175, Method 1033. The bond strength between the honeycomb core and the inner and outer facings was determined by trepan test. The trepan test is a flatwise tensile test of a 1-in.-dia specimen that is cut from the bonded assembly (Figure 227). A minimum of one test was performed on each core segment of the total circumferential assembly. After the test, the trepan test hole was repaired by filling the cavity with Epon 913 epoxy and a 5-in. doubler of the identical facing material and thickness bonded with Epon 913 epoxy over the repair area. Trepan retests were required if the strength values were below minimum as a result of improperly obtained specimens and/or improperly performed test procedures; no retests were required. Ultrasonic inspection was used to detect bondline defects after each bonding operation. It should be noted that the bond between the honeycomb core and the inner and outer facings cannot be inspected by the ultrasonic technique. Bond areas, in which percentage of voids exceeded the allowable limit, and specimen test values, which did not meet minimum requirements, were recorded in Suppliers Discrepancy Action Report for Material Review Board disposition. A summary of the ultrasonic inspection and bond specimen test results for the 260-SL-1 and -2 exit cone assemblies are shown in Figures 228 and 229, respectively. All test results were within specification limits. The complete exit cone assembly was leak tested to assure no gas flow in the bondline between the plastic liner and honeycomb structure and the honeycomb sandwich and end flanges. The leak detector and leak detection medium were the same as those used on the nozzle assembly.



IX, A, 260-SL Nozzle (cont.)

Leak-check tooling was installed on the forward end of the exit cone assembly, the Freon was introduced at the interface bond between the plastic liner and honeycomb structure, and all adhesive bond joints within the honeycomb sandwich and the interface bond between plastic liner and honeycomb facing were checked for leakage. No leakage was detected in the exit cone assembly.

B. 120-SS-1 NOZZLE

The in-process testing and inspection methods used during fabrication of the 120-SS-1 nozzle were the same as those employed for the 260-SL nozzle described above. The same Aerojet process specifications were used to define quality control requirements used during fabrication and processing. Ablative component properties, which were obtained from end rings made simultaneously with the component, are shown in Figures 230 through 234. The properties were within specification limits.

Tests were also conducted on 120-SS-1 ablative material specimens to verify the mechanical property values used in the structural analysis of the 260-SL-1 nozzle. The specimens were obtained from end test rings except for the entrance-insert meridional specimens which were obtained from the parent material of the postfired component. The tensile strength and tensile modulus of MX-4926 and MX-2646 were determined. The results are shown in Figure 235. The values obtained exceed the values used in the structural analysis.

Radiographic inspection of the plastic inserts indicated the parts to be free of cracks and delaminations, however, the inspection indicated a resin-rich area in the throat extension as discussed in Section VIII.

IX, B, 120-SS-1 Nozzle (cont.)

Ultrasonic inspection of the plastic insert to steel bonding indicated that the unbondness was within specification requirements; however, the entrance insert to shell had relatively large areas of unbondedness as shown in Figure 236. Nozzle-assembly bond strength and gap-inspection data are shown in Figures 237 and 238, which indicate acceptable bonds and gaps. The trepan test results and in-process bond data for the exit cone assembly are shown in Figures 239 and 240, respectively. The exit cone bond data were acceptable.

Leak tests were conducted on the nozzle and exit cone assemblies; no leakage occurred.

C. 44-SS NOZZLES

The in-process testing and methods used during fabrication of the 44-SS nozzles were generally similar to those employed for the 120-SS-1 and 260-SL-1 nozzles, although the test methods and specifications of the larger nozzles had not been completely established at the time of the 44-SS nozzle fabrication.

The results of mechanical property tests obtained from tag end specimens of the plastic inserts are shown in Figures 241 through 243. A summary of the bondline inspection is shown in 244.

1. 44-SS-1 Nozzle

Physical properties of the 44-SS-1 plastic inserts, shown in Figure 241, were within limits. Bondlines were satisfactory as shown in Figure 244. A leak test revealed a small leak between the entrance insert and shell. This leak was blocked when the entrance insulation was bonded in place.

IX, C, 44-SS Nozzles (cont.)

2. 44-SS-2 Nozzle

Physical properties of the plastic inserts were within limits as shown in Figure 242. Bondline inspection results, shown in Figure 244, were acceptable. A leak check revealed a 5-oz/year leakage at the forward end of entrance insert. This was repaired by injecting Epon 913; the area was covered subsequently with rubber insulation.

3. 44-SS-3 Nozzle

Physical properties of the ablative plastic inserts, shown in Figure 243, were acceptable as well as the bondline inspection results (Figure 244). No leaks were detected during leak check of the assembly.

X. INVESTIGATION OF FABRICATION PROCESSES AND QUALITY ACHIEVED

A. 260-SL NOZZLES

1. 260-SL-1 Nozzle

Analyses of the in-process and final quality control data indicated that the 260-SL-1 nozzle and exit cone assemblies met Aerojet engineering and quality control requirements and were acceptable for use in motor 260-SL-1.

a. Material Conformance

The materials used in the 260-SL-1 nozzle met the specified acceptance requirements. Experience gained during fabrication of the 44-SS and 120-SS-1 nozzles was used in assessing and accepting minor deviations in chemical and physical properties and, in certain instances, initial specification requirements were modified. Special tests were conducted where acceptance test values were somewhat beyond specification. For example, flow and tack values at room temperature were not acceptable particularly after 90-day storage retest. Tack tests at elevated temperatures (200 to 275°F) determined that the material tape wrapped at these temperatures was acceptable.

b. Dimensional Conformance

Only minor in-process dimensional discrepancies occurred during fabrication and assembly of the components and were readily corrected or accepted, based on their having negligible effect on the final dimensions and performance of the components. Details of discrepancies are discussed under Section VIII, Fabrication.

X, A, 260-SL-1 Nozzle (cont.)

c. Tape Wrapping

Tape-width reduction during tape wrapping of the throat insert indicated that a smooth and wrinkle-free wrap was attained and uniform. This was confirmed by inspection of the end ring specimens. Material tack was excellent; roller pressure and mass temperature were well maintained. As wrapped-density of the carbon liner was 85 to 90% of the 1.44 specific gravity ultimate value. Visual quality and density of the carbon were considered excellent.

Initial wrapping of the entrance insert presented certain problems which were corrected eventually. As a result of improper knit, 83.2 lb of MX-4926 were removed from the part. Additionally, the silica tape pulled away from the mandrel slightly at the forward end, but was corrected as the wrapping progressed. The as-wrapped densities of the carbon and silica were 79% and 75% of ultimate, respectively.

Throat extension No. 2, used in motor 260-SL-1, was wrapped in a very uniform and wrinkle-free manner. The as-wrapped specific gravity of the carbon liner was 1.24 or 86% of ultimate. The parallel-to-surface FM-5131 overwrap was roller debulked to 89% of ultimate specific gravity.

The exit cone was tape wrapped to a very uniform, wrinkle-free part. The carbon and silica portions were roller debulked to 89% and 95% of ultimate specific gravity, respectively. The wrapping plan specified the buildup of various tape widths to minimize waste. The variation of tape width caused variations and adjustments of roller force, heat flux for tape preheating and wrapping speed. It was decided to eliminate all of the above variables on the 260-SL-2 exit cone by using a uniform tape width.

X, A, 260-SL-1 Nozzle (cont.)

d. Hydroclave Bagging

Vacuum-bag failures continued to exist in the hydroclave operations similar to those experienced with the 120-SS-1 nozzle. A bag leakage occurred during the preform cycle of the entrance insert and throat inserts No. 1 and 2. Throat insert No. 1 was rejected because of high volatile content. Throat insert No. 2 and the entrance insert were not wetted and were used. Based on the repeated occurrence of hydroclave bag failure and the potential loss of the expensive components, it was decided to conduct subsequent preform and final-cure operations in the autoclave.

In the process of developing methods of improving hydroclave reliability, bag mandrels were reworked, end rings were redesigned and fabricated, and an extension to the mandrel was made. All of these tools and procedures were eliminated by changing to the autoclave process.

e. Autoclave Preform and Cure

As discussed previously, the autoclave was selected for subsequent preform and cure cycles. The autoclave process was considered to yield nearly the same end-product properties obtained with the higher-pressure hydroclave process, with much less risk of damaging the quality of the part or the reliability of fabrication. Preform and cure temperatures used in the autoclave were the same as used in the hydroclave; however, the pressure was changed from 1000 psig to a range of 275 to 325 psig. The autoclave cycles were accomplished as scheduled without incident. The preform and cure cycles for the various components are shown in Figures 245 through 251. All components achieved acceptable physical properties.

X, A, 260-SL-1 Nozzle (cont.)

f. Nylon Tension Wrap

The exit cone insert was tape wrapped, overwrapped, bagged, and cured at approximately 85 psi in the oven, eliminating the liner preform cycle. The high roller debulk and nylon tension wrap process permitted the elimination of the preform cycle. The physical properties of the cured liner were acceptable.

g. Component Integrity

Physical property tests and nondestructive inspection indicated that the components were of acceptable quality. The cause of the delaminations, which were detected in the exit cone, throat, and first throat extension, was not determined. The existence of delaminations in an oriented wrapped part presents no problems in component integrity; the laminates are mechanically locked in place, and thermal expansion seal the delaminations. In a parallel-to-center line wrapped part the delaminated component must rely on the adhesive bond to hold the part in place. The risk of possible bond failure or gas pressure getting behind the delaminated component must rely on the adhesive bond to hold the part in place. The risk of possible bond failure or gas pressure getting behind the delaminated part and ejecting it is too high for large, expensive nozzles. As a consequence, the first (parallel-wrapped) throat extension was rejected and replaced with a tape-oriented part. The very small delaminated part of the exit cone was considered to be of a minor nature, and loss of this piece would not jeopardize the nozzle integrity or performance. This component was rebonded in place and also bonded to the nozzle assembly.

h. Nozzle Assembly

The nozzle assembly consists primarily of bonding sequences of the inserts and rubber insulation to the shell. Bonding procedures and

X, A, 260-SL-1 Nozzle (cont.)

sequence of operation were satisfactory. Removal of the first throat extension and subsequent replacement was accomplished efficiently and maintained integrity of the assembly. Ultrasonic inspection gave small indications on each bond; these were attributed to trowel marks leaving void areas, which were not completely filled with adhesive from the mating part. The total unbondedness was less than 1% of the total bond area and was acceptable. The lap shear-test values for the rubber and throat extension were below specification values but were acceptable. The low values were attributed to faulty cleaning of the test panels.

The bond gap of the rubber insulation to the plastic insert and shell were out of tolerance, particularly at the plastic joint where the rubber is thinner. The excessive bond gap is the result of the rubber insulation shrinking and pulling away from the mandrel during its cure process. The bond gap was filled with Epon 948 and was acceptable. The excessive plastic-to-rubber bondline occurs at a relatively high Mach number and may enhance rubber erosion or removal; however, the plastic components are designed to accept the gas stream exposure even if the rubber was not initially present.

i. Exit Cone Assembly

The exit cone assembly consists primarily of bonding sequences. The bond quality was considered acceptable as verified by ultrasonic inspection, bond sample tests and trepan tests. The assembly procedures and cure cycles were adequate except for minor discrepancies. Two of these discrepancies requiring processing modifications are as follows:

(1) The edges of the inner doublers did not lay flat during bonding due to inadequate vacuum pressure. The flatness discrepancy was minor and readily repaired.



X, A, 260-SL-1 Nozzle (cont.)

(2) The aft flange would not seat as predicted during cure. As a result, the distance between flanges was out of tolerance by 0.04 in. This was acceptable and would not affect component assembly or performance. A leak test indicated that the assembly was acceptable.

The fit of the nozzle and exit cone assemblies were adequate. Deviations due to the repair of the exit cone liner resulted in bonding the assemblies together and eliminating the expansion joint at the interface. The effect of removing the expansion joint on nozzle performance is considered negligible.

## 2. 260-SL-2 Nozzle

Fabrication and quality control experience obtained from the 260-SL-1 nozzle was applied to that of the 260-SL-2 nozzle. Except for the minor discrepancies discussed in Section VIII, the material and dimensional conformance, tape wrapping, curing cycles, and component integrity were obtained successfully.

In-process and final quality control data indicated that the 260-SL-2 nozzle and exit cone assemblies met engineering and quality control requirements and were acceptable for use in motor 260-SL-2.

## B. 120-SS-1 NOZZLE

### 1. Tape Wrapping

Tape wrapping the various oriented bias and warp tapes presented no major problems in obtaining uniform wrinkle-free parts. The first oriented throat extension was wrinkled after preform due to inadequate end

X, B, 120-SS-1 Nozzle (cont.)

support. This part was wetted during preform and replaced with a parallel-wrapped part.

The targeted percent for roller debulk was not obtained initially. The 72- to 87-degree oriented entrance insert attained 45 to 70% of ultimate specific gravity instead of the targeted 80%. The parallel-wrapped throat extension attained 83 to 85% debulk instead of the targeted 93 to 94%. The lower roller debulk values presented no problem due to final debulk attainment with the hydroclave pressure. Experience in tape wrapping indicated that a minimum of 70% debulk is adequate for providing the predicted orientation in the center of the part. Finally, the exit cone liner did achieve the targeted 93% debulk. Factors contributing to the higher debulk were receipt of raw material with better tack properties, and incorporation of a cooling system which cooled the tape to 140°F as it passed the roller. The addition of the cooling system also eliminated tape slippage which occurred during initial tape wrapping of the exit cone liner. Other roller parameters which were used during tape wrapping were a roller pressure of 200 lb/in. of width, roller temperature of 100°F, and a tape temperature upstream of the roller of 300 to 400°F (infrascopy measurement).

## 2. Nylon Tension-Wrap Process

The nylon tension-wrap process demonstrated the ability to fabricate ablative plastic components with adequate properties without a hydroclave or autoclave. Comparison of the physical properties of the exit cone insert with those properties obtained with 1000-psi molding pressure are shown in Figures 233 and 234. The specific gravity of the nylon tension-wrap parts were 95% of the ultimate attained with 1000-psi hydroclave pressure for the carbon cloth and 100% of ultimate for the silica cloth. Postfired performance of these components were as predicted. Comparison of the physical

X, B, 120-SS-1 Nozzle (cont.)

properties of the component under the longitudinal tension straps and between tension straps are shown in Figure 234. There is no apparent difference in properties; however, surface indentation occurred under the straps, indicating that minimizing the spacing between straps would improve the process and provide a more uniform molded laminate orientation. This improvement was incorporated in the 260-SL exit cone fabrication.

### 3. Tape Orientation in Molded Part

Determination of the laminate orientation was attempted by inserting a lead foil into the laminate; subsequent X-ray examination of the laminate was not successful. The laminate orientation was determined visually from the end ring specimens. The required laminate orientations were obtained with good uniformity; only slight local reorientation occurred.

### 4. Hydroclave Bagging

Water leakage during the preform cycle was a common occurrence. A bag failure occurred during preforming of the entrance insert and the first throat extension. The entrance insert was not wetted, but the extension insert was wetted and eventually rejected and replaced. A hydroclave line breakage occurred during preforming of the throat insert causing a loss in vacuum. As the throat was at a temperature of 187°F for less than 1 hr, the effects of the exposure were insignificant. The throat was subjected to a second preform cycle. Analysis of the cycle and tag-end tests indicated that the throat had attained 93% debulk with a small degree of resin advancement. Various studies and changes to the bagging system were made throughout the program.

### 5. Preform Cycle

The preform cycles were established from the subtask data, accurately planned, and determined to be very adequate. The system used a

X, B, 120-SS-1 Nozzle (cont.)

hot-air recirculating system inside the mandrel to transfer heat to the part. Thermocouples were imbedded in the part to monitor the temperature during the cycle.

The preform cycle of the entrance insert was similar to the planned cycle. The physical properties results indicate that the cycle was adequate. The first attempt at preforming the throat insert was aborted after less than 1 hr at 187°F. Data from the process evaluation subtasks indicate that the change in properties are insignificant after a 6-hr exposure at 187°F. The second preform cycle was similar to the planned cycle except the temperature reached 193°F instead of 185°F for 2 hr. Subtask data and tag-end test data indicated that maximum debulk of 93% was obtained while retaining a low degree of resin advancement.

During preforming of the second throat extension, an operational error resulted in an extended preform cycle. Duration at 187°F was 84 hr instead of the planned 5-1/2 hr. As a result of the extended cycle, the part was 85% polymerized. This advancement had no effect on the physical properties of the final cured part.

A malfunction in the temperature recording instrumentation caused the temperature of the exit cone preforming cycle to reach 193 to 200°F instead of the planned 187°F. The effect of the higher temperature on resin advancement was slight. An equipment check prior to each cycle was investigated to prevent similar malfunctions.

#### 6. Cure Cycle

The cure cycle was also established from data obtained in the subtasks. The equipment setup was the same as that employed for preforming.

X, B, 120-SS-1 Nozzle (cont.)

The cure cycle of the entrance insert was in accordance with the planned cycle. The initial preheat portion of the throat-insert cure cycle consisted of 7-hr duration instead of the planned 4-hr duration. Data from the subtasks indicated that the extended duration at 187°F had negligible effect on the final-cured throat. This was verified by the physical properties of the final-cured part. The cure cycle of throat extension No. 2 was extended 1-1/2 hr longer than planned at a temperature of 300 to 315°F; this excess in time did not affect the part. The exit cone was final-cured as planned. A shutdown in the plant vacuum facility occurred during the exit cone cure cycle, and an aspirator, producing a vacuum pressure of 7 psi, was used. The loss in vacuum had no effect on the part as evidenced by the exceptionally low volatile content of the part (0.21% for MX-4926 and 0.11% for FM-5131).

#### 7. Postcure Cycles

The first throat extension, which was wetted during preforming, was subjected to postcure cycles to reduce the volatile content. Whereas the volatile content was reduced to an acceptable level, the part density was unacceptable. The overall effects of extended curing cycles is not completely known.

#### 8. Material Conformance

Material conformance of the ablative parts was generally quite good. Initially, the properties were more variable and the tack was low. Properties of the material improved as the program progressed.

#### 9. Dimensional Conformance

Dimensional conformance was acceptable. No major problems in obtaining the dimensions required were encountered during fabrication.

X, B, 120-SS-1 Nozzle (cont.)

10. Nozzle Assembly

No major problems were experienced during nozzle assembly. Bond-gap requirements were met for all components, except for the rubber insulation to nozzle shell, which had a smaller gap thickness. This bond thickness was considered acceptable. Bond-cure cycles were adequate, as verified by bond sample tests and ultrasonic inspections. A leak test indicated no leakage in the assembly.

11. Exit Cone Assembly

The forward flange slipped during adhesive cure, causing problems in forward-flange alignment with the liner and the aft flange; the discrepancies were accepted. Improved techniques for securing the parts during cure were established. Bonding test specimens indicated that bond-cure cycle and strength were as required. Trepan tests and ultrasonic inspection substantiated the adequacy of the bonds. Leak tests showed no leakage.

12. Conclusions

Fabrication of the 120-SS-1 nozzle and exit cone adequately demonstrated all the processes and fabrication procedures to be used on the 260-SL nozzles. The experiences occurring throughout the fabrication revealed the various problem areas in the procedure which required modification. All problems were resolved with the exception of hydroclave bag leakage.

C. 44-SS NOZZLE

The 44-SS nozzles, the first nozzles fabricated by TRW on the program, were not intended initially for nozzle evaluation. However, many

X, C, 44-SS Nozzle (cont.)

materials and fabrication procedures were similar to those to be used on the 260-SL nozzles, and considerable knowledge was obtained which was applicable to 260-SL nozzle fabrication.

1. Material Conformance

Initially, the ablative plastic broadgoods were rejected by TRW due to deviations in acceptance properties with the material vendors. The deviations were the result of an interpretation of acceptance test procedures which were subsequently solved.

2. Dimensional Conformance

Dimensional conformance of the parts was achieved satisfactorily. Early in the program, problems occurred in determining proper tape width and percentage of debulk. As a result, undersized areas occurred in the tape-wrapped parts which required repair.

3. Die-Cut Molding

At the time of 44-SS nozzle fabrication, the experience of ablative plastic nozzle parts indicated that the throat and portions of the entrance insert could not be tape wrapped. Tape wrapping was limited to OD/ID tape ratios of 1.3 maximum. Therefore, these components were made by laying up die-cut circular arc segments in a die mold, and by hydroclave preforming and final curing in the mold.

Considerable difficulty was experienced in obtaining satisfactory die-molded throat inserts. One part was rejected due to delaminations resulting from improper removal of the preform from the mandrel. A second

X, C, 44-SS Nozzle (cont.)

5. Hydroclave Bagging

Hydroclave bag leakages occurred during fabrication of several 44-SS nozzle components. The exit cone of 44-SS-1 was wetted during preforming, but the volatile content was reduced during an extended postcure cycle and the component was used. Throat inserts Nos. 3 and 4 were both wetted due to bag failure during final cure. The parts were rejected due to the wetting and the delaminations which incurred earlier in the fabrication process.

6. Tape Orientation

Tape orientation of the parts were within requirements and were quite uniform.

7. Preform and Cure Cycles

Documentation of the preform and cure cycles of the 44-SS nozzles was not as detailed as subsequently required for the larger nozzles. The temperatures, pressures, and duration of the cycles were generally the same as those specified on the larger nozzles. No major problem occurred as a result of the curing cycles used. One extended postcure cycle was used on the exit cone of 44-SS-1, in which the volatile content was reduced from 7.88 to 2.55%, while the specific density remained within requirements. The part performed satisfactorily during motor firing.



X, C, 44-SS Nozzle (cont.)

8. Nozzle Assembly

Bonding of the inserts into the shell was performed successfully with conformance to bond gap and strength requirements. A leak check revealed small leakages in the entrance insert of the 44-SS-1 and 44-SS-2 nozzles. These leaks were repaired by injecting Epon 913 and subsequently covering the component with the entrance insulation. Ultrasonic inspection indicated adequate bond coverage. The assemblies met all requirements.

XI. HANDLING AND HANDLING EQUIPMENT

A. 260-SL NOZZLES

The ablative plastic components were handled by means of the wrapping mandrel during fabrication and assembly. These components were supported by the mandrel from the start of fabrication until they were bonded to the structural shell, except for a short duration during the radiographic inspection of the liner.

Two fixtures were built for handling the steel structural shell and the subsequent handling of the nozzle assembly. A holding fixture was designed and built by Sun Shipbuilding for fabrication of the steel shell. After completion of OD machining on the shell, the two halves of the fixture were placed on the exterior surface and attached so that the roundness of the nozzle-shell end flanges was maintained during machining of the interior surface. The fixture has trunnions on both ends for lifting and rotating the shell. The fixture was removed from the shell for hydrostatic test with the chamber and reassembled to the shell after the completion of the test.

A lightweight handling fixture was built to replace the Sun Shipbuilding holding fixture for further processing of the nozzle assembly. This fixture was designed and built by Aerojet and supplied to TRW. The lightweight fixture was used for rounding the flange diameters of the nozzle shell. The ring for rounding the large flange diameter was separable from the handling fixture and was used to provide restraint until final assembly of the nozzle to the motor. The smaller shell diameter that mates with the exit cone was rounded by the positioning of eight pads around a circumference. Trunnions are provided on both ends of the fixture for rotating the nozzle assembly, in addition to four lugs on each end that were used for vertical lift.

During fabrication and processing of the exit cone assembly, two rings, (one on each end) were used for handling. A split ring is used for

XI, A, 260-SL-Nozzles (cont.)

rounding and handling on the small diameter end which mates with the nozzle assembly. This ring, designed and provided by TRW, is attached to the exit cone flange through 22 holes. Four eyebolts, 90 degrees apart, are provided for vertical lift and rotation of the assembly. A two-piece ring, designed and provided by Aerojet, is attached to the large diameter through 36 bolt holes. Three equally spaced lugs are provided for vertical lift and four equally spaced attachment points are used for rotation. It was found that the attachments for rotating the completed assembly are marginal. The design of the ring was revised by the addition of two trunnions for processing of the 260-SL-2 exit cone assembly. These rings were assembled to the exit cone prior to removal of the wrapping mandrel for the ablative liner.

The handling fixtures for both the nozzle and exit cone assemblies were designed to be structurally adequate for a minimum of 3g acceleration load imposed on the assemblies in any direction. This design load provides a minimum safety factor of 2 on the actual anticipated load and yet is well within the calculated acceleration load capacity of the assemblies, as shown in Figure 252.

B. 120-SS-1 NOZZLE

The 120-SS-1 nozzle ablative plastic components were handled by means of the wrapping mandrel, similar to the 260-SL components, during fabrication and assembly. The mandrels, which were provided by TRW, remained in each component during processing until the component was bonded to the structural shell.

A holding fixture was designed and built by Sun Shipbuilding for fabrication of the steel shell. The two halves of the split type fixture were assembled to the shell after completion of OD machining. Thereafter, the fixture remained in place until the nozzle was assembled to the motor except for

XI, B, 120-SS-1 Nozzle (cont.)

the period during hydrostatic test. The ends of the fixture have stiffening rings for maintaining roundness of the corresponding flanges of the steel shell. Four eyebolt attachments are provided on each end of the fixture for lifting and rotation.

A one-piece fixture was used for handling the exit cone assembly; this fixture was designed and built by Aerojet. The fixture has two rings for maintaining roundness on the end flanges of the exit cone. A tubular structure was used to connect the two rings of the fixture. The fixture was assembled to the exit cone assembly after completion of processing and prior to removal of the mandrel from the plastic liner. Four eyebolts are provided at each end of the fixture for lifting and rotation.

Both the nozzle and exit cone handling fixtures were designed for a 3g minimum acceleration load imposed on the assemblies in any direction. This design load is within the calculated acceleration load capacity of the assemblies as shown in Figure 252.

C. 44-SS NOZZLES

Handling of the 44-SS nozzle required no special equipment because of the relatively small size and high margin of safety of the nozzle. The shortness and stiffness of the nozzle shell precluded the use of rounding rings. The attachment flanges are strong enough for handling purposes. Three equally spaced eyebolts in the attachment flange were used to attach handling cables, or slings were wrapped around the middle portion of nozzle shell to permit handling.

The insulation and plastic liner components were handled by their respective fabrication mandrels.

XII. PACKAGING AND SHIPPING

A. 260-SL NOZZLES

After completion of processing, the nozzle and exit cone assemblies were packaged and prepared for shipment. All material used for packaging was supplied by TRW. Both assemblies were packaged with the nozzle center line in the vertical position and with the assemblies resting on their forward diameters.

The assemblies were packaged for protection against exposure to weather. A plastic sheet was placed on the top and bottom diameters of the assembly as a sealant against moisture. Excess air within the barrier was extracted after completion of packaging. The sheet on the top end was cemented to the underside of a plywood cover which was installed and bolted to the end flange of the assembly. Desiccant bags for absorbing moisture were placed on a tray which was attached to the cover. A color-change humidity indicator was installed on the inner surface of the vapor-proof barrier. An impact recorder was attached to the handling fixtures of each assembly prior to sealing with the barrier material.

Each assembly was supported by a wooden pallet. A 5.5-in.-thick wooden ring spacer was used to provide clearance between the nozzle insulation and the pallet. The ring spacer was secured to the nozzle assembly by eight lag screws through the forward flange. The nozzle assembly was bolted to the pallet with 12 lag screws through the forward flange and the ring spacer into six stringers. A 1.5-in.-thick wooden ring was cemented to the exit cone pallet to support the assembly. In addition, six spacers were used to support the exit cone handling ring on the pallet. The exit cone assembly was bolted to the pallet with six lag screws through the spacers and handling ring into the stringers. Four 5/16-in.-dia wire cables were used to stabilize the assembly by securing the aft diameter of the exit cone to the corners of the pallet.

XIII, A, 260-SL Nozzles (cont.)

The overall dimension of the nozzle assembly package was 17 by 18 ft at the base (the size of the pallet) with a height of 11 ft 9 in. The dimension of the exit cone package was 16 by 17 ft at the base with a height of 11 ft 11 in. The total package weights of the nozzle and exit cone assemblies were 48,600 and 14,000 lb, respectively.

Both assemblies were transported by low-bed trailers from TRW, Cleveland, Ohio, to the Aerojet-Dade Division, Florida. A 60-ton trailer driven by a tandem axle tractor was used for the exit cone. Outriggers were placed on the sides of the trailers to support the oversized load. A 2-in.-thick resilient material (Ethafoam) was placed on the bed of the trailer for cushioning the load. The packaged assembly was loaded on the trailer and the pallet was tied to the trailer with ratchet-type chain binders. Each assembly was covered with a 40-ft-square tarpaulin tied to both the trailer and the assembly. Three 1-by-6 in. planks were placed on top of the assemblies as protection from overhead wires while enroute. A wooden frame barrier extending to the maximum height and width of the assembly was placed in front of the assembly to serve as a warning device for low obstacles enroute. Impact recorders were placed on the bed of each trailer and were checked periodically enroute.

The nozzle and exit cone assemblies were accepted for static firing after ultrasonic inspection indicated that no assignable shipping damage occurred.

B. 120-SS-1 NOZZLE

The 120-SS-1 nozzle and exit cone assemblies were packaged for shipping in accordance with Aerojet specifications AGC-36448 and AGC-36447, respectively. Each assembly with the installed holding fixture was covered

XII, B, 120-SS-1 Nozzle (cont.)

and sealed with reinforced plastic sheets. Desiccant bags were enclosed in the assembly. After the plastic sheets were sealed, a partial vacuum was applied to remove the excess air.

Each assembly was secured to a palletted container with the nozzle center line in the vertical position and the large diameter resting on the pallet. A builtup ring supported each assembly on the pallet. The pallet had provision for fork-lift handling and was structurally adequate for handling 3g loads in any direction. Cushions and braces were used to secure the assembly to the pallet; a wooden container was used to enclose each assembly. The inside surface of the container was sealed against water. The total weight of both assemblies was 10,700 lb.

The assemblies were shipped in their containers by a closed van from TRW, Cleveland, Ohio, to the Aerojet-Dade Division, Florida.

C. 44-SS NOZZLES

The nozzle shells were packaged in wooden crates and secured by bolts through the attachments flanges. The internal surface of the nozzle rubber insulation was encased in a plaster cast to protect the rubber during handling and shipping. The insulation was shipped while on the fabrication mandrel.

The nozzle assembly was wrapped in a polyethylene bag which was filled with desiccant bags. The nozzle was bolted through the aft attachment flange to a wooden packing crate. Rubber pads were placed between the crate and the nozzle flanges.

XIII. NOZZLE PERFORMANCE

A. 44-SS MOTORS

1. Motor 44-SS-1

The 44-SS-1 nozzle components were in excellent postfiring condition with the exception of the aft portion of the throat insert, shown in Figures 253 and 254. The nozzle surface recession is shown in Figures 255 and 256. The nozzle throat and exit cone surface recession was obtained by measuring the diameters with calipers before and after the test. The surface recession of the entire nozzle contour was obtained with a contour follower tool, which measured the surface before and after firing on Mylar templates. Accuracy of the follower tool is approximately  $\pm 1/64$  in. The results taken with the follower tool were in agreement with the throat and exit cone measurements taken with the calipers. The forward portion of the throat insert was eroded smoothly and uniformly with a throat surface recession rate of approximately 0.00336 in./sec (Figure 255), which is less than the predicted 0.0042 in./sec. However, 0.20- to 0.48-in.-deep by 0.50-in.-wide gouges occurred downstream of the geometric throat. The gouges extended around the entire circumference. Also, white circumferential lines were evident in the upstream surface of the throat insert and were attributed to aluminum deposition. A cross-sectional view of the nozzle (Figure 257) showed a striated effect in the region of the throat insert gouges.

The throat insert was fabricated by layup of die-cut 90-degree-arc segments which were compression molded at 1000 psi. The striated appearance of the gouged area indicated that some fabrication discrepancy could have contributed to the gouging. However, as gouging also occurred in the region adjacent to the aft-end igniter, the ignition phenomena was also considered a possible cause of the gouging. Additional analysis of the gas dynamics of the igniter motor and 44-SS-1 motor exhaust stream substantiated the previous



XIII, A, 44-SS Motors (cont.)

analysis, which concluded that there is no igniter motor gas impingement on the throat insert, Reference (5).

A section of the nozzle was sent to TRW for further analysis of the throat-insert gouging problem. The striation effect was analyzed by TRW to be the result of the method of stacking and overlapping the throat laminates which supposedly has no effect on strength or performance. However, the results of the physical property tests conducted by TRW showed several factors which could account for the poor performance of the striated aft portion.

a. The interlaminar shear of specimens taken from the striated section ranged from 600 to 1900 psi (1200 psi average), whereas the interlaminar shear of specimens from the nonstriated section was higher, ranging from 900 to 2800 psi (1800 psi average).

b. The compressive strength readings of the striated portion ranged from 37,500 to 45,400 psi (41,200 psi average), whereas the readings of the nonstriated section ranged from 40,100 to 47,800 psi (44,100 psi average).

c. The Shore D hardness of the char in the striated section ranged from 66 to 85, whereas the char hardness of the nonstriated section ranged from 50 to 69. The hardness of the parent material was similar for both sections.

d. The tensile strength of the raw carbon material, as taken from the three rolls used in the throat insert, varied considerably, ranging from 32 to 70 lb/in.-width in the warp direction and from 28 to 70 lb/in.-width in the fill direction. The location of the rolls with respect to the insert is not known.

XIII, A, 44-SS Motors (cont.)

The variations in the above four properties, plus variations in stacking and processing of the laminates, could have accounted for the gouging in the aft portion of the throat insert. This was confirmed later by the testing of the 44-SS-3 nozzle, which had a tape-wrapped throat insert instead of the stacked die-cut insert.

The rubber entrance insulation eroded smoothly and uniformly with a maximum radial spread of 0.18 in. The recessions at various radial and axial locations are tabulated in Figure 256. The recession was generally higher than predicted at the forward end and considerably less than predicted at the aft end. The valleys of the grain configuration were aligned with the insulation at an area ratio of approximately 3.86:1 (Figure 258). The results do not indicate any effect of grain geometry on the insulation surface recession as was evidenced in the motor 120-SS-1. Also, Figure 258 shows that the throat recession is very uniform and does not reflect any deviation observed on the rubber insulation.

The surface recession of the entrance insert was fairly smooth and uniform, but the recession rate was two to three times higher than that predicted. The higher surface recession is attributed to the non-optimum contour of the rubber entrance insulation, which did not provide smooth flow to the entrance insert. Also, the insulation had been predicted to erode more rapidly in the area adjacent to the entrance insert. As a result of the insulation contour and the fact that the insulation did not erode as rapidly in the aft area, the flow detached near the aft end of the rubber insulation and reattached on the silica entrance insert, resulting in a higher heat flux. The silica entrance insert was designed with a safety factor of two and could withstand the more severe flow environment.

The exit cone insert had less surface recession than predicted, without cracks or delaminations. The fact that the exit cone was of the same

XIII, A, 44-SS Motors (cont.)

material as the throat insert, but was made by a different process (tape-wrapped vs die-cut molded), would also indicate that the throat insert gouging was due to the method of fabrication.

The char depth was measured at the 60-, 90-, 180-, and 210-degree radial stations where the nozzle was sectioned. The results (Figures 255 and 259) indicate the char depth was approximately twice that predicted in the throat insert, and 50% greater than that predicted in the entrance and exit cone inserts. The measured char was expected to be greater than predicted since the actual erosion was less than predicted. Also, the quench system did not function for the full quench duration.

The V-61 insulation around the nozzle retainer ring charred slightly (less than 0.10 in.) at the aft plane; no char occurred on the outside diameter or at the forward plane.

The silicone sealant between the plastic inserts was squeezed and/or eroded out to depths of 1/8 to 1/2 in., corresponding to the char depths of the inserts; however, a seal was maintained between the inserts. The gap sealant, O-rings, and bond between the inserts and steel shell were intact after firing, thus preventing any gas leak to the shell. This was verified by the temperature readings from the thermocouples located along the nozzle exterior which did not exceed 102°F (Figures 260 and 261), indicating a maximum increase of only 19°F.

With the exception of the throat insert, all materials and components of the 44-SS-1 nozzle performed as predicted and confirmed their selection for use in the 260-SL nozzles.

XIII, A, 44-SS Motors (cont.)

2. Motor 44-SS-2

The performance of the 44-SS-2 nozzle was essentially identical to that of the 44-SS-1 nozzle, which was as expected, since their nozzle design and fabrication techniques were similar. The nozzle surface recession is shown in Figures 262 and 263.

The rubber entrance insulation eroded smoothly in a manner similar to that of 44-SS-1. The surface recession was higher than predicted at the forward end and considerably less than predicted at the aft end. A radial plot of recession does not indicate any extreme recession effect due to grain geometry (Figure 264). However, the recession at locations aligned with the valleys of the grain is greater than at locations between the valleys.

The surface recession of the entrance insert was fairly smooth and uniform, but the recession rate was approximately twice that predicted, similar to that of 44-SS-1. As discussed in Section XIII,A,1, the higher surface recession was attributed to the contour of the rubber entrance insulation, which resulted in a separated gas flow from the rubber insulation and reattachment with a high heat flux on the entrance insert.

The throat surface recession rate was approximately 0.00315 in./sec (average), less than the predicted rate of 0.0042 in./sec. The forward portion of the throat insert was eroded smoothly and uniformly; however, 0.19- to 0.49-in.-deep by 0.50-in.-wide gouges occurred downstream of the geometric throat. The gouges extended around the entire circumference. A posttest view of the nozzle is shown in Figure 265.

The exit cone insert had less surface recession than predicted, without cracks or delamination, similar to that of 44-SS-1. As discussed in Section XIII,A,1, the fact that the exit cone was of the same material as the

XIII, A, 44-SS Motors (cont.)

throat insert, but was fabricated by a different process, would indicate that the throat insert gouging was due to the method of fabrication. This was further demonstrated in the second 44-SS motor firing, because the throat insert of 44-SS-1 was 0.75-in. shorter than that of the 44-SS-2 throat insert. Gouging occurred in the last 0.75 in. portion of the 44-SS-2 throat insert but not in the comparable location (the exit cone insert) of the 44-SS-1 nozzle, i.e., gouging occurred only in the die-cut molded inserts and not in the tape-wrapped inserts.

Since the surface recession of 44-SS-2 nozzle was similar to that of 44-SS-1 nozzle, the 44-SS-2 nozzle was not sectioned and char depth data were not obtained.

The silicone sealant between the inserts was removed to a depth of approximately 1/8 to 1/2 in. but remained intact within the gap. Four thermocouples were positioned on the exterior of the nozzle shell opposite insert joints, as shown in Figure 266. The data from these thermocouples (Figure 267) indicated that there were no joint leaks or insert anomalies which could provide gas paths to the shell. There were no visible discoloration on the nozzle shell due to excessive heating.

The V-61 insulation around the nozzle retainer ring was charred less than 1/8 in. at the aft plane, similar to that incurred in motor 44-SS-1.

3. Motor 44-SS-3

The nozzle components were in excellent postfiring condition, as shown in Figures 268 through 272. The nozzle surface recession at various stations is shown in Figures 273 and 274.

XIII, A, 44-SS Motors (cont.)

The rubber insulation in the nozzle entrance was eroded in a fairly uniform manner; no areas of selective erosion were observed (Figure 268). The surface recession was higher than predicted in the forward end and less than predicted at the aft end. The surface recession with respect to grain geometry is shown in Figure 275, which indicated higher recession at locations opposite the valleys of the grain.

The throat surface recession rate was approximately 0.00373 in./sec, which was less than the predicted 0.0042 in./sec and slightly higher than the 0.00336- and 0.00315-in./sec rates obtained in the 44-SS-1 and -2 motor nozzles, respectively. The throat insert surface recession was very smooth (Figures 271 through 273) and did not have the gouging which occurred downstream of the throat in the 44-SS-1 and -2 motor nozzles. The gouged throat inserts of motors 44-SS-1 and -2 were made by laying up and compression molding the die-cut segments. The insert portion, which was gouged in the 44-SS-1 and -2 motor nozzles, was replaced with a tape-wrapped section in the 44-SS-3 motor nozzle. It was concluded that the throat gouging of the 44-SS-1 and -2 motor nozzles was due to the method of fabrication. The upstream portion of the 44-SS-3 throat insert was die-cut molded, similar to that of the 44-SS-1 and -2 nozzles, and performance was very similar.

The surface recession of the entrance and exit-cone inserts was fairly uniform and performed similarly to comparable inserts in the 44-SS-1 and -2 motor nozzles. No delamination or cracks were observed. The surface recession of the exit cone was lower than predicted, whereas the entrance insert surface receded approximately twice as much as predicted. This higher surface recession is attributed to the contour of the rubber entrance insulation for the 44-SS-1 and -2 nozzles. The entrance insert was designed with a high erosion safety factor and could withstand the more severe flow environment. Since the recession of the 44-SS-3 nozzle was similar to that of the 44-SS-1 and -2 nozzles, the component was not sectioned to determine char depth.

XIII, A, 44-SS Motors (cont.)

The silicone sealant between the plastic inserts was removed for a depth of 1/8 to 1/2 in., but maintained a seal between the joints during the motor firing.

Five thermocouples were positioned along the nozzle exterior to coincide with the ablative insert joints in the nozzle as shown in Figure 276. The thermocouple data (Figure 277) indicated that essentially no change in exterior temperature occurred due to gas leakage through the insert joints. The maximum temperature increase of 17°F is attributable to the heat from the exhaust plume. There were no visual areas of paint or metal discoloration on the nozzle shell.

The V-61 insulation around the nozzle retainer ring was charred to a depth of less than a 0.10 in. on the aft face (Figure 270). No charring occurred on the OD or the forward face of the V-61.

The performance of the materials and components in the three 44-SS nozzles was quite reproducible and confirmed their selection and predicted performance in the 260-SL motor nozzles.

XIII, Nozzle Performance (cont.)

B. 120-SS-1 NOZZLE

1. General

The nozzle and exit cone assemblies performed successfully throughout the motor firing. The objectives of the test, a subscale version of the 260-SL motor nozzle with similar design and fabrication processes, were accomplished.

The surface-erosion contour was irregular upstream from the throat and was relatively smooth and uniform downstream from the throat. Irregular erosion in the nozzle entrance section was caused by the combined effects of the erosion pattern in the Germax-modified V-44 insulation in the aft end of the chamber and the nonuniform gas flow generated by the configuration of the propellant grain.

The surface recession of all nozzle liner materials was within design limits, which were based on twice the predicted recession depth. At the throat, the average recession rate was 0.0048 in./sec, as compared with a predicted rate of 0.00405 in./sec. At the entrance section, the maximum deviation of recession rate from the predicted rate occurred at the 1.6 area ratio; the average recession rate was 0.004 in./sec compared with a predicted rate of 0.0028 in./sec. At stations downstream from the throat, the average recession rates were generally lower than predicted.

The char formation on the ablation surfaces was greater than predicted; maximum char layer occurred in the throat insert. The predicted values were based on motor burn time and did not include postfiring heat-soak. The motor quench system did not function properly, and the quench boom was not inserted into the nozzle until 132 sec after tailoff.



XIII, B, 120-SS-1 Nozzle (cont.)

The laminae orientation of the nozzle inserts were uniform with only slight local reorientation. The orientation angles were all within tolerance limits specified by the design.

The aft 12 in. of the external surface of the exit cone showed evidence of heating, apparently due to blow back of the exhaust gases during motor tailoff. The remainder of the nozzle and exit cone surfaces showed no thermal or structural damage.

Posttest diameter measurements were taken at the throat and exit plane. Pretest and posttest contour measurements were taken of the nozzle ablation surfaces to provide data for analysis of the erosion characteristics. Posttest surfaces were wire-brushed to remove the loose char prior to measurement. The nozzle and exit cone contour profile was traced longitudinally with a tracing tool on a Mylar sheet, which was held by a fixture. The tracings on the Mylar sheets were subsequently converted back to the actual contour by a template.

Numerous profiles of the nozzle assembly were taken to establish the variation in erosion of the nozzle entrance region. In addition to the profiles taken at 45-degree intervals (Figure 278), profiles from 10 other selected radial locations were taken. By superimposing the pretest and posttest contours, a direct measurement of the recession depth for each location was provided. The accuracy of the resultant measurements was within  $\pm 0.030$  in. A summary of the nozzle recession depths for all these radial locations is shown in Figure 279. These recession depths were plotted in the proper radial orientation (Figure 280) for comparison with the predicted recession at three stations of the nozzle entrance. A comparison of the maximum and minimum surface recession with the predicted recession of the nozzle assembly is shown in Figure 281.

XIII, B, 120-SS-1 Nozzle (cont.)

Measurements were also taken of the V-44 insulation contour at the nozzle attachment-joint interface to determine the circumferential variation of erosion. The measurements taken are tabulated in Figure 282.

The nozzle assembly inserts were subsequently removed from the steel shell and sectioned to determine the char depth and laminae orientation. Char depths were determined from Shore D hardness readings taken at intervals through the thickness of each insert. The char interface corresponds to the point of sudden change in hardness readings and is verified by a test that shows high water absorption within the char layer. Four equally spaced circumferential locations were sectioned, and hardness readings were recorded. A tabulation of the maximum, average, and minimum hardness readings taken on the throat insert is shown in Figure 283. The laminae orientation within each insert was obtained by tracing the laminates at each of the four cross sections. The laminae orientation of the throat insert is shown in Figure 283.

The exit-cone assembly was cut longitudinally at four locations, 90-degrees apart, after 4-in.-long sections had been cut from the forward and aft ends to remove the end flanges. Shore D hardness readings were taken at each longitudinal cross section. The maximum, average, and minimum readings are tabulated in Figure 284; the laminae orientation of the exit cone insert is also shown in Figure 284.

Tensile mechanical properties were determined from ablative material specimens obtained from components of the 120-SS-1 nozzle to verify the values used for ablative material mechanical properties in the structural analysis of the 260-SL-1 nozzle. The values obtained from these tests exceeded the values used in the structural analysis of the 260-SL-1 nozzle. The average tensile strength of MX-2646 measured in specimen tests was 7700 psi in the meridional direction. The calculated maximum meridional stress in this

## XIII, B, 120-SS-1 Nozzle (cont.)

material in the 260-SL-1 nozzle is 10,000 psi, and occurs locally on the ablative surface in the aft (large) end of the entrance cap. Thus, if the calculated stress actually exists, and the actual meridional tensile strength is the same as that indicated by the specimens tested, it is probable that surface cracks will occur in the heat-affected layers of the ablative material. Such cracks in the ablation surface would be closed by thermal expansion of the char layer. Such cracks in the ablation surface would be closed by thermal expansion of the char layer. Such cracks would not extend into the hoop overwrap, and thermal protection for the structural shell would continue to be provided by this overwrap. Since the measurement of meridional tensile strength for MX-2646 was accomplished on a specimen from the postfired 120-SS-1 nozzle entrance insert, the tensile strength may have been degraded by the test firing exposure.

Tests of interlaminar shear, density and percent volatile were conducted on specimens obtained from postfired 120-SS-1 nozzle components. The results are shown in Figure 285. The results indicated that the physical property values were above the minimum requirements; however, the interlaminar shear of the carbon throat insert was much lower than that obtained in the carbon located in the entrance and throat extension inserts. The mechanical property data obtained verified the structural adequacy of ablative components designed for the 260-SL nozzles.

Forward and aft sections of the postfired 120-SS-1 nozzle throat extension are shown in Figures 286 and 287. The section shows the exceptional uniformity achieved in the tape wrap. The appearance of the char layer is shown at the top of the section.

The aft section of the postfired nozzle throat is shown in Figure 288. Uniformity in the transition in the tape orientation resulting from debulk in the 1000-psi hydroclave molding and uniformity throughout the

XIII, B, 120-SS-1 Nozzle (cont.)

entire section can be seen. The appearance of the char layer in the throat shows both the separations occurring in the disintegration of the resin and the irregular erosion occurring on the exposed surface. Using the scale shown, the erosion reaches a maximum depth of 0.150 in. from the primary eroded surface, with an average depth of 0.075 in. The separations are confined to the char layer. The dots shown in the char layer are perforations made in conducting the Shore durometer hardness test.

The entrance cap section, showing the interface between the FM-5131 wrapped 82 degrees to center line, the MX-4926 wrapped 82 degrees to center line, and the FM-5131 parallel-to-surface overwrap, is presented in Figure 289. The interface between all these components indicate a well-defined interface bond and uniformity in tape-laminate orientation. The enlarged photograph of the section shows the nature of the char developed in the 82-degree-to-center-line laminate. The cracks developed are confined to the char depth, and a maximum erosion of 0.050 in. in depth was noted.

Two sections of the exit cone liner are shown in Figures 290 and 291. Uniformity in the parallel-to-center-line tape-wrapped liner was achieved in the high-debulk tape wrap and the subsequent low-pressure, prestressed, nylon-tape, tension-molding method. An intimate bond line was achieved in the FM-5131 silica tape overwrap. Uniformity in the adhesive bond line was achieved in the stainless steel skins, using low vacuum-bag molding pressures. It can be seen that the required degree of filleting around the contacting edges of honeycomb core was attained. The irregular edges of the honeycomb core are due to machining of the sample sections.

Figure 292 shows the thermal separation at the carbon-to-silica tape interface in the exit cone liner. The separation appears to have been formed during the cool-down period by the sharp trailing edge of

XIII, B, 120-SS-1 Nozzle (cont.)

the carbon tape. Exceptional uniformity of the tape-wrapped FM-4926 and FM-5131 is to be noted. Although some distortion in the overwrap is discernible, the overwrap is considered to be functionally acceptable.

The adhesive filleting of the honeycomb core exposed by removal of the exterior stainless-steel outer skin and the adhesive bond between two honeycomb core blankets is shown in Figure 293.

2. Nozzle Entrance Section

Maximum surface erosion occurred in the nozzle entrance region. All of the V-44 insulation was eroded at the aft end. The forward portion of the insulation was eroded irregularly. The least eroded area occurred at approximately the 180-degree location and the most eroded area at approximately the 150-degree location. The orientation of the nozzle with respect to the propellant-grain configuration is shown in Figure 280. The silica-cloth insert, which was initially protected by the V-44 insulation, was eroded irregularly to coincide with the pattern of erosion of the insulation; the insert surface showed no indications of delamination. The carbon-cloth insert forward of the throat was eroded more uniformly than the silica-cloth insert. However, variations of erosion in the circumferential direction were still noticeable as a result of extension of the pattern of erosion in the aft head.

The erosion pattern of the V-44 insulation in the nozzle entrance insert (Figure 280) showed six locations, approximately 60 degrees apart, that exhibited higher than predicted erosion. The maximum erosion at the 150-degree location was 55% more than that predicted (3.0 area ratio). The high erosion was the result of the Germax-modified V-44 material used at the six insulation joints of the aft chamber. The faster erosion of the

XIII, B, 120-SS-1 Nozzle (cont.)

modified V-44 caused a wide variation of recession depths for both the silica cloth and the carbon cloth in the nozzle entrance insert. The recession depth varied from 0.45 to 1.04 in. (0.78 in. predicted) at the 2.26 area ratio for the silica cloth, and from 0.21 to 0.60 in. (0.254 in. predicted) at the 1.60 area ratio for the carbon cloth. In addition to these phenomena, the variation of erosion in the nozzle entrance region was also affected by the configuration of the propellant grain. The aft chamber insulation joints of the 260-SL motor were filled with Gen-Gard V-61 material, which has higher erosion resistance.

Downstream from the entrance area ratio of 1.6 at the silica/carbon interface, the erosion became more uniform circumferentially except at the 180-degree location. The variation of recession depth at the 1.20 entrance area ratio was from 0.35 to 0.50 in., except at the 180-degree location where the recession depth was from 0.26 to 0.29 in. Since the carbon cloth in the entrance insert exhibited better erosion uniformity than the silica cloth, the carbon-cloth entrance section was extended upstream to a 2:1 area ratio in the 260-SL nozzles.

The average char thicknesses at the 1.6 and 2.26 area ratios were 0.24 and 0.07 in., respectively, and agreed closely with the predicted thicknesses of 0.29 and 0.08 in., respectively. However, because of the much higher erosion in this region, the char thickness would be expected to be much less than predicted.

The laminae orientation of the entrance insert is shown in Figure 294. Only a slight reorientation was observed in the silica-cloth insert. Both the carbon cloth and the silica cloth have orientation angles from 80 to 86 degrees, which are within the design limits of 72 to 87 degrees.

## XIII, B, 120-SS-1 Nozzle (cont.)

3. Nozzle Throat Insert

The nozzle throat insert eroded evenly around the circumference except for a slight hump that appeared at the 180-degree location. At the throat, the recession-depth variation from contour measurements was 0.35 to 0.51 in., with an average depth of 0.43 in. (Figure 279). The predicted depth was 0.365 in.; the average recession depth at the throat obtained by comparing the pretest and posttest diameter measurements taken at four locations was 0.39 in. The recession depth at the 180-degree location was 0.35 in.

The physical appearance of the throat surface (Figure 295) showed a general roughness with numerous ridges. These ridges are perpendicular to the gas flow and are more numerous at the aft end of the insert, numbering approximately 12 to 15 per in. The ridges are approximately 1/16 to 1/8 in. deep and are continuous for about 120 degrees of the circumference. At the center of the insert (nozzle throat), the frequency of the ridges was 5 to 7 per in. The forward position of the insert was eroded smoothly and only a few ridges appeared. This type of roughness did not occur in the 44-SS motors or on the 120-SS-1 nozzle entrance insert. The fact that the interlaminar shear of the throat insert was much lower than the entrance or throat extension inserts (Figure 285) indicates that the throat insert was a lower quality component which could account for the postfired ridges and the higher than predicted surface recession.

The char thicknesses of the throat insert were much higher than predicted. At the upstream 1.2 area ratio, throat, and downstream 1.1 area ratio, respectively, the average char thicknesses were 0.43, 0.65, and 0.72 in., respectively, as compared with predicted thicknesses at motor burnout of 0.26, 0.24, and 0.25 in. The 0.65 in. thickness at the throat was

XIII, B, 120-SS-1 Nozzle (cont.)

more than 2.5 times the predicted char thickness of 0.24 in. at motor burnout and was higher than the 0.43-in. thickness predicted for an unquenched condition. The design safety factor of the insert permitted the insert to accept the additional char.

The laminae orientation of the throat insert is shown in Figure 29<sup>4</sup>. A slight waviness in the laminae is seen at the middle section of the insert; the laminae at both ends were straight. The orientation angle was from 63 to 69 degrees, which is within the design limits of 60 to 75 degrees. The laminae orientation of this throat insert was much more uniform compared with the half-length throat insert that was previously fabricated for a process evaluation task.

4. Throat Extension Insert

The throat extension insert presented a smoothly eroded surface with the exception of three circumferential gaps. Approximately 6 in. apart and measuring along the nozzle center line from the aft end, gaps due to delamination between layers of carbon fabric were opened for approximately 180 to 270 degrees circumferentially (Figure 29<sup>6</sup>). The gaps would accept a 0.020-in. feeler gage for a depth of approximately 1 in. The step that existed at each gap location was caused by breakage of the sharp edge of the charred laminates. At each location, a white deposit was observed, which was attributed to be aluminum oxide. The edge of the gaps did not erode, indicating that the gaps may have occurred during cooldown. Since the depth of delamination extended only 0.12 in. below the char layer, adequate thermal protection for the structure component existed for the full firing duration.



XIII, B, 120-SS-1 Nozzle (cont.)

The recession depth of the throat extension is lower than predicted. Average and predicted recession depths at the 1.10 area ratio are 0.300 and 0.314 in., respectively. The average recession depth at the 1.9 area ratio is 0.07 in.

The char thickness of the throat extension is a relatively constant 0.54 in., which is approximately twice the predicted thickness or approximately that amount predicted for an unquenched condition. Because of the decrease in ablation depth, the char thickness would be expected to be greater than, but not twice, that predicted.

The laminae orientation was uniform throughout. No reorientation or waviness was observed, and the orientation angle was parallel to the nozzle center line.

5. Nozzle Assembly

The overall recession profile of the nozzle assembly is shown in Figure 281. The actual and predicted recession rates are tabulated in Figure 297. Maximum and minimum recession contours are compared with the predicted recession contour (Fig 281). It can be seen that a step occurs at the forward and aft interface to the nozzle throat insert. In either case, the recession depth of the throat insert is greater than the adjacent inserts, indicating that the erosion resistance of the throat material may have been inferior. As previously discussed, the interlaminar shear of the throat insert was much lower than that of the surrounding inserts.

Sealant remained in the expansion joints at the forward and aft ends of the throat insert. A 0.125- to 0.344-in.-thick layer of sealant was missing, leaving a 1/8- to 1/4-in.-wide gap. Thermal expansion

XIII, B, 120-SS-1 Nozzle (cont.)

of the inserts during firing caused the sealant to be squeezed out of the joint. A gap occurs at the joint after firing as a result of contraction of the inserts during quench and subsequent cooldown.

Prior to separating the postfired plastic components from the steel shell, an ultrasonic inspection of the nozzle was conducted to determine bond integrity. The area of the entrance cap-to-shell bond was inspected and mapped in its entirety; the results of this inspection are shown in Figure 298. The figure covers four 90-degree radial sections of the fired nozzle assembly. The results indicated that the bonded area covered only 20 to 30% of the surface. Prefired ultrasonic inspection did not reveal this magnitude of unbonded area. It was learned during the posttest sonic investigation that a typical steel shell section, coated with adhesive, has very nearly the same attenuation of ultrasonic signal as does a complete and properly bonded steel-to-plastic assembly. This finding initiated an investigation, which has resulted in the development of sonic calibration masters for improving ability to differentiate between proper and improper bonds.

The throat-to-shell and the throat extension-to-shell bonds also were checked sonically, at four 6-in.-wide axial sections, each 90 degrees apart. Results are also shown in Figure 298. Zones of these tests lie at the 45-, 135-, 225-, and 315-degree locations. Only small areas of unbondedness were detected.

The plastic components were separated from the shell by rapid heating in an oven. The individual components were then inspected visually. Results of the apparent bond, as interpreted from the individual plastic components, are shown in Figure 298. Good correlation was obtained between the ultrasonic data and visual observation.

XIII, B, 120-SS-1 Nozzle (cont.)

The percentage of entrance-cap-to-steel bond is less than acceptable, although the bonded area functioned properly during the firing. The throat-to-shell and throat extension-to-shell bonds were excellent. It was noted that the entrance cap was bonded to the shell after adhesive was applied to both surfaces, while the throat and throat extension were bonded after adhesive was applied to the plastic parts only. It is not apparent why the application of adhesive to both surfaces could result in unbonding. Further investigations of bonding techniques were conducted in an effort to assure reliable bonds in the 260-SL nozzles. It was determined that elevated cure temperatures caused unbonding of the insert to the steel shell due to the differences in coefficients of thermal expansion. Therefore, the 260-SL nozzle inserts were bonded to the shell, using an ambient cure cycle.

6. Exit Cone Assembly

Pretest and posttest recession profiles of the exit cone were taken at eight locations (Figure 299). Recession depths obtained from these profiles are summarized in Figure 300.

The ablation surface of the exit cone was smooth except at four delamination gaps, which occurred in the carbon-cloth section, located at distances of 6, 11, 15, and 17 in. from the forward end (Figure 301). The characteristics of the delaminations and the evidence of a white deposit are similar to those of the throat extension insert. The depth of the delaminations were determined to extend 0.12 in. beyond the char thickness into the heat-affected layer.

Longitudinal grooves existed in the forward end of the exit cone at 17 locations. These 4-in.-long, 1/8-in.-deep grooves were spaced approximately 5 in. apart (Figure 302). The grooves are related to folds in

XIII, B, 120-SS-1 Nozzle (cont.)

the material that existed from the fabrication process. During tape wrapping of this component, the tape slipped away from the mandrel, loosening some of the laminae. The subsequent pressurization cure cycle resulted in these folds.

The average recession contour of the exit cone assembly is compared with the predicted recession contour in Figure 303. The erosion characteristics of the exit cone material were better than predicted.

A comparison of the pretest and posttest profiles showed that maximum erosion is located downstream of the carbon-cloth to silica-cloth interface. At that location (area ratio of 3.6), maximum erosion was expected to occur because of the change to the less erosion-resistant silica material. The average recession depth of 0.31 in. is comparable to the predicted depth of 0.314 in. Negligible erosion occurred from an area ratio of 3.0 to 3.5. The posttest profile is slightly smaller than the pretest profile at these area ratios due to thermal expansion of the laminae within the char layer. This condition is expected to be less pronounced in silica cloth than in carbon cloth, since the char depth of the former is only half that of the latter.

The 0.080-in.-wide gap at the interface laminae between the carbon-cloth and silica-cloth materials is the result of contraction of the insert during quench and cool-down. From the sectioned insert, the depth of the gap was determined to extend beyond the char depth into the heat-affected layer.

After sectioning, the char depth was obtained by Shore D hardness readings (Figure 284). The char-depth line is shown in Figure 303. The average char thicknesses are slightly higher than the predicted thickness. At

XIII, B, 120-SS-1 Nozzle (cont.)

the 3.4 area ratio in the MX-4926 carbon cloth, the average char thickness was 0.48 in. as compared with a predicted 0.40 in. In the FM-5131 silica cloth, the average char thickness was a constant 0.25 in., as compared with a predicted thickness that varied from 0.15 in. at the 3.5 area ratio to 0.20 in. at the 6.0 area ratio. As previously discussed, the actual char thickness would be expected to be higher, since the predicted thickness is based on motor burnout time and does not include postfiring heat effects.

The laminae orientation for both materials below the char layer was uniform with no evidence of reorientation or wrinkling. The orientation was parallel to the nozzle center line.

The V-61 potting compound at the exit plane performed as expected. The thickness of insulation was sufficient to protect the metal flange for the full duration, although the erosion was nonuniform in the circumferential direction. The potting compound was charred approximately 0.4 in. deep on the aft surface of the flange; the remaining uncharred V-61 was approximately 0.3 in. thick. The forward face of the flange showed no evidence of heating between 30 and 225 degrees radially, and the remaining surface indicated only slight heating.

Heating of the external nozzle surface occurred near the exit plane. The paint was blistered for the full circumference and was from 2 to 12 in. wide adjacent to the aft flange (Figure 304). Temperature-sensitive paint indicated that the maximum temperature experienced was 400°F. At this temperature, the bond between the honeycomb core and facings is degraded, as shown by a separation of approximately 4 to 5 in. between the doubler and the facing (Figure 305). After the honeycomb structure was sectioned, a separation was observed between the core and outer facing within this heat-affected area. The heating of the external surface was

XIII, B, 120-SS-1 Nozzle (cont.)

the result of flame impingement during tailoff and radiation from exhaust gases. A layer of cork insulation was bonded to the aft 2 ft of the 260-SL nozzle exteriors to prevent this external heating.

C. 260-SL NOZZLE

1. General

The nozzle and exit cone assemblies of the 260-SL-1 and -2 nozzles maintained structural integrity for the full firing duration. Erosion performance of the entrance section V-44 insulator and all ablative plastic liner components was excellent. The postfiring average throat diameter of the 260-SL-1 nozzle was 1.46 in. greater than the prefiring diameter, yielding an average material loss rate of 5.7 mils/sec during the motor action time of 128.2 sec. The average postfiring throat diameter of 260-SL-2 was 1.25 in. greater than the prefiring diameter, yielding an average throat erosion rate of 4.8 mils/sec during an action time of 129.8 sec.

Posttest erosion profiles of the nozzle and exit cone liner were taken at 60-degree intervals starting at the 0-degree radial location. The loose char on the V-44 insulation surface and the oxide deposit most pronounced on the silica cloth and phenolic portion of the exit cone were removed prior to profile measurement.

Char thickness, laminate orientation and joint integrity were determined for 260-SL-1 nozzle by removing and examining sections of the liner. This expensive operation was not performed on 260-SL-2 nozzle since the nozzle erosion and appearance was essentially similar to that of 260-SL-1.

XIII, C, 260-SL Nozzle (cont.)

Thermocouples were used to monitor the temperature of the external surface of the nozzle and exit cone. No heat was transmitted through the nozzle interior to the structural members. The aft portion of the exit cone exterior was slightly heated by the exhaust gases during tailoff, but was intact.

2. 260-SL-1

a. Erosion Performance

A summary of erosion values obtained from contour tracings is tabulated in Figure 306. Erosion profiles of the nozzle and exit cone are shown in Figures 307 and 308.

(1) Nozzle Inlet Insulation

The performance of the V-44 nozzle insulation was within design limits and was comparable to the performance of the nozzle insulation in motor 120-SS-1. The maximum surface recession occurred between area ratios of -3.10:1 and -1.60:1, with a maximum insulation material loss of 9.6 in. measured at the -2.04:1 area ratio station. Measurements taken are tabulated in Figure 306 and the maximum surface recession profile is shown in Figure 309. Erosion in the area of the step joint is shown in Figure 310.

Downstream of the -3.10:1 area ratio, the surface recession was higher than predicted, based on the thickness-loss rate vs Mach number data previously obtained for V-44 rubber; however, the maximum surface recession rate was approximately equal to the maximum rate obtained in the nozzle insulator of motor 120-SS-1.

XIII, C, 260-SL Nozzle (cont.)

The erosion contour over approximately 12 in. of length at the aft end of the insulator, spanning the -2.04:1 area ratio station, showed significant irregularity about the circumference, with as much as a 3.5-in. variation in material loss. This uneven erosion (Figure 311) is attributed to the high gas velocity and effect of flow area configuration where the insulator fails into the surface of the plastic insert. The excessive thickness of the adhesive bondline between the insulation and plastic insert may also have contributed to the uneven erosion. It is probable that some impairment of bond strength resulted from the excessive thickness. When combined with nonuniform degradation of the bond, this thickness may have affected local material loss, which would then be exaggerated by the high Mach number flow. Posttest inspection revealed areas along the bond line where significant degradation of adhesive was apparent.

Upstream of the -3.10:1 area ratio station, surface erosion was quite uniform, and total magnitude was equal to or less than predicted. Very little evidence of variability resulting from the grain configuration was apparent.

(2) Entrance Insert

Maximum surface erosion in the entrance insert occurred in the silica cloth portion of the insert at the surface of the V-44 insulation. The silica cloth section, which was initially fully covered by V-44 insulation, was eroded irregularly and coincided with the erosion pattern of the V-44 insulation. There is no evidence that variability in erosion of the plastic resulted from any cause other than variation in protection afforded by the V-44 insulation.



XIII, C, 260-SL Nozzle (cont.)

The carbon cloth portion of the insert, which interfaced with the silica at the -2.0:1 area ratio station, was more uniformly eroded, with small variability near the silica interface reflecting the variation in V-44 insulation erosion. The measured depth of erosion at the -1.6:1 area ratio station was 0.15 to 0.45 in., with an average of 0.37 in., as compared to the predicted 0.35 in. Moving from the -1.60:1 area ratio station toward the throat, measured erosion exceeded prediction by successively higher percentages; at the -1.06:1 area ratio station, the average measured erosion was 0.84 in., as compared with a predicted 0.47 in.

Figure 312 shows the posttest surface condition of the entrance insert. No delaminations were observed in the surface of the silica cloth; numerous short circumferential delaminations existed in the surface of the carbon cloth.

(3) Throat Insert

The nozzle throat insert was eroded uniformly around its circumference. At the throat station, the erosion depth obtained in contour measurements was 0.62 to 0.80 in., with an average of 0.70 in., as compared to the predicted 0.48 in. Average erosion at the throat obtained from the difference between pre- and posttest diameter measurements taken at six angular locations was 0.728 in. The total erosion was greatest at the entrance end of the insert (-1.06:1 area ratio station) and decreased progressively over the length of the insert; at the aft end (1.10:1 area ratio station); the average measured erosion was approximately equal to that predicted.

The physical appearance of the surface of the throat is shown in Figure 313. Small surface pits were observed, and the area downstream from the throat showed surface roughness similar in appearance to, but

XIII, C, 260-SL Nozzle (cont.)

of lesser magnitude than, that observed at this location in the 120-SS-1 nozzle throat insert. This surface condition appears to be the result of greater than optimum laminate orientation angle in this area.

(4) Throat Extension Insert

The measured depth of erosion of the throat extension insert was less than predicted over the entire length of the insert. At the upstream end of the insert (1.10:1 area ratio station), the average measured erosion was 0.28 in. as compared to predicted 0.42 in.; near the downstream end (1.9:1 area ratio station), the average measured erosion was 0.15 in. as compared to a predicted 0.22 in.

The surface appearance of the throat extension insert was excellent, as shown in Figure 31<sup>4</sup>. Erosion was uniform. Short circumferential delaminations were apparent.

(5) Exit Cone Liner

A comparison of pretest and posttest contour tracings shows that erosion of the carbon cloth portion of the exit cone liner (between the 2.0:1 and 3.0:1 area ratio station) was approximately equal to, or slightly less than, that predicted. Erosion of the silica cloth over the remainder of the exit cone varied from slightly in excess of prediction at the upstream end (3.0:1 area ratio station) to somewhat less than predicted at the downstream end (6.0:1 area ratio station). Maximum erosion of the silica cloth occurred a short distance downstream from the carbon-cloth to silica-cloth interface (3.1:1 area ratio station), as was expected.

## XIII, C, 260-SL Nozzle (cont.)

The ablation surface of the carbon cloth portion of the exit cone was smooth, with long circumferential delaminations as shown in Figure 315. These delaminations were similar in appearance to those observed in the throat extension insert and exit cone of motor 120-SS-1, which were also tape wrapped with parallel-to-nozzle center line orientation. Two major delaminations existed at the forward end of the exit cone liner at locations corresponding to ultrasonic and X-ray inspection indications.

The ablation surface of the silica cloth is shown in Figure 316. An oxide deposit covered the entire surface of the silica cloth and was heaviest near the carbon-cloth to silica-cloth interface, decreasing progressively toward the exit plane. Analysis of samples of this deposit by emission spectrograph and X-ray diffraction showed the oxide to be basically mullite ( $3\text{Al}_2\text{O}_3 \cdot 2\text{SiO}_2$ ) with additional silicon present as  $\text{SiO}_2$ . This oxide was apparently produced as a melt of  $\text{SiO}_2$  from the silica cloth of the liner and  $\text{Al}_2\text{O}_3$  from the aluminum of the propellant. The molten oxide apparently collected on the surface late in motor tailoff and tended to flow downward from the exit plane.

Circumferential delaminations, spaced 6 to 12 in. apart, were observed over the entire surface of the silica cloth portion of the liner. Longitudinal depressions were also observed, being most pronounced at the upstream end of the silica cloth section. The pattern of these depressions correlates with locations of steel strips used to retain the nylon tension wrap during liner cure and appear to result from small fiber reorientation occurring between each of the first layer of these strips.

In summary, the erosion performance of ablative components in the expansion section (downstream of the throat) was in substantial agreement with predictions based on heat transfer analysis, while actual erosion

## XIII, C, 260-SL Nozzle (cont.)

exceeded prediction by as much as 50% at the throat and locations in the entrance section. Since results of the same nature were obtained in the sub-scale nozzle tested on motor 120-SS-1, the procedures for prediction of erosion at the throat and in the entrance section must be revised.

## b. Char Thickness and Structural Integrity

After firing, a section of each plastic component was removed to examine char thickness, laminate orientation, and joint integrity. Using a portable circular-bladed saw, two longitudinal cuts were made near the 0-degree location, extending over the full length of plastic components. One cut was made perpendicular to surface; a second cut, made at an angle of approximately 60 degrees to surface near the interface of the overwrap and innerwrap, intersected the first cut such that a longitudinal strip, triangular in cross section, was removed.

Observed laminate orientations were uniform, with no evidence of significant reorientation or wrinkling during cure, and in close agreement with design values as shown below.

<u>Component</u>	<u>Measured Approximate Laminate Orientation Angle, Degrees to Nozzle Center Line</u>	<u>Required Laminate Orientation Angle, Degrees to Nozzle Center Line</u>
Entrance Insert	79	72 to 87
Throat Insert	62 to 72	60 to 75
Throat Extension	27	20 to 35
Exit Cone	0	-1 to +3

XIII, C, 260-SL Nozzle (cont.)

Integrity of all joints between plastic components appeared excellent with no evidence of gas penetration into the joint areas. The silicone rubber sealant was eroded away to a depth of 0.25 to 0.38 in. below the eroded surface of the plastic but was intact with apparent normal physical properties at greater depths.

An examination was made of the section of plastic that was removed to further evaluate the circumferential delaminations observed in the surface of the components. The majority of these delamination cracks were found to extend only to the depth of the heat-affected zone; thus, the cracks would appear to have resulted from differential thermal expansion in cooling of the char layer. Those delaminations which extended through the innerwrap to the surface of the overwrap showed no evidence of gas circulation or oxide deposit, and there was no indication of increased depth of the heat-affected zone in the local area of the delamination.

As shown in Figures 317 and 318, the measured thickness of the char layer exceeded the predicted value at all locations. However, predicted char thickness was based on the water quench stopping growth of the char layer at 140 sec, while actual quench start occurred at 247 sec. Char thickness at the throat station only was recalculated based on actual motor ballistic performance and elapsed time prior to quench, and the value obtained was still substantially less than predicted. It thus appears that the values of material thermal properties at elevated temperature, which were used in the heat-transfer calculations to obtain char thickness, are incorrect.

In general, values of material thermal properties used in past heat-transfer calculations have been extrapolated from low-temperature test data with very limited data from tests actually conducted at elevated temperatures. Using thermal properties at temperatures of up to 750°F, as

XIII, C, 260-SL Nozzle (cont.)

determined in tests of MX-4926 carbon cloth and phenolic recently reported by Southern Research Institute, Reference (8), the heat-transfer computer program was repeated for the throat station. This calculation yielded a calculated depth from the eroded surface to the 500° isotherm of 1.04 in., as compared to a calculated depth from the eroded surface to the 500°F isotherm of 0.67 in., using the same computer program and material property values on which past calculations were based. The measured char thickness (depth below eroded surface) was 0.85 in. Based on Southern Research Institute material property data, this measured depth coincides closely to the calculated depth at the 700°F isotherm. Recently reported data, Reference (9), indicate that the lower limit temperature of pyrolysis of phenolics is 689°F, and charring occurs at some temperatures above this value.

Although further analysis, covering the entire range of entrance and expansion section flow conditions and correlation with other test results is required, it appears that future predictions of char thickness should be based on calculated depth of the 700°F isotherm, using material property data as reported by Southern Research Institute.

The V-61 potting compound applied to the exit-cone aft flange afforded adequate thermal protection. The external surface of the exit cone showed evidence of heating, in that the cork-sheet insulation placed over the outer skin of the honeycomb structure was charred or blackened over approximately three-quarters of its circumference (Figure 319), and small unbonding of one outer doubler occurred just forward of the cork insulation. This heating resulted from exhaust gas circulation during late tailoff; this is confirmed by the motion picture footage and thermocouple data. The remainder of the nozzle and exit cone show no evidence of overheating or structural damage.

XIII, C, 260-SL Nozzle (cont.)

The thermocouple data indicated no significant temperature rise along the nozzle shell. The exit cone skin temperature increased 20 to 30°F due to motor tailoff. A temperature rise of 415°F was recorded at 180 sec at the exit cone aft flange adjacent to the V-61 insulation.

c. Bonding Analysis

Specimens were removed from the nozzle and exit cone assemblies to determine the adhesive bond characteristics. Specimens were obtained from the nozzle assembly for each plastic insert at the 0-, 120- and 240-degree orientations (the 0-degree location is defined by the index hole in the attachment joint). The 120- and 240-degree orientations coincided with the unbonded areas between the throat insert and the steel shell that were observed in ultrasonic inspection. In the exit cone assembly, specimens were obtained at the 0- and 120-degree orientation in the carbon cloth and phenolic, carbon cloth-to-silica cloth interface, and silica and cloth and phenolic regions.

The specimens were removed with either a 2-in.-dia diamond cutter or a Skill saw with a diamond blade. The nozzle assembly specimens were machined to the steel shell interface and subsequently were removed by prying at the bond line between the plastic insert and the steel shell. The exit cone assembly specimens were removed by machining through the plastic liner and honeycomb structure.

Visual examination of the specimens showed that the bond between the plastic inserts and the steel shell were adequate except for local areas of the nozzle throat insert at the 120- and 240-degree locations. The ease of removal of the specimens at these locations and the characteristic of the adhesive surfaces, Figure 320, verified that unbonding occurred as previously observed from ultrasonic inspection. The remaining nozzle assembly

XIII, C, 260-SL Nozzle (cont.)

specimens indicated adhesive bond on the entire surface. Removal of these specimens resulted in interlaminar tensile failure of the overwrap, in some cases, as shown in Figure 321, and in adhesive failure between the epoxy primer and steel shell. Both types of failures indicated excellent bond strength in the adhesive.

Examination of the exit cone specimen cross section showed that the bonds between the plastic liner and honeycomb structure and between the honeycomb core and facings were adequate. Two specimens were unbonded between the inner doubler and inner facing and three specimens were unbonded between the outer doubler and outer facing. The unbonding was apparently caused by peeling of the adhesive bond during machining of the specimens.

The laminate orientation and interlaminar bond characteristics observed in the specimens verified the integrity of the component. The laminate orientation was uniform in both the ablative liner and overwrap and interlaminar bonds were excellent between the liner and overwrap. Delamination in the liner existed only within the char thickness. The carbon cloth to silica cloth interface was not delaminated in the nozzle entrance insert, but was delaminated to the overwrap in the exit cone.

3. 260-SL-2 Nozzle

a. Erosion Performance

A summary of erosion depths obtained from profile measurements is tabulated in Figure 322. The average erosion profile of the nozzle assembly is shown in Figure 323. The average nozzle throat erosion is 0.624 in. and agrees with the average of six posttest throat diameter measurements taken. Figure 324 compares nozzle insert erosion of motors 260-SL-1 and -2.



## XIII, C, 260-SL Nozzle (cont.)

The nozzle erosion profile showed a step at the downstream 1.32 area ratio and reflected contraction of the aft 16 in. of the throat extension insert. Further visual inspection of the end of the throat extension insert indicated gaps up to 0.12 in. at the bond line between the plastic insert and steel shell and within the overwrap material. The unbonding and subsequent contraction during cool-down of this portion of the throat extension insert are apparently due to the bond strength being exceeded by thermal expansion stresses and are the result of additional heating of the nozzle inserts from the quench system malfunction after motor burnout. Contraction of the insert renders the erosion values unrealistic and inaccurate within this area; however, the average erosion appeared to be less than that for the 260-SL-1 nozzle.

The exit-cone erosion data were unobtainable as a result of excessive heating caused by the quench system malfunction. Visual inspection showed separation of bonds between the liner and honeycomb facings and within the honeycomb sandwich structure. Dimensional inspection indicated apparent contraction of the plastic liner after excessive heating and subsequent cool-down. The appearance of the surface is similar to that of the 260-SL-1 exit cone, and the erosion depths are not anticipated to have exceeded the 260-SL-1 values.

## (1) Nozzle Insulation

The performance of the V-44 nozzle rubber insulation was within design limits and was comparable to the nozzle insulation performance in motors 120-SS-1 and 260-SL-1. The 260-SL-2 nozzle insulation maximum surface recession profile is shown in Figure 325; the initial surface contour for both the 260-SL-1 and -2 nozzle insulation, and the maximum surface recession profile for 260-SL-1 nozzle insulation are included in Figure 325 for comparison. A posttest view of the entrance insulation is shown in Figure 326.

XIII, C, 260-SL Nozzle (cont.)

As shown in Figure 325, the erosion contour at the downstream edge of the nozzle insulation, spanning the -2.04:1 area ratio station, was considerably smoother than the 260-SL-1 posttest contour. Apparently, the effort expended to control the nozzle insulation shrinkage in the mandrel during and after cure produced a closer fit with the nozzle plastic components. As a result, a thinner bondline was formed between the rubber and plastic at the blend area, and the irregular erosion experienced in 260-SL-1 from degradation of the rubber-to-plastic bond was averted.

(2) Entrance Insert

The erosion characteristics of the entrance insert is similar to that of the 260-SL-1 nozzle. Maximum surface erosion occurred in the silica cloth portion of the insert, which was initially fully covered by V-44 insulation. There is no evidence that variability in erosion of the plastic resulted from any cause other than variation in protection afforded by the V-44 insulation.

The carbon cloth portion of the insert, which interfaced with the silica at the -2.0:1 area ratio station, was more uniformly eroded, with small variability near the silica interface reflecting the variation in V-44 insulation erosion. The average erosion contour was similar to 260-SL-1 in this portion of the entrance insert. The average measured depth of erosion at the -1.6:1 area ratio station was 0.27 in., as compared to 0.37 in. for motor 260-SL-1. Moving from the -1.60:1 area ratio station toward the throat, measured erosion exceeded 260-SL-1 erosion by a maximum of 30% at the 1.41 area ratio and then progressively decreased. At the -1.06:1 area ratio station, the average measured erosion was 0.81 in., as compared with 0.84 for motor 260-SL-1.

XIII, C, 260-SL Nozzle (cont.)

Figure 327 shows the posttest surface condition of the entrance insert adjacent to the V-44 insulation. No delaminations were observed in the surface of the silica cloth; numerous short circumferential delaminations existed in the surface of the carbon cloth.

(3) Throat Insert

The nozzle throat insert was eroded uniformly around its circumference except for a local deep erosion at the 140-degree location. The local erosion shown in Figure 328 is 0.20 in. deeper than the adjacent surface and is an extension of the irregular V-44 insulation erosion pattern into the nozzle throat. At the throat station, the erosion depth obtained in contour measurements was 0.56 to 0.71 in., with an average of 0.61 in., as compared to 0.70 in. for motor 260-SL-1. Average erosion at the throat obtained from the differences between pretest and posttest diameter measurements taken at six angular locations was 0.624 in. The action time throat recession rate is 4.8 mils/sec. The total erosion was greatest at the entrance end of the insert (-1.06:1 area ratio station) and decreased progressively over the length of the insert.

The physical appearance of the surface of the throat is shown in Figure 329. Numerous circumferential delaminations were apparent. The area downstream from the throat showed surface roughness similar in appearance to that observed at this location in the 260-SL-1 nozzle throat insert.

XIII, C, 260-SL Nozzle (cont.)

(4) Throat Extension Insert

The measured depth of erosion of the throat extension was less than the 260-SL-1 erosion over the entire length of the insert. At the upstream end of the insert (1.01:1 area ratio station), the average measured erosion was 0.28 in. as compared to 0.42 in. for 260-SL-1; near the downstream end (1.9:1 area ratio station), the average measured erosion was 0.15-in. as compared to 0.22 for the 260-SL-1 nozzle.

The surface appearance of the throat extension insert is shown in Figure 330. Numerous surface pits were observed, and erosion was uniform. Short circumferential delaminations were apparent with two long circumferential delaminations near the aft end of the insert. These two delaminations are shown in Figure 330. By insertion of steel scales, it was determined that the depth of these delaminations extend approximately to the overwrap material interface.

(5) Exit Cone

The ablation surface of the carbon portion of the exit cone was smooth, with long circumferential delaminations as shown in Figure 331. Numerous radial cracks were also observed. These delaminations and cracks were similar in appearance to those observed in the exit cone of the motor 260-SL-1, except that more radial cracks were apparent. The interface layer between the carbon cloth and silica cloth was delaminated and inspection indicated that the delamination extended to the overwrap material interface.

The ablation surface of the silica cloth is shown in Figure 332. An oxide deposit similar to that observed on the 260-SL-1 exit cone

XIII, C, 260-SL Nozzle (cont.)

covered the entire surface of the silica cloth. Previous analysis of samples of this deposit showed the oxide to be basically mullite ( $3\text{Al}_2\text{O}_3 \cdot 2\text{SiO}_2$ ) with additional silicon present as  $\text{SiO}_2$ . This oxide was apparently produced as a melt of  $\text{SiO}_2$  from the silica cloth of the liner and  $\text{Al}_2\text{O}_3$  from the aluminum of the propellant.

Circumferential delaminations were observed over the entire surface of the silica cloth portion of the liner. Longitudinal depressions were also observed, being most pronounced at the upstream end of the silica cloth section. The pattern of these depressions correlates with locations of steel strips used to retain the nylon tension wrap during liner cure and appear to result from small fiber reorientation occurring between each of the first layer of these strips.

The V-61 potting compound applied to the exit cone aft flange afforded adequate thermal protection. The external surface of the exit cone showed evidence of heating, in that the cork-sheet insulation placed over the outer skin of the honeycomb structure was charred or blackened over approximately three-quarters of its circumference (Figure 333) and extended 2 ft further below the exit plane than observed on motor 260-SL-1. Unbonding of the edge of the outer doublers and two repair panels was observed. Inspection by tapping showed that large areas of the bond between the outer facings and honeycomb core were separated. Although no discoloration of the honeycomb external surface was observed, overheating and subsequent degradation of the bond line was evident.

b. Char Thickness, Structural Integrity and Bondline

The surface erosion and general appearance of the 260-SL-2 nozzle was similar to that of 260-SL-1. It was not considered necessary to section the 260-SL-2 nozzle. Therefore, char thickness, structural evaluation, and bondline analysis were not obtained.

XIV. CONCLUSIONS

The objectives of the 260-SL motor nozzle development program were achieved and demonstrated the feasibility of fabricating reliable 260-in.-dia motor nozzles with ablative plastic liners. The experience of ablative nozzle components from programs such as Minuteman, Polaris, Large Solid Rocket, and related R&D programs, provided the background data necessary to establish the approach to the current program. Based on the analytical studies, process evaluation studies, and test data obtained during the program, the following conclusions have been reached.

1. The process evaluation programs provided sound bases for the selection of materials, fabrication processes, and assembly procedures, and for the establishment of quality control requirements.
2. The subscale nozzles fired on the 44-SS and 120-SS-1 motors verified the design criteria, analytical stress and heat transfer analyses, and performance predictions for components of the 260-SL nozzles.
3. The 44-SS nozzles adequately demonstrated the performance of nozzles subjected to aft-end ignition.
4. The predictability of erosion performance for ablative components in large nozzles was demonstrated in test firing performance on the 120-SS-1 and the 260-SL motor nozzles.
5. The feasibility of fabricating ablative components for nozzles with throat diameters up to 71.0 in. was demonstrated.
6. Ablative components, which were preformed and cured in autoclave cycles at approximately 300 psi, have properties comparable to those cured in a hydroclave at 1000 psi.

XIV, Conclusions (cont.)

7. The nylon tension-wrap process demonstrated attainment of adequate physical properties, permitting curing of large, ablative exit-cone liners without the use of an autoclave or hydroclave.

8. The exit-cone honeycomb sandwich structure consisting of aluminum honeycomb and stainless steel facings, was demonstrated to be a relatively lightweight structure capable of supporting aft-end ignition loads. The fabrication process of building up the sandwich structure directly on the liner was also demonstrated.

LIST OF REFERENCES

1. Aerojet-General Corp., 260-in.-dia Motor Feasibility Demonstration Program, Final Phase Report, Volume V: 260-SL Motor Chamber and Nozzle Shell fabrication of 18%-Nickel Steel, Contract No. NAS3-6284, Report NASA CR 72126, dtd 8 April 1966
2. Aerojet-General Corp., 260-in.-dia Motor Feasibility Demonstration Program, Volume IV: 260-SL Motor Internal Insulation System, Contract No. NAS3-6284, Report NASA CR 54930, dtd 8 April 1966
3. Aerojet-General Corp., 260-in.-dia Motor Feasibility Demonstration Program, Final Report, Static Test Firing of Motor 260-SL-1, Report NAS3-6284 FT-5, dtd 25 October 1965
4. Aerojet-General Corp., 260-in.-dia Motor Feasibility Demonstration Program, Final Report, Static Test Firing of Motor 260-SL-2, Report NAS3-6284 FT-6, dtd 25 March 1966.
5. Aerojet-General Corp., 260-in.-dia Motor Feasibility Demonstration Program, Volume I: 260-SL Motor Aft-End Ignition System Development, Final Phase Report, Contract No. NAS3-6284, Report NASA CR 54454, dtd 20 August 1965
6. Aerojet-General Corp., Structural Analysis Report, 260-in.-dia Motor, 623A Program, dtd 27 September 1963
7. Aerojet-General Corp., Structural Analysis Report, 120-SS Subscale Motor, 623A Program, dtd 7 November 1963
8. Southern Research Institute, The Thermal and Mechanical Properties of Five Ablative Reinforced Plastics from Room Temperature to 750°F, Report No. AFML-TR-65-133, April 1965
9. S. L. Madorsky, Thermal Degradation of Organical Polymers, Interscience Publishers, 1964



LIST OF NOMENCLATURE

A	Local nozzle area, sq ft
A	Effective heat transfer area in hydroclave heat exchanger
$A_t$	Throat area, sq ft
$\dot{g}$	Recession rate, mil/sec
c	Specific heat, Btu/lb-°R
$C_W$	Propellant mass flow coefficient, sec <sup>-1</sup>
$c_p$	Specific heat at constant pressure, Btu/lb-°R
D	Nozzle diameter, in. or ft
$D_t$	Nozzle throat diameter, in. or ft
$E_p$	Modulus of elasticity of plastic, psi
$E_s$	Modulus of elasticity of steel, psi
h	Height of arc, ft
$h_{eff}$	Effective lower heat of ablation temperature, °R
K	Thermal conductivity, Btu/sec ft-°F
L	Half specimen length
$h_c$	Convective heat transfer coefficient, Btu/sq ft-sec-°R
m	Water circulating rate
$\theta$ or t	Time, sec
$P_c$ or P	Chamber pressure, lb/sq ft abs. or lb/sq in. abs. (psia)
Pr	Prandtl number
$Q_c$	Convective heat flux, Btu/sq ft-sec
r	Radial coordinate, ft
r	Radius of curvature
$T_{aw}$	Adiabatic wall temperature, °R
$T_w$	Wall temperature, °R
$T_a$	Effective ablation temperature, °R
T	Temperature
$T_{s_{av}}$	Average temperature of steam in hydroclave heat exchanger
T	Hydroclave water temperature at any time
To	Starting temperature of water in hydroclave

LIST OF NOMENCLATURE (cont.)

W	Weight, lb
U	Overall heat transfer coefficient in hydroclave heat exchanger
$\alpha$	Thermal diffusivity
$\mu$	Absolute viscosity, lb/ft sec
$\rho$	Density, lb/cu ft